Preparation and properties of flame-retarded vermiculite composites

by

Hermínio Francisco Muiambo

Thesis submitted in partial fulfilment of the requirements for the degree

Philosophiae Doctor in Chemistry

in the

Faculty of Natural & Agricultural Sciences,

University of Pretoria

Pretoria

February 2015

Preparation and properties of flame-retarded vermiculite polymer composites

Author: Hermínio Francisco Muiambo

Supervisor: Prof. Walter W. Focke

Department: Chemistry

University: University of Pretoria

Degree: PhD (Philosophiae Doctor)

SYNOPSIS

Polymeric materials are increasingly used in several applications. However, their relatively high flammability presents a danger to people and property. Their use therefore requires that they are made more resistant to both the initiation and propagation of fires.

Vermiculite is a fire-resistant material which can be utilised as a flame retardant (FR) additive in polymers. Industrial expansion of natural vermiculite is made at temperatures above 800 °C. However, vermiculite's expansion onset temperature is around 450 °C and effective FR additives have their onset temperatures in the range of 200 to 350 °C. With the aim of resolving this disparity, Palabora vermiculite was modified by different procedures and methods to render it more suitable for its application in flame-retarded LLDPE, PU and PVC polymer composites.

Palabora vermiculite was modified using inorganic cations, urea complexes and organic surfactants. Urea complexes and some organic surfactants reduced vermiculite's expansion onset temperature, but did not significantly affect its

maximum expansion ratio. The latter was found to be independent of the flake thickness and the nature of the modification.

Application of a compressive force sufficient to compact an expanded worm-like vermiculite flake reconstituted the vermicular structure to the original dimensions. At low compressive forces the vermicular structure showed spring-like behaviour with hysteresis. The interlayer mosaic-like bonding holds the sheets together and stabilises the system via mechanical interconnects that prevent complete expansion or exfoliation.

In this work the expansion onset temperature of vermiculite was successfully tuned to within the activation temperature range of intumescent systems (209 ± 35 °C) through the intercalation of metal-urea complexes. These complexes feature both urea and water molecules as blowing agents. To the best of our knowledge, this is the first time that vermiculite's exfoliation onset temperature has been lowered to such temperatures, using ion-exchange methods and specifically urea complexes.

The organic intercalation was successful and was restricted to the ion-exchange level, despite vermiculite's pre-treatment with Na^+ ions. The d-spacing values were proportional to the surfactant's chain length. These values also increased with increasing surfactant:vermiculite ratio up to ca. 150% CEC and assumed an average value of 4.4 nm.

All organo-vermiculite/LLDPE composites were translucent. Their XRD diffractograms were featureless, suggesting excellent dispersion throughout the matrix. However, the presence of mica agglomerates was detected. The organo-vermiculite improved significantly LLDPE's mechanical and flammability properties.

In PU composites the urea-vermiculite was unable to form a cohesive protective barrier layer during the cone calorimeter test. The poor compatibility between the molten PU and the exfoliated flakes also led to the consumption of the underlying PU. Nevertheless, the addition of urea-vermiculite lowered significantly the pHRR of PU composites.

Flexible PVC cone calorimeter tests proceeded without a visible flame following an initial short-lived ignition which degenerated into a bulk pyrolysis, in combination with a surface glowing-combustion event. Urea-vermiculite formed an exfoliated protective barrier layer which allowed thermal stabilisation of the condensed phase. The simultaneous release of halogen species by the PVC and the action of the exfoliated barrier layer prevented the formation of a flammable air–fuel mixture. The addition of urea-vermiculite lowered the pHRR and the tHR significantly.

Keywords: Vermiculite, Ion exchange, Exfoliation, Composites, Flame retardancy.

.

Preparação e propriedades de compósitos poliméricos de vermiculita modificada para retardamento de chama

Autor:	Hermínio Francisco Muiambo
Supervisor:	Prof. Walter W. Focke
Departmento:	Química
Universidade:	Universidade de Pretória
Grau académico:	Doutoramento (PhD)

RESUMO (PORTUGUESE)

Materiais poliméricos estão sendo progressivamente usados em diversas aplicações. Entretanto a sua alta inflamabilidade representa um risco enorme para pessoas e bens. Assim, o seu uso responsável requer que materiais poliméricos sejam adequadamente modificados e feitos mais resistentes à ignição e propagação de chamas.

A expansão (geralmente chamada exfoliação) industrial da vermiculita natural é feita a temperaturas que excedem 800 °C e a temperatura inicial de expansão se situa acima dos 450 °C. Retardantes de chama eficientes para materiais poliméricos possuem uma temperatura inicial de expansão na região entre 200 °C – 350 °C. Com este propósito, a vermiculita de Palabora foi quimicamente modificada através de diferentes métodos e procedimentos para a sua posterior aplicação como retardante de chama em matrizes poliméricas de LLDPE (polietileno de baixa densidade linear), PU (poliuretano) e PVC (cloreto de polivinil).

Catiões inorgânicos de baixo potencial iónico, complexos metálicos de ureia e surfactantes (orgânicos) foram usados no presente estudo para modificação das

propriedades da vermiculita de Palabora. Os complexos metálicos de ureia e alguns surfactantes foram eficientes na redução da temperatura inicial de exfoliação embora, ainda, tenham mostrado um relativamente baixo índice de expansão térmica. A expansão térmica relativa da vermiculita mostrou-se ser independente da espessura do floco e da natureza da modificação química.

O uso de uma força de compressão, suficiente para compactar um floco de vermiculita expandida a altas temperaturas, reconstituiu a estrutura vermicular até às suas dimensões iniciais, a baixas temperaturas. A baixas forças de compressão a estrutura vermicular exibiu características de uma mola com clara histerese. A composição mosaica da região interlamelar propicia uma diversidade de ligações entre as camadas estabilizando assim o sistema de ligações mecânicas que previnem a expansão completa das camadas ou exfoliação/delaminação.

A temperatura inicial de expansão da vermiculite foi ajustada com sucesso para a sua aplicação em sistemas intumescentes (209 ± 35 °C) através da co-intercalação de complexos metálicos de ureia. Estes complexos (ureia-vermiculita) dispõem de ureia e água (ligados aos catiões interlamelares) como agentes de expansão. Este novo método de co-intercalação de complexos de ureia para a redução da temperatura de início de esfoliação da vermiculita é inovador.

A vermiculita pré-tratada com iões Na^+ intercalou surfactantes de cadeia longa quase na mesma extensão que a Mg-vermiculita natural e a reacção se restringiu ao nível de troca iónica. O espaçamento interlamelar (d_{001}) se mostrou proporcional ao tamanho da cadeia carbónica. Este também aumentou proporcionalmente ao incremento do rácio surfactante/vermiculita até 150% CTC (capacidade de troca catiónica) e assumiu um valor médio de 4.4. nm.

Compósitos poliméricos de LLDPE, com diferentes composições, foram preparados usando uma organo-vermiculita de cadeia dupla (DC10) como único aditivo. Todas as composições não exibiram reflexões típicas da vermiculita sugerindo

boa dispersão (exfoliação e/ou intercalação) através da matriz polimérica embora tenham mostrado alguns aglomerados de argila (mica).

A organo-vermiculita melhorou significativamente a resistência à tracção e o módulo de Young dos compósitos poliméricos de LLDPE. Estes compósitos também apresentaram uma camada exfoliada protectora homogénea que reduziu a taxa de emissão de fumo e de CO, CO_2 e do pHRR.

Em composições de PU a vermiculite expansível não pôde formar uma camada protectora homogénea. A fraca compatibilidade entre a matriz fundida de PU e os flocos exfoliados permitiu que houvesse consumo da parte interna de PU. Entretanto a adição da vermiculite expansível permitiu a redução significativa do pHRR dos compósitos de PU embora não tenha sido foi suficiente para diluir a mistura de vapores inflamáveis, na fase gasosa

Testes de cone calorimetria dos compósitos de PVC decorreram sem chama visível seguida de uma curta ignição que degenerou numa pirólise geral em combinação com combustão superficial sem chama. A libertação simultânea de espécias halogénicas pelo PVC e a acção protectora da camada de vermiculita exfoliada impediu a formação de uma mistura de gases inflamáveis. A adição de ureia-vermiculita em PVC flexível reduziu drasticamente o pHRR e o tHR.

Palavras-chave: Vermiculite; Troca iónica; Exfoliação; Compósitos, Retardamento de chama;

ACKNOWLEDGEMENTS

My special and sincere thanks to:

God Almighty for His grace and endless blessings.

My Supervisor Prof. Walter Focke for his guidance, patience, inspiration and encouragement.

My fellow researchers at the Institute of Applied Materials (IAM), University of Pretoria, (especially Dan Molefe, Mthokozisi Sibanda, Washington Mhike, Sheppard Tichapondwa, Nontete Nhlapo, Lumbi Moyo, Maria Atanasova and Afonso Macheca) for their friendship and companionship, as well as all staff members at the IAM (Suzette Seymore, Ollie del Fabbro, Isbe van der Westhuizen and Reiner Schumacher) for their daily support.

Prof. Joseph K. O. Asante (Tshwane University of Technology) for valuable assistance with the cone calorimeter tests.

Xyris stuff for their valuable support throughout my post-graduation studies.

Students and staff members at the Center for Engineering Sciences, Martin Luther University Halle-Wittenberg (Prof. Radusch, Prof. Androsch, Dr. Wutzler, Matthias, Melanie, Andreas) for their cordiality and support. My colleagues and friends at Université A. Mira de Bejaïa (especially Dr. Aida Benhamida and Prof. Mustafa Kaci) for their friendship and collaboration.

My colleagues at Eduardo Mondlane University (especially *Tios* Carvalho Madivate, Arão Manhique and Pedro Massinga Jr.) for their support and encouragement to further my studies.

My parents Francisco Muiambo and Olinda Tembe for their endless love and guidance throughout all stages of my education. My brothers César Muiambo, Ivo Muiambo, Fídel Muiambo and André Muiambo for their brotherhood and support.

My wife Inês Cossa Muiambo and my lovely daughters Keila Muiambo, Flora Muiambo and Inês Muiambo for their inspiration, motivation and unconditional support, especially during those long periods of absence.

Eduardo Mondlane University (UEM) and the Technology Processing of Natural Resources Program of the Swedish International Development Cooperation Agency (SIDA) for financial support.

DECLARATION

I, Hermínio Francisco Muiambo, declare that the thesis which I hereby submit for the degree PhD in Chemistry, at the University of Pretoria, is my own work and has not previously been submitted by me for a degree at this or any other tertiary institution.

……

February 2015

THESIS OUTLINE

The thesis is structured in eight chapters:

The aims and the methodology applied in the present research work are described in Chapter 1.

The second chapter presents a literature review on clays and clay minerals, focusing on vermiculite. A brief history of research on vermiculite is provided. The geological origin, properties, structure and potential applications of Palabora vermiculite are presented.

Chapter 2 also reviews polymer flame retardancy (FR). It provides an overview of the common analytical techniques used for the characterisation of vermiculite and vermiculite's polymer composites.

Vermiculite's properties vary according to its origin and composition. Chapter 3 therefore provides characterisation data on Palabora vermiculite.

Chapter 4 discusses the ion exchange of Palabora vermiculite by inorganic cations and by metal-urea complexes.

Chapter 5 describes the organic modification of vermiculite by intercalation of organic surfactants. Previous work, aimed at modifying hydrophilic vermiculite to hydrophobic vermiculite for various applications, with particular focus on polymer layered silicate nanocomposites (PLSNs), is discussed. Experimental results related to the structure of the hybrids are presented and discussed.

Chapter 6 discusses the thermal expansion properties of vermiculite and its modified forms. A brief literature review of the inorganic modification and expansion properties of vermiculite is also presented. In the Results Section, this chapter considers the possibility of reversible expansion (and contraction) of neat and modified vermiculites.

Chapter 7 assesses the effectiveness of a selected organo-vermiculite in LLDPE composites and of one metal-urea-vermiculite complex as flame-retardant additive in PU and PVC.

The overall conclusions and recommendations are summarised in Chapter 8.

Additional relevant information and data are provided in the Appendices.

TABLE OF CONTENTS

LIST OF FIGURES

LIST OF TABLES

LIST OF SCHEMES

LIST OF ABBREVIATIONS

ASTM	American Society for Testing and Materials
CEC	cation exchange capacity
cmol	centimol
CNT	carbon nanotube(s)
DC10	N,N′-didecyldimethylammonium chloride
DMA	dynamic mechanical analysis/analyser
DSC	differential scanning calorimeter
DTG	derivative thermogravimetry
EG	expandable graphite
ESEM	environmental scanning electron microscope/microscopy
FR	flame/fire retardant/retardancy
FT-IR	Fourier transform infrared spectroscopy
HBCD	hexabromocyclododecane
HRR	heat release rate
ICP-OES	inductively coupled plasma–optical emission spectrometer
ISO	International Organization for Standardization
IR	infrared spectrometer/spectroscopy
IUPAC	International Union of Pure and Applied Chemistry
Ksp	constant of solubility product
LLDPE	linear low-density polyethylene
L.O.I.	loss on ignition
LOI	limiting oxygen index
MMT	montmorillonite
PBDE	polybromodiphenylether
PE	polyethylene
pH	potential hydrogen

pHRR	peak heat release rate
PLSN	polymer layered silicate nanocomposite
POSS	polyhedral silsesquioxanes
PP	polypropylene
PVC	poly(vinyl)chloride
PU	polyurethane
SC8	octylammonium chloride
SC12	dodecylpyridinium chloride
SC14	tetradecyl-trimethylammonium bromide (Cetrimide BP)
SC16	hexadecyltrimethyl-ammonium bromide (CTAB)
SEM	scanning electron microscopy
SPR	smoke production rate
TBPA	tetrabromophtalic anhydride
TGA	thermogravimetric analysis/analyser
TMA	thermomechanical analysis/analyser
TEM	transmission electron microscopy
tHR	total heat release rate
t_{ign}	time to ignition
TMA	thermomechanical analysis/analyser
TBBPA	tetrabromobisphenol A
XRD	X-ray diffraction
XRF	X-ray fluorescence
WAXS	wide-angle X-ray scattering
WLHS	water layer hydration state
0-WLHS	zero water layers hydration state
1-WLHS	one water layer hydration state
2-WLHS	two water layers hydration state
wt.%	weight percentage

CHAPTER 1
GENERAL INTRODUCTION

1.1 BACKGROUND

Clay minerals attract interest in science and technology due to the huge effect that they can have on structural and functional materials, even at very low dosage levels.

Applications of clay minerals include nanocomposites, catalysis, adsorbents, sensors, nuclear waste storage, antibacterials, pharmaceuticals, pesticide carriers and others (Grim, 1968; Bergaya *et al.*, 2006; Liu *et al.*, 2007; Annabi-Bergaya, 2008). Clay minerals are also seen as a low-cost and environmentally friendly option in the abovementioned applications (Tjong *et al.*, 2002; Tjong, 2006; Bergaya and Lagaly, 2013).

Clay minerals possess several advantages as additives. For instance, their polymer nanocomposites can be transparent, flexible and have some synergistic activity with other additives, etc. The enhancement of polymeric material properties such as flame retardancy, thermal and chemical resistance, permeability, etc. is usually related to factors such as compatibility of the clay layers with the host polymer and with the degree of dispersion (exfoliation and/or intercalation) in the polymer matrix (Giannelis, 1996; Alexandre and Dubois, 2000; Tjong *et al.*, 2002; Sinha Ray and Okamoto, 2003).

Vermiculite is a natural cationic clay. It belongs to the phyllosilicate category with a layered nanostructure and a relatively high cation exchange capacity (CEC). Its most striking property is the thermal expansion also known as sudden exfoliation. Natural vermiculite with its lamellar structure and high aspect ratio can potentially provide good barrier properties (Utracki, 2004). However, during the modification of vermiculite, it is important to control its lamellar structure and flake size in order to retain its expansion properties (Pérez-Maqueda *et al.*, 2001).

Commercially, the expansion of vermiculite is performed in an exfoliation furnace with temperatures in excess of 1 000 °C. Dwelling time in the high heat area of the furnace is usually less than five seconds. The industrial exfoliation process adds value by changing the physical properties of the material undergoing exfoliation into a new material with commercial uses. Crude ore, high-density vermiculite flakes have limited applications. Yet, when converted into non-combustible, lightweight particles, they have several commercial and industrial uses.

Since the 1980s, there has been a growing interest in non-halogenated and environmentally friendly flame-retardant solutions. Mineral fillers, as raw materials or as precursors, are often considered (Dufton, 1995).

Expandable graphite (EG) is a good intumescent fire retardant (FR) for many polymers (Nakagawa, 2006; Weil and Levchik, 2008; Chen and Wang, 2010; Weil, 2011) and in particular for polyethylene (Qu and Xie, 2003; Focke et al., 2014a), polyurethane foam (Camino *et al.*, 2001; Nakagawa, 2006) and poly(vinyl) chloride (PVC) (Focke *et al.*, 2014b). On exposure to heat, the EG exfoliates, forming a low-density, fire-resistant layer covering the exposed surface.

Natural vermiculite also expands abruptly when heated to high temperatures, resembling EG. Exfoliated vermiculite is lightweight, chemically inert and incombustible with excellent absorption and thermal insulation properties (Schoeman, 1989; Tomanec *et al.*, 1997; Obut and Girgin, 2002; Bergaya *et al.*, 2006). So, by analogy to EG, vermiculite could act as a good FR for polymers. However, its onset temperature is about 450 °C. At this temperature organic polymers are usually already fully degraded. Hence the exfoliation temperature of vermiculite must be reduced in order for it to be an effective FR additive.

1.2 RESEARCH OBJECTIVES

The properties of vermiculites are closely related to the nature of the interlayer cation and to the chemical environment surrounding it (ligands). The main aim of the present work was to prepare and study flame-retarded modified-vermiculite/polymer composites, using different processing techniques and polymeric matrices. For this purpose the following specific objectives were set:

⇒ Chemically modify Palabora vermiculite, using different (inorganic) cations and their complexes and (organic) cationic surfactants, by ion exchange.

⇒ Lower the expansion onset temperature of Palabora vermiculite to temperatures in the range of 200 °C to 250 °C.

⇒ Evaluate the flammability of different polymer composites prepared with these modified vermiculites.

1.3 RESEARCH METHODOLOGY

The present study involved three basic steps:

(1) Modifications of Palabora vermiculite

(2) Dispersion of modified vermiculite into polymeric matrices

(3) Evaluation of the FR properties of the composites.

All modification experiments were carried out at room temperature and were intentionally designed to also preserve vermiculite's expansion properties by maintaining its lamellar structure.

The modification of the interlayer chemical environment of the neat vermiculite was carried out using the following three experimental designs:

⇒ Ion exchange of neat vermiculite with some selected inorganic cations

⇒ Ion exchange of neat vermiculite with some selected cationic urea complexes

⇒ Intercalation of neat vermiculite and Na-vermiculite with different long-(carbon) chain surfactants

Neat vermiculite and its modified samples were widely characterised using several techniques and the main focus was on the determination of the expansion onset temperature and the expansion ratio by thermomechanical analysis (TMA).

Successfully modified-vermiculites were dispersed in linear low-density polyethylene (LLDPE), PVC and polyurethane (PU). Melt compounding by extrusion (and then injection moulding), the plastisol route and casting were, respectively, the methods used for the preparation of modified-vermiculite/polymer composites.

REFERENCES

Alexandre, M., Dubois, P., 2000. Polymer-layered silicate nanocomposites: preparation, properties and uses of a new class of materials. Materials Science and Engineering: R: Reports 28, 1-63.

Annabi-Bergaya, F., 2008. Layered clay minerals. Basic research and innovative composite applications. Microporous and Mesoporous Materials 107, 141-148.

Bergaya, F., Lagaly, G., 2013. Handbook of Clay Science. Elsevier Science, Amsterdam.

Bergaya, F., Theng, B.K.G., Lagaly, G., 2006. Handbook of Clay Science. Elsevier, Amsterdam.

Camino, G., Duquesne, S., Delobel, R., Eling, B., Lindsay, C., Roels, T., 2001. Mechanism of Expandable Graphite Fire Retardant Action in Polyurethanes, Fire and Polymers. American Chemical Society, pp. 90-109.

Chen, L., Wang, Y.Z., 2010. A review on flame retardant technology in China. Part I: Development of flame retardants. Polymers for Advanced Technologies 21, 1-26.

Dufton, P.W., 1995. Fire - Additives and Materials. Smithers Rapra Technology.

Focke, W.W., Kruger, H.J., Mhike, W., Taute, A., Roberson, A., Ofosu, O., 2014a. Polyethylene flame retarded with expandable graphite and a novel intumescent additive. Journal of Applied Polymer Science 131, n/a-n/a.

Focke, W.W., Muiambo, H., Mhike, W., Kruger, H.J., Ofosu, O., 2014b. Flexible PVC flame retarded with expandable graphite. Polymer Degradation and Stability 100, 63-69.

Giannelis, E.P., 1996. Polymer layered silicate nanocomposites. Advanced Materials 8, 29-35.

Grim, R.E., 1968. Clay mineralogy. 2nd edition. McGraw Hill.

Liu, Y., Xiao, D., Li, H., 2007. Kinetics and Thermodynamics of Lead (II) Adsorption on Vermiculite. Separation Science and Technology 42, 185-202.

Nakagawa, Y., 2006. Recent development of flame retardant polymeric materials containing expandable graphite. Bulletin of Japan Association for Fire Science and Engineering 56, 37-43.

Obut, A., Girgin, I., 2002. Hydrogen peroxide exfoliation of vermiculite and phlogopite. Minerals Engineering 15, 683-687.

Pérez-Maqueda, L.A., Canea, O.B., Poyato, J., Pérez-Rodríguez, J.L., 2001. Preparation and characterization of micron and submicron-sized vermiculite. Physics and Chemistry of Minerals 28, 61-66.

Qu, B., Xie, R., 2003. Intumescent char structures and flame-retardant mechanism of expandable graphite-based halogen-free flame-retardant linear low density polyethylene blends. Polymer International 52, 1415-1422.

Schoeman, J.J., 1989. Mica and vermiculite in South Africa. Journal of The South African Institute of Mining and Metallurgy 89, 1-12.

Sinha Ray, S., Okamoto, M., 2003. Polymer/layered silicate nanocomposites: a review from preparation to processing. Progress in Polymer Science 28, 1539-1641.

Tjong, S.C., 2006. Structural and mechanical properties of polymer nanocomposites. Materials Science and Engineering: R: Reports 53, 73-197.

Tjong, S.C., Meng, Y.Z., Hay, A.S., 2002. Novel Preparation and Properties of Polypropylene–Vermiculite Nanocomposites. Chemistry of Materials 14, 44-51.

Tomanec, R., Popov, S., Vučinič, D., Lazič, P., 1997. Vermiculite from Kopaonik (Yugoslavia): Characterization and processing. Fizykochemiczne Problemy Mineralurgii 31, 247-254.

Utracki, L.A., 2004. Clay-Containing Polymeric Nanocomposites, Volumes 1-2. Smithers Rapra Technology.

Weil, E.D., 2011. Fire-protective and flame-retardant coatings - A state-of-the-art review. Journal of Fire Sciences 29, 259-296.

Weil, E.D., Levchik, S.V., 2008. Flame retardants in commercial use or development for polyolefins. Journal of Fire Sciences 26, 5-43.

CHAPTER 2
LITERATURE SURVEY

2.1 CLAYS AND CLAY MINERALS

According to the charge of the interlayer cation, clays and clay minerals are categorised into two broad classes: cationic clays and anionic clays. While the cationic clays are widespread in nature, the anionic clays or mixed metal hydroxides are rarely found but are relatively simple and inexpensive to synthesise (Reichle, 1986; Vaccari, 1998).

Clay minerals are defined as natural or synthetic phyllosilicate minerals that impart plasticity to clay and that harden upon drying or firing (Bergaya *et al.*, 2006). According to Bergaya *et al.* (2006), the properties of clay minerals are usually associated with those of smectites and are characterised by:

- a layered structure with one dimension in the nanometre range
- anisotropy of the layers
- different types of surface (basal, edge and interlayer)
- cation and anion exchange capacity
- relatively easy capacity for chemical, physical or thermal modification
- interlayer swelling in appropriate solvents
- plasticity.

The structures of phyllosilicates are all based on tetrahedral (T, with four sites) and octahedral (O, with six sites) sheets that may condense anisotropically in a proportion of either 1:1 (TO) or 2:1 (TOT) (Newman, 1987; Vaccari, 1998; Bergaya *et al.*, 2006).

The unit cell of a 1:1 phyllosilicate layer structure is characterised by four tetrahedral sites and six octahedral sites, while a 2:1 layer unit cell is composed of eight tetrahedral sites and six octahedral sites. The oxygen atoms are responsible for

connecting the sheets (Newman, 1987; Frank and Edmond, 2001; Bergaya *et al.*, 2006; da Fonseca *et al.*, 2006).

$$(Si_{8-x}M_x)^T(Al_{4-y}M'_y)^O(OH)_4O_{20}M''^{n+}M''^{n+}_{(x+y)/n}mH_2O$$

Scheme I: General formula of dioctahedral clay minerals

In dioctahedral clay minerals (Scheme I) only four of the six octahedral sites are occupied, while in trioctahedral clay minerals all the sites – either the octahedral (six) or the tetrahedral (four) sites – are occupied, as shown in Scheme II (Newman, 1987; Vaccari, 1998; Bergaya *et al.*, 2006).

$$(Si_{8-x}M_x)^T(Al_{6-y}M'_y)^O(OH)_4O_{20}M''^{n+}M''^{n+}_{(x+y)/n}mH_2O$$

Scheme II: General formula of trioctahedral clay minerals

In clay minerals the thickness of the 1:1 layer is about 0.7 nm, while in 2:1 the layer is about 1 nm (Bergaya *et al.*, 2006).

2.2 VERMICULITE

Vermiculite was first described by Thomas H. Webb, in 1824, while studying a mineral from Worcester, Massachusetts, US (Grim, 1968; Anthony *et al.*, 2004; Bergaya *et al.*, 2006; Hindman, 2006). He defined it as a variety of talc mineral that during thermal expansion looks like small worms having the *vermicular* motion, hence its name "vermiculite" (from Latin *vermiculari,* which means to breed worms). Due to slight variations in colour and chemical composition, commercial vermiculites have also been traded as dugarlite, mandolite, strong-lite, zonolite, etc. (Hindman, 2006).

Vermiculite's remarkable exfoliation, when subjected to high temperatures, has attracted the attention of researchers. Available relevant literature on vermiculite dates back to the 1930s. Gruner (1934) and, later on, Hendricks and Jefferson (1938) were the first to elucidate the vermiculite (and hydrobiotite) crystal structure(s).

Due to the high cation exchange capacity (CEC) and surface area of vermiculites, research has been focused on the improvement of its surface area and porosity, the replaceability of the interlayer cations, as well as its hydration/dehydration properties (Barshad, 1950; Fripiat *et al.*, 1960; Saehr *et al.*, 1992; Beyer and Reichenbach, 1998; Jiménez de Haro *et al.*, 2005).

According to some authors (Justo *et al.*, 1993; Marcos *et al.*, 2009), vermiculite-mica interstratification materials show larger expansion at relatively lower temperatures and the thermal effects are also observed at these temperatures. In addition, this modified and interstratified vermiculite is amenable to producing a durable exfoliated material (Frank and Edmond, 2001). In fire barrier applications, it is desirable for exfoliation of vermiculite to occur at temperatures in the range of 200 to 350 °C.

2.2.1 Composition of trioctahedral vermiculite

Natural vermiculite consists mainly of macroscopic and microscopic types. Macroscopic vermiculite (large plate-like morphology crystal) is trioctahedral and has a relatively narrow range of CEC, whereas microscopic or clay vermiculite may be either trioctahedral or dioctahedral (Basset, 1961; Brindley and Brown, 1980; Newman, 1987).

Vermiculite is a magnesium, iron, aluminium, silicate, hydroxide hydrate mineral. Structural water occurs between the silicate layers, depending on the interlayer cation, and non-structural water also occurs in an amount depending on the porosity and relative humidity (Brindley and Brown, 1980; Newman, 1987; Harben and Bates, 1990; Frank and Edmond, 2001; da Fonseca *et al.*, 2006).

In vermiculites, most of the octahedral cations are trivalent, such as Al^{3+} or Fe^{3+}. The layers carry a net negative charge owing to isomorphous substitutions of Si^{4+} in the tetrahedral sites by trivalent ions such as Al^{3+} or Fe^{3+}. However, this is partially compensated for by substitution of Mg^{2+} in the octahedral sites by trivalent ions, e.g. Fe^{3+}. The excess sheet charge is neutralised by alkali metal or alkaline earth interlayer cations, e.g. Mg^{2+}, present in the interlayer space and lying in plane midway between adjacent 2:1 layers. These cations are hydrated and can be exchanged (Brindley and Brown, 1980; Newman, 1987; Pérez-Maqueda *et al.*, 2003; Bergaya *et al.*, 2006).

According to Farmer (1974), the surface charge in vermiculite is concentrated on oxygens of Al-O-Si linkages and adjacent oxygens of Si-O-Si connections.

Vermiculite shows similarities in its crystalline structure and expansibility with smectites (Basset, 1961; Grim, 1968; Jiménez de Haro *et al.*, 2005; Tjong, 2006). However, the electrostatic charge of the vermiculite layer is larger and more heterogenic than that of smectites due to the variations in charge density from layer to layer or within the individual layers (Grim, 1968; Jiménez de Haro *et al.*, 2005; Xu *et al.*, 2005; Tjong, 2006).

2.2.2 Geological origin of Palabora vermiculite

The Palabora Proterozoic igneous complex resulted from an alkaline intrusive activity. The Palabora mine (also known as Loolekop) is a zoned deposit with ultramafic intrusive rocks (pyroxenite), most of which are syenitic in composition (Frank and Edmond, 2001; Hindman, 2006).

Palabora vermiculite is a product of the hydration of phlogopite/biotite under the influence of percolating meteoric water at the weathering surface. During the vermiculisation process there was progressive leaching of potassium ions, an increase in the total water content, a change in colour and a simultaneous loss in elasticity and transparency on the part of the mica (Basset, 1961; Schoeman, 1989; Hindman, 2006).

$$(Mg_{3-x}Fe^{2+}_{x})[Si_{4-y-z}Al_{y}Fe^{3+}_{z}]O_{10}(OH)_{2}K^{+}_{y+z} \rightarrow \alpha(Mg_{3-x}Fe^{2+}_{x})[Si_{4-y-z}Al_{y}Fe^{3+}_{z}]O_{10}(OH)_{2}K^{+}_{y+z} + (1-\alpha)(Mg_{3-x}Fe^{3+}_{x})[Si_{4-y-z}Al_{y}Fe^{3+}_{z}]O_{10}(OH)_{2}Mg^{2+}_{(y+z-x)/2}.nH_{2}O$$

Scheme III: Simplified representation of the partial conversion of biotite into vermiculite (Newman, 1987). It is assumed that Fe^{3+} is present in the tetrahedral sheets and that the Fe^{2+} in the octahedral sheets is completely oxidised during the vermiculisation process.

Scheme III illustrates the partial transformation of biotite to vermiculite in a decidedly simplified manner. It is assumed that Fe^{3+} is present in the tetrahedral sheets and that the Fe^{2+} in the octahedral sheets in vermiculite is completely oxidised during the vermiculisation process. The process entails the replacement of the interlayer potassium ions by hydrated cations (usually Mg^{2+} and, less frequently, Ca^{2+} ions) and the oxidation of the octahedral Fe^{2+} ions (Newman, 1987; Hindman, 2006). Thus, the net negative charge is lower than that of the parental biotite and usually falls in the range 0.6 to 0.9 per $O_{10}(OH)_2$ unit. The decreased charge density facilitates the stripping of K^+ ions and their replacement by (most commonly) hydrated Mg^{2+} ions (Brindley *et al.*, 1983; Moore and Reynolds, 1989).

The co-intercalation of water increases the distance between the 2:1 layers. The hydration energy of the cation (i.e. its ionic potential, which is a function of charge density and ionic radius) attracts water. A monovalent cation has lower ionic potential than an equivalent-sized divalent cation. The interlayer distance is therefore dependent on the balance of forces necessary to dehydrate the cation and the forces of attraction between the layers and the cation (Brindley and Brown, 1980; Brindley *et al.*, 1983).

During the transformation from mica to vermiculite, numerous intermediate mixed-layer phases with various compositions and ordering are formed. In general, a more ordered structure results in a higher layer charge and this is also the case when the humidity is high enough to give stable water layer hydration states (WLHS) (Brindley *et al.*, 1983).

Actually, Palabora vermiculite is not pure vermiculite but rather a mixed-layer vermiculite-mica (Schwellnus, 1938; Basset, 1961; Schoeman, 1989). In fact, "commercial vermiculite" is a generic name for minerals with characteristics similar to those of pure vermiculite (Justo *et al.*, 1989; Jiménez de Haro *et al.*, 2005; Hindman, 2006). Schoeman (1989) proposed the name "hydrophlogopite" for the mineral being considered here.

Palabora vermiculite mining and concentration were started during 1946 by Dr Hans Merensky (Palabora Mining Company Limited, 1976; Schoeman, 1989).

At the Palabora complex there are three separate open pits (see Fig. 1). The vermiculite open-pit mine (represented by number 2 in Fig. 1) is operated by the Palabora Mining Company and since 1990 has become the world's largest producer (Evans, 1987;1993; Hindman, 2006). This vermiculite is mined from a coarse-grained zoned ultramafic body consisting of phlogopite-serpentine rock enveloped by phologopite-diopside rock (Palabora Mining Company Limited, 1976; Evans, 1993).

The crude vermiculite is transported by rail from the mine in Phalaborwa to the port of Richards Bay on the Indian Ocean in KwaZulu-Natal province, South Africa.

From this port it is shipped in bulk to a diversity of destinations and is also stored in the Netherlands and the United Kingdom (Eaves, 2006; Rushton, 2014).

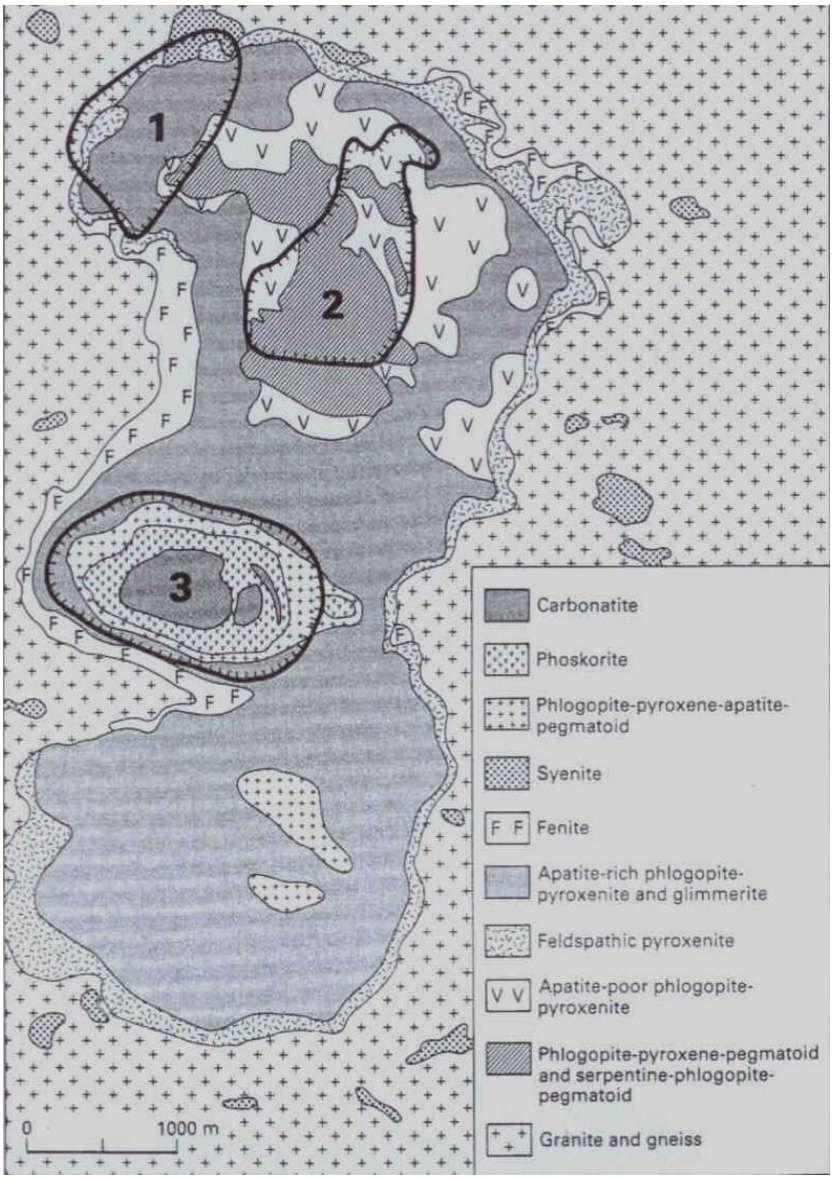

Figure 1. Simplified geological map of the Palabora igneous complex (Evans, 1993). (1) Open pit which produces phosphate; (2) Vermiculite open pit; (3) Open pit which produces basically copper and magnetite

Environmentally, Palabora vermiculite is described as essentially free of asbestiform fibres and crystalline silica (Evans, 1993; Symons, 1999; Eaves, 2006) and,

by the same token, as a potential raw material for application in environmentally friendly technologies.

2.2.3 Physical properties of Palabora vermiculite

Vermiculite resembles mica and varies in colour. It can exhibit a wide range of compositions which are affected by the composition of the parent mica, changes during weathering and ion exchange (Basset, 1961; Frank and Edmond, 2001; Hindman, 2006).

Palabora vermiculite's main properties are summarised in Table 1. It shows properties close to those of the parental biotite: odourless, non-corrosive, non-combustible, non-allergenic and harmless if swallowed (Symons, 1999).

Table 1. Physical properties of Palabora vermiculite (Symons, 1999; Anthony et al., 2004; Hindman, 2006)

Property	Characteristics
Melting point	1 315 °C
Sinter temperature	1 260 °C
Thermal conductivity	0.062–0.065 w m^{-1} $°C^{-1}$
Colour	Brownish, golden yellow
Hardness	1.5–2.5 (Mohs scale)
Density	2.2–2.8 (g cm^{-3})
Specific heat	0.2 J g^{-1} K^{-1}
Bulk density	50–130 g L^{-1}
Cleavage	d_{001}, perfect, typically relict
Tenacity	brittle to flexible

2.2.4 Ion exchange in vermiculite

Bergaya *et al.* (2006) have identified and discussed in detail different ways of modifying 2:1 clay minerals, as follows:

(i) Adsorption

(ii) Ion exchange with inorganic cations and cationic complexes

(iii) Ion exchange with organic cations

(iv) Binding of inorganic and organic cations

(v) Grafting of organic compounds

(vi) Reaction with acids

(vii) Pillaring by different types of poly(hydroxo metal) cations

(viii) Interlamellar or interparticle and interparticle polymerisation

(ix) Dehydroxilation and calcination

(x) Delamination and reaggregation.

Ion exchange generally consists of the stoichiometrical and reversible replacement or swapping of ions between two electrolytes in different media (Grim, 1968; Harland, 1994). Many authors (Walker, 1959; Grim, 1968; Harland, 1994; Tan, 1996) also describe ion exchange, in clay minerals, as a diffusion process of substitution of the ions held electrostatically on the surface of the ion exchanger (condensed phase) and a solution phase.

According to Grim (1968) and Harland (1994), the ion exchange of phyllosilicates is frequently accompanied by a change in the d-spacing and is basically made to occur by:

- *Replacement in the interlayer space:* The exchangeable cations are mostly located on cleavage surfaces and in vermiculite this region contributes approximately 80% of the total CEC. This charge results from isomorphous substitutions within the lattice structure.

- *Replacement on the edges of the platelets owing to the breaking of chemical bonds:* The availability of these exchange sites is seriously affected by the particle size, lattice distortions and crystallinity. Broken bands are responsible for up to 20% of total CEC in vermiculite.
- *Exchange of hydrogens of exposed hydroxyl groups:* Obviously, the availability of these sites during the exchange reaction is highly influenced by the pH of the medium and is of particular significance for layered minerals such as vermiculite.

The ion exchange phenomenon is quantitatively measured by the CEC, which is defined as the average of the quantity of cations available to be exchanged at a certain pH. Due to the neutral character of the clay, the CEC is also related to the clay surface charge and is traditionally expressed in (mEq)/100 g of calcinated clay, which is equivalent to cmol(+)/kg, units recommended by IUPAC (Sinha Ray and Okamoto, 2003; Bergaya *et al.*, 2006).

Table 2. CEC of some clay minerals (Bergaya *et al.*, 2006)

Clay	CEC (mEq/100 g)
Vermiculite	130–210
Montmorillonite	70–20
Illite	10–40
Kaolinite	3–15

The CEC values of selected clay minerals are presented in Table 2. It appears that the broad intervals given are due to diverse factors that may influence the clay properties. The main aspects that affect CEC measurements are: pH, temperature, ionic strength, nature of the index cation, nature of the interlayer cation(s), particle morphology and size, and surface area (Raman and Jackson, 1963; Grim, 1968; Stone and Wild, 1978; Harland, 1994; Bergaya *et al.*, 2006; Peralta, 2009).

Due to its wide use in the literature, in this work the term "ion exchange" is used to designate the exchange of interlayer inorganic ions adsorbed on vermiculite (Ca^{2+} and Mg^{2+}) by other inorganic cations. Some of their relevant properties are summarised in Table 3.

The "ionic potential" is defined as the ratio of the ion's electrical charge to its radius. It is a measure of density of charge and gives an idea of the strength of the ionic bond that can be formed by the cation, as well as the extent of hydration. Many authors (Wild and Keay, 1964; Gier and Johns, 2000; Badreddine *et al.*, 2002b; Ferrage *et al.*, 2005; Vidal and Dubacq, 2009) have observed, in their work with clay minerals, that cations with high ionic potential possess high selectivity coefficients. As a result, they are able to create a richer interlayer hydration and consequent better enlargement of the interlayer space.

Table 3. Dehydrated and hydrated ionic radii and respective calculated ionic potentials (Grim, 1968).

Ion	Dehydrated ionic radius (nm)	Hydrated ionic radius (nm)	Ionic potential [z/r] (-)
NH4+	0.143	0.537	7.0
K+	0.133	0.380	7.5
Na+	0.098	0.560	10.2
Mg^{2+}	0.078	1.080	25.6
Ca^{2+}	0.106	0.960	18.9
Ba^{2+}	0.143	0.880	14.0

The work done by Thomas Jr. and Bohor (1969) in their study of the surface area of ion-exchanged vermiculite gave further insight. They stated that "Mg-vermiculite would retain coordinated water more tenaciously at comparable elevated temperatures than would the other vermiculites studied". According to them, this is due to three combined effects: (1) high ionic potential; (2) a stronger polarising effect;

and (3) high covalent character. These results were later confirmed and augmented by Couderc and Douillet (1973), Stone and Wild (1978) and Justo *et al.* (1989).

2.2.5 Thermodynamics of ion exchange in vermiculite

The ion exchange reaction in vermiculite can be systematically represented by Scheme IV (Barrer and Klinowski, 1977; Inoue, 1984; Harland, 1994).

$$Z_A B_V^{Z_B}[\text{Vermiculite}] + Z_B A_s^{Z_A}[\text{Solution}] \rightleftharpoons Z_B A_V^{Z_A}[\text{Vermiculite}] + Z_A B_s^{Z_B}[\text{Solution}]$$

Scheme IV: Ion exchange reaction involving vermiculite and another electrolyte

By applying the mass action law to the exchange reaction (Scheme IV) between the vermiculite interlayer cations $B_V^{Z_B}$ and a solution containing $A_s^{Z_A}$ cations, the equilibrium constant (K) can be determined by Scheme V (Barrer and Klinowski, 1977; Inoue, 1984):

$$K = \frac{A_V^{Z_B}\left(m_S^B\right)^{Z_A} f_A^{Z_B} \gamma_B^{Z_A}}{B_V^{Z_A}\left(m_S^A\right)^{Z_B} f_B^{Z_A} \gamma_A^{Z_B}}$$

Scheme V: Ion exchange equilibrium constant in vermiculite

where A_V and B_V, and Z_A and Z_B are the equivalent fractions and respective charges of ions A and B in vermiculite; m_S^B and m_S^A represent the molalities in the solution; and f_A, f_B, γ_A and γ_B are the activity coefficients in vermiculite and in solution, respectively.

The standard free energy change (ΔG°) for the reaction demonstrated by Scheme VI can be determined by the expression:

$$\Delta G^\circ = -\frac{RT}{Z_A Z_B} \ln K$$

Scheme VI: ΔG° of the ion exchange reaction on vermiculite

where R is the universal gas constant and T is the absolute temperature.

On the other hand, the standard enthalpy change (ΔH°) can be estimated by the Van't Hoff equation (Scheme VII):

$$\Delta H^{\circ} = -\frac{R}{Z_A Z_B} \cdot \frac{\partial(\ln K)}{\partial(1/T)}$$

Scheme VII: Van't Hoff equation for the determination of ΔH°

and the standard entropy change (ΔS°) can be calculated from the following relationship (Scheme VIII):

$$\Delta S^{\circ} = \frac{1}{T}(\Delta H^{\circ} - \quad \Delta G^{\circ})$$

Scheme VIII: ΔS° that accompanies the ion exchange on vermiculite

The standard free energies (ΔG°) determined by Wild and Keay (1964) and (Inoue, 1984) indicate the following affinity of alkali and alkaline metal ions to vermiculite: $Na^{+} < Ba^{2+} \sim Ca^{2+} < Mg^{2+} < K^{+}$.

According to Wild and Keay (1964) and Inoue (1984), vermiculite selectivity, in the above series, is determined mostly by the entropy increase rather than the enthalpy change since both enthalpy and entropy are positive during ion exchange. For instance, Wild and Keay (1964) found that vermiculite's preference for divalent cations is due mainly to an increase in the (configurational) entropy during the replacement of monovalent cations by corresponding half-divalent cations.

2.2.6 Exfoliation of vermiculite

Commercial vermiculite features the desirable property that it expands by more than eight times in volume when heated rapidly to elevated temperatures (Walker, 1961; Wada, 1973a;b; Justo *et al.*, 1989; Friedman *et al.*, 1994; Tomanec *et al.*, 1997; Hindman, 2006).

During exfoliation it is desirable to preserve the relevant properties for vermiculite applications. Besides its light weight, sound absorption, heat insulation and attractive appearance, properties such its ion exchangeability, humidity control,

high water-holding capacity and elimination of odours are advantageous and should be conserved.

Exfoliation of vermiculite can be achieved by means of various processes. The conventional processes for the manufacture of exfoliated vermiculite is the thermal exfoliation which employs temperatures exceeding 800 °C. This occurs as a sheet exfoliation process (i.e. normal to the basal cleavage), which is driven by an explosive release of interlayer water as steam (Baumeister and Hahn, 1976; Justo *et al.*, 1989; Obut and Girgin, 2002; Pérez-Maqueda *et al.*, 2003; Bergaya *et al.*, 2006). The interlayer water is said to escape easily and explosively between the layers (pushing them apart), favouring the degree of exfoliation when the particle size is relatively small (Bergaya *et al.*, 2006).

For the application of vermiculite in intumescent fire barriers, exfoliation of vermiculite has been made to occur at relatively lower temperatures than the usual by impregnating it with urea, thiourea or a mixture of them. The resulting composition is heated at temperatures (160–300 °C) not lower than the decomposition point of the urea or thiourea compound (Wada, 1973a;b).

Langer and Marlor (1981) also describe the exfoliation of vermiculite via the addition of inorganic ammonium salts, such as ammonium dihydrogen phosphate, ammonium hydroxide and ammonium carbonate, as well as urea. When this inorganically treated vermiculite is heated to 400 °C, it expands by more than 200%.

Exfoliation of vermiculite also occurs by sudden decomposition on heating to 100 °C after pre-treatment and the penetration of large quantities of H_2O_2 into the interlayer space at 4 °C (Baumeister and Hahn, 1976).

Early research also focused on vermiculite expansion through irradiation of electromagnetic waves in a specific range of frequencies. This process was carried out for ore vermiculite and previously intercalated vermiculite (Wada, 1973a).

2.2.7 Interstratification in vermiculite

Interstratified minerals are compositions in which individual crystals are made up of elementary layers of two or more different types (MacEwan *et al.*, 1961; Moore and Reynolds, 1989; Bergaya *et al.*, 2006). These minerals are structurally and chemically more complex than minerals with a one-unit structure (Newman, 1987).

Newman (1987) and (Bergaya *et al.*, 2006) classify interstratified minerals according to the stacking order or periodicity along the *c* direction as:

- Ordered or regular mixed-layer structures – if the layers arrange in an alternate order, like ...ABABAB...; ...AABAABAAB...; ...AAABAAAB...; etc.
- Disordered or irregular mixed-layer structures – when the stacking order is random, like ...ABAABA...; ...ABBAABAB...; ...AABABBABBBBA...; etc.

The literature reveals two types of interstratification in clay minerals. One form is due to the types of mineral forming the mixed layers (e.g. vermiculite/mica, vermiculite/chlorite, mica/montmorillonite) and the other is due to the difference in terms of the water layer hydration states (WLHS) of the interlayer cations (e.g. 1-WLHS mixed with 2-WLHS). Apparently, mixed mineral layers occur naturally, while the WLHS interstratifications are usually observed during the dehydration and/or rehydration of clays (Gruner, 1934; Brindley *et al.*, 1983; Reichenbach and Beyer, 1997; Frank and Edmond, 2001; Marcos *et al.*, 2009).

Justo *et al.* (1993) and Marcos *et al.* (2009) have shown that vermiculite-mica interstratification materials have the highest expansion and the thermal effects occur at lower temperatures compared with pure vermiculite.

a) Mineral interstratifications in vermiculite

Hydrobiotite is a regular 1:1 interstratification of vermiculite and biotite layers (Brindley *et al.*, 1983; Newman, 1987). By the same token, hydrophlogopite is described as a regularly interstratified 1:1 mix of phlogopite/vermiculite. It has basal reflections with d = 2.43 nm, 1.223 nm, 0.827 nm, 0.490 nm and 0.349 nm (Gruner, 1934;

Palabora Mining Company Limited, 1976; Brindley *et al.*, 1983; Frank and Edmond, 2001).

However, the name "hydrobiotite" is not internationally recognised as a valid mineral name, although it has long been used in the literature and is associated with interstratified biotite/vermiculite minerals found in commercial vermiculite deposits (Boss, 1967; van der Marel and Beutelspacher, 1976; Brindley *et al.*, 1983; Hudson *et al.*, 1999; Zhu *et al.*, 2008).

Mixed-layer clay minerals with any appreciable degree of randomness show a seemingly irrational series of reflections that make their identification and interpretation quite a complex exercise. However, computer programs are available for predicting the diffraction patterns of one-dimensional mixed-layer clays (Reynolds Jr., 1985).

The presence of mixed-layer vermiculite-mica in ore vermiculite makes it more valuable, taking into account the following facts:

- The interlayer spacing of hydrobiotite (2.5 nm), for instance, is largely higher than that of pure vermiculite (1.5 nm) and/or biotite (1.0 nm). In fact, this first-order reflection is close to the algebraic sum of the component interlayer spacing of the unit minerals (Newman, 1987; Ruiz Amil *et al.*, 1992).
- Two chemically different exchange sites are available owing to the existence of two different structural unities (Na-vermiculite and K-vermiculite) in bi-ionic Na- and K-vermiculites while in equilibrium with aqueous solutions of NaCl and KCl. X-ray diffraction (XRD) results showed the interlayer spaces of K-vermiculite (1.08 nm), Na-vermiculite (1.41 nm) and the ordered interstratified Na/K-vermiculite (2.50 nm).
- The interlayer space created after intercalation of interstratified vermiculite by organic surfactants is also much higher than that from pure vermiculite and biotite, as well as their exfoliated forms (Ruiz Amil *et al.*, 1992; Justo *et al.*, 1993).

- Furthermore, this interstratified vermiculite is amenable to producing a durable exfoliated material (Frank and Edmond, 2001).

b) Water layer hydration states (WLHS) and dehydration of vermiculites

Water bound to the interlayer cations in vermiculite is arranged in a series of layers, i.e. the water layer hydration states (WLHS). These WLHS define the basal reflection and are intrinsically related to the interlayer cation(s), relative humidity and temperature (Barshad, 1950; Fripiat *et al.*, 1960; Marcos *et al.*, 2003).

According to Barshad (1948) and Ferrage *et al.* (2005), at room temperature and relative humidity around 35%, cations such as Mg^{2+}, Ca^{2+} and H^{+} will exhibit 2-WLHS; Ba^{2+}, Li^{+} and Na^{+} only 1-WLHS, and NH_4^{+}, K^{+}, Rb^{+} and Cs^{+} 0-WLHS. In the case of the latter cations, exhibiting 0-WLHS, their relatively smaller d-spacing is caused by the size and the position (in the cavities) of the dehydrated interlayer cation.

In natural biotite (vermiculite parent mica) the interlayer ions are potassium and the interlayer space contains no water (0-WLHS). By contrast, pure vermiculite (Mg-vermiculite) contains the equivalent of up to two sheets of interlayer water (2-WLHS) (Barshad, 1950; Harben and Bates, 1990; Bergaya *et al.*, 2006).

During dehydration, initially there is a release of water from external surfaces and mesopores (unbound water), then the water of hydration (bound with the interlayer cation) and finally the water derived from dehydroxylation (combination of surface clay hydroxyl groups) (Bergaya *et al.*, 2006).

The dehydration and/or rehydration of vermiculite is, to a certain extent, a reversible process (Grim, 1968; Newman, 1987). It progresses stepwise during the elimination and/or accumulation of one or several water layer structures, with some overlap, accompanied by a change in the d-spacing (Fripiat *et al.*, 1960; Kresten and Berggren, 1978; Bergaya *et al.*, 2006).

Reichenbach and Beyer also conducted several experiments with alkaline earth-exchanged vermiculites and published an interesting series on dehydration and rehydration of vermiculites (Reichenbach and Beyer, 1994;1995;1997; Beyer and

Reichenbach, 1998). They applied thermo-analysis and in situ XRD to study the relationship between temperature and the WLHS of homionic vermiculites. Some of their results are presented in Table 4.

Furthermore, Reichenbach and Beyer (1994) also concluded that Mg-vermiculites are more thermally stable due to the well-defined WLHS (2-WLHS, 1-WLHS and 0-WLHS) compared with other ion-exchanged vermiculites studied. Several WLHS were also found by Marcos *et al.* (2003) in their work with natural commercial vermiculites (including Palabora vermiculite), supplementing preceding findings.

In previous work a vacuum was also applied to study the dehydration and rehydration of vermiculite (Okhotnikov *et al.*, 1989; Marcos *et al.*, 2003). The results showed that during thermal dehydration of vermiculite there is no destruction of the crystals: water molecules are released by interlayer diffusion and escape through the cracks (Walker, 1959; Wild and Keay, 1964; Okhotnikov *et al.*, 1989).

Marcos *et al.* (2003) found that exposing vermiculite to a vacuum causes rapid dehydration and that below 120 °C the vacuum dehydration is arrested at 1-WLHS. They also observed that exfoliation under vacuum conditions is not dependent on the presence of water above 120 °C.

Table 4. Vermiculite WLHS properties (Grim, 1968; Hougardy et al., 1970; Reichenbach and Beyer, 1997)

Interlayer cation	WLHS	Thickness of water layer (nm)	d-spacing (nm)	Water content (mol/ion)
Mg^{2+}	2	0.51	1.38–1.44	4.00–4.71
	1	N/A	1.15–1.16	1.57–1.88
	0	N/A	0.93–1.00	0.00–0.51
Ca^{2+}	2	0.58	1.47–1.59	4.59–5.39
	1	N/A	1.18–1.19	1.23–1.83
	0	N/A	095–0.98	0.00–0.21
Ba^{2+}	1	0.34	1.24	2.36–2.53
	0	N/A	0.99–1.00	0.00–0.50
Na^{+}	2	N/A	1.48	5.6–6.0
	1	0.56	1.18	2.0
	0	N/A	N/A	N/A
NH_4^{+}	0	~ 0.15	1.08 (diffuse)	N/A
K^{+}	0	~ 0.13	1.06 (diffuse)	N/A

[1] N/A = data not available

2.2.8 Potential applications of vermiculite

Neat vermiculite has been used effectively as an absorbent in water purification due to its capacity to exchange its interlayer cations with some toxic ions such as Sr, Pb, Zn and Cd (Schoeman, 1989; Das and Bandyopadhyay, 1991; Konta, 1995; Mekhamer and Assaad, 1999). It is effective as an adsorbent for the removal of natural and artificial organic matter, as well as for the controlled release of fertilisers and pesticides (Bailey and White, 1964; Schoeman, 1989; Abate *et al.*, 2006).

NH_4-vermiculite has been used to prepare intumescent gaskets for the automotive industry. Some patents claim that appropriately intercalated vermiculites show lowered expansion onset temperatures (Langer and Marlor, 1981). Acid-

activated vermiculite is used as a catalyst, especially during the cracking of heavy fuels to the highest gasoline portion in the petroleum industry (Suquet *et al.*, 1994).

Organo-vermiculite has been used in the removal of herbicides from water and in herbicide formulations for the controlled release of active components in soils (Plachá *et al.*, 2008; Holešová *et al.*, 2010; Yu *et al.*, 2010). Organo-vermiculite polymer nanocomposites with improved mechanical properties, as well as good flame-retardant and intumescent properties, are also reported in the literature (Connell *et al.*, 1994; Connell *et al.*, 2000; Liu *et al.*, 2005; Gomes *et al.*, 2009; Qiu *et al.*, 2011).

Most vermiculite is consumed in its thermally exfoliated form. This lightweight (low bulk density) vermiculite finds use in a variety of areas, according to the particle size and mechanical disintegration (Konta, 1995; Hindman, 2006). Expanded vermiculite is of industrial interest because it is chemically inert, incombustible and shows excellent absorption and thermal insulation properties (Wada, 1973b; Schoeman, 1989; Tomanec *et al.*, 1997; Obut and Girgin, 2002; Bergaya *et al.*, 2006). It is used as aggregate in concretes and plasterboards (Wada, 1973b; Konta, 1995; da Silva Jr *et al.*, 2003; Hindman, 2006).

Expanded vermiculite is used in commercial and residential construction for fire protection to prevent warping, bending or collapse of the reinforced-concrete or steel-beam framework. Due to its inertness with respect to heat and fire, expanded vermiculite is also used as a high-temperature insulator, as well as for ambient-temperature refrigeration and sound dissipation (Schoeman, 1989; Evans, 1993; Association, 2000; Bergaya *et al.*, 2006). It is also used as thermal protection and shock-proof filling material for glass containers and vessels in the packaging industry (Konta, 1995; Bergaya *et al.*, 2006).

Since expanded vermiculite is able to retain liquids and gases better than natural soils, it is used in agriculture and animal feeds as a growth medium and as a filler and carrier for powdered fertilisers and animal nutrients (Schoeman, 1989; Evans, 1993; Konta, 1995; Association, 2000; Hindman, 2006). Expanded vermiculite, with its layered structure and surface characteristics, is used in the friction brake linings

market (as a replacement for asbestos) for high-temperature insulation, for loft/ceiling insulation, and in intumescent coatings and gaskets (Konta, 1995).

A mixture of exfoliated vermiculite, modified bentonite and peat is currently applied as a deodorising agent in the protection of the environment. Exfoliated vermiculite is also recommended as a bio-remediate aid to clean contaminated soils and sites, as an absorbent or filter in water purification and beverages, for the controlled release of fertilisers and pesticides, as well as for the treatment of nuclear and other toxic waste (Schoeman, 1989; Konta, 1995; Association, 2000; Hindman, 2006).

2.2.9 Commercial value of vermiculite

Basically, a vermiculite ore contains vermiculite (proper), interstratified vermiculite/mica and unaltered mica. The distribution and efficient recovery of relatively large particles determine its value and the concentrated ore is marketed with a specific particle size distribution (Hindman, 2006). South Africa's exports to the US have been reducing gradually. They amounted to about 99% from 1992 to 1995, 59% from 2005 to 2008, but during the period 2010 to 2013 accounted for only 44% (Survey, 1996;2009;2010;2015).

The decrease in exports is due to the emergence of new suppliers such as Australia, Brazil, China and Zimbabwe. Even with the emergence of these new sources, the price of vermiculite has been relatively stable, from US$100–400 in 2010 to US$150–580 in 2014 per ton. During the last decade the production has also remained relatively stable (Survey, 2010;2015).

2.3 VERMICULITE/POLYMER COMPOSITES

Polymer composites are extensively used in various areas due to their relatively low cost and the broad range of properties that can be attained (Giannelis, 1996).

The outstanding performance of polymer layered silicate nanocomposites (PLSNs) is intrinsically related to the clay's high aspect ratio. The clay's delamination, homogeneous dispersion and compatibility with the polymer matrix are the main challenges faced while preparing PLSNs. Fully exfoliated composites have been claimed, but some studies have shown that delamination and dispersion of individual clay layers is still a challenge (Giannelis, 1996; Alexandre and Dubois, 2000; Fischer, 2003; Sinha Ray and Okamoto, 2003; Pavlidou and Papaspyrides, 2008).

According to Tjong (2006), the properties of nanocomposites depend greatly on the chemistry of the polymer matrices, the nature of the nanofillers, and the way in which they are prepared.

Most of the vermiculite-polymer composites were prepared using heat-expanded vermiculite as raw materials in highly polar matrices. Vermiculite-polymer nanocomposites with improved mechanical properties, as well as good flame-retardant and intumescent properties, are discussed in the literature, although less frequently than other clay minerals (montmorillonite, hectorite and saponite) which are relatively less abundant and much more expensive (Sinha Ray and Okamoto, 2003; Tjong and Meng, 2003; Liu *et al.*, 2005; Gomes *et al.*, 2009; Qiu *et al.*, 2011).

On the other hand, vermiculite-polyethylene (PE) or -polypropylene (PP) nanocomposites are also much less studied due to the non-polar chemical structure of the olefin chain.

Flame-barrier compositions have been proposed that rely on vermiculite's expansion properties (Wada, 1973a). It is believed that vermiculite could impart fire resistance to polymers, provided the exfoliation temperature can take place at temperatures just below the volatilisation of the polymer. Some patents claim that

appropriately intercalated vermiculites show lowered expansion onset temperatures (Langer and Marlor, 1981).

The improvement in flame retardancy by organo-clays does not occur by a process in the vapour phase but rather by a modification of the combustion process in the condensed phase, i.e. the formation of an insulator and mass transport barrier char layer obtained through the collapse of the exfoliated and/or intercalated structures (Alexandre and Dubois, 2000).

The development of halogen-free and environmentally friendly flame-retardant polymeric material, especially for the construction, mining and shipbuilding industries, has become an important trend (Rosa *et al.*, 2008).

2.4 FLAME RETARDANCY

Polymer combustion is an exothermic reaction driven by thermally induced decomposition (pyrolysis) of solid material into smaller fragments, which then volatilise, mix with oxygen and combust. If enough energy is released, which reradiates onto the unburned polymer, the combustion is sustainable until a lack of heat/fuel/oxygen causes the fire to extinguish (Dufton, 1995; Laoutid *et al.*, 2009; Morgan and Gilman, 2013).

The thermal degradation of polymers depends on the C-H bond energy. It can be by either non-oxidising or oxidising thermal degradation mechanisms. During the decomposition of the molten polymer, there is chain scission which can occur in two ways, namely by (Laoutid *et al.*, 2009):

⇒ formation of free radicals, or

⇒ migration of hydrogen atoms and the formation of stable molecules, one of which has a reactive carbon-carbon double bond.

The burning behaviour of each material is characterised by ease of ignition, contribution to flame spread, smoke density and toxicity, and corrosiveness of the combustion products, among other factors.

The development of a fire consists of three basic stages (Fig. 2): (a) ignition and early development; (b) total involvement or full development; and (c) extinguishment (Crompton, 2006). Fig. 2 also shows the difference in burning behaviour of thermally thin and thick materials (Schartel and Hull, 2007).

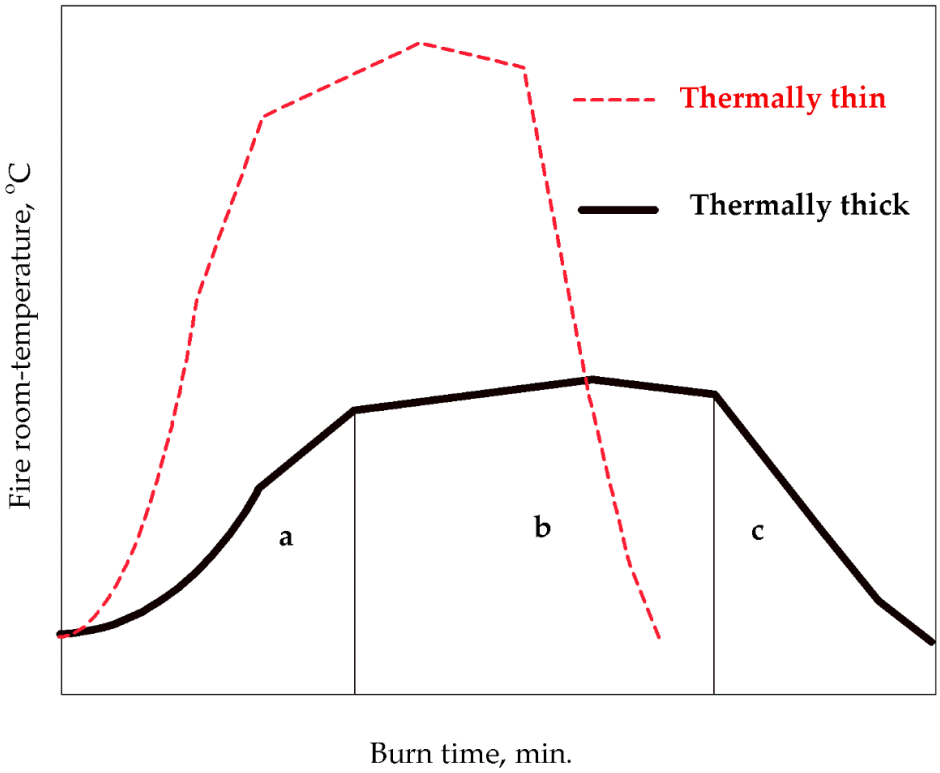

Figure 2. Temperature–time fire profile of thermally thin and thick materials. (a) ignition and propagation; (b) full development; and (c) extinguishment

Current methods for the protection of materials from fire risk are based on engineering approaches, the use of inherently low flammable polymers and FR additive materials (Morgan and Gilman, 2013).

A FR is an additive or reactive material which delays ignition or reduces flame spread of the resulting material when exposed to flame impingement (Weil and Levchik, 2009).

According to Dufton (1995), an effective FR material has to be able to impede or reduce heat supply to below the critical levels required for flame stability. This prerequisite can be accomplished by:

(i) limiting the heat and mass transfer between the solid and gas phases

(ii) scavenging of the free radicals in the gas phase

(iii) creating a heat sink.

Existing FR materials in polymers are generally based on (Laoutid *et al.*, 2009):

⇒ halogenated additives and antimony trioxide (as synergist)

⇒ inorganic fillers

⇒ melamine derivatives

⇒ phosphate-based materials.

To be effective, a FR material has to supply the flame inhibitor (for fuel starvation) in the same temperature range as the decomposing polymer (Dufton, 1995). This criterion complies with the "right place at the right time" theory. FR materials play an important role in reducing the incidence and severity of a fire, despite not giving absolute protection against it (Weil and Levchik, 2009).

The categorisation of FR materials is somewhat inconsistent. This dilemma is related to the multiplicity of polymer processing techniques and, on the other hand, to the fact that the very same FR material can exhibit different FR mechanisms. Nevertheless, all types of FR materials can be classified according to the mode of action or the means of incorporation into the polymer matrix.

2.4.1 Classification of FR materials by mode of action

a) Physical action

FR materials based on physical action act basically on the condensed phase by reacting and forming a carbonaceous layer on the material's surface. This residual protective layer should obstruct the heat and mass transfer between the pyrolysis zone (vapour phase) and the molten polymer (condensed phase). On the other hand, the volatile decomposition products (such as H_2O, CO_2, NH_3, etc.) can, also, dilute the flammable vapours mixture. Phosphorous and nitrogen compounds are the most-used char-forming flame retardants (Laoutid *et al.*, 2009; Kind and Hull, 2012; Morgan and Gilman, 2013; Wang, 2013; Company, 2014).

To this class we can also consider adding the endothermic FR materials which use the "quench and cool mechanism". These additives, also known as "heat sinks", degrade endothermically (and cool the condensed phase) while releasing non-flammable molecules (e.g. H_2O and CO_2) that can dilute the vapour phase and induce a decrease in the temperature. For the quenching and cooling mechanism, inorganic compounds (or hydrated minerals) are the commonly used FR materials (Dufton, 1995; Wang, 2013; Company, 2014).

b) Chemical action

Chemical FRs modify the fire process in either the vapour or condensed phase. In the vapour phase they act by scavenging the free radicals, by successful competition with oxygen, thus terminating the propagation of the reaction. Chemical action can also take place by promoting the successive conversion of the polymer to compounds with high molecular weight, high thermal stability and barrier properties. Such reactions can include dehydrogenation (leading to unsaturation), cross-linking and cyclisation. Chlorine-, bromine- and phosphorous-based FR systems are the main representatives of this class (Dufton, 1995; Morgan and Gilman, 2013; Wang, 2013; Company, 2014).

2.4.2 Classification of FR by means of incorporation

According to the means of incorporation, FRs are classified as:

⇒ *Additive* – usually added after being made compatible with the polymer matrix and can have physical or chemical action.

⇒ *Reactive* – covalently bound to the polymer chain. They are part of the modified polymer and may be added during polymerisation or later grafted as side-chain.

⇒ *Coatings* – also known as intumescent coatings, provide an insulating barrier for mass and heat transfer by swelling or foaming on heating.

2.4.3 Halogen-based FRs

Halogenated chemical FR materials eliminate halogen acids on heating. They act essentially in the vapour phase as flame poison. Halogen radicals, while in the vapour phase, react with free radical species, stopping the chain reactions and therefore the combustion of the molten polymer. Their potential flame-inhibition activities decrease in the series: I > Br > Cl > F. Chlorinated and brominated FR materials are the most used in polymer composites and the latter is the most effective radical scavenger. Tetrabromobisphenol A (TBBPA) and polybromodiphenylether (PBDE) have been widely used but are being phased out due to environmental concerns, while hexabromocyclododecane (HBCD) and tetrabromophtalic anhydride (TBPA) are still commonly used as FR materials (Camino and Costa, 1988; Dufton, 1995; Laoutid *et al.*, 2009; Morgan and Gilman, 2013).

In synergistic systems, halogenated flame retardants may also act in the condensed phase by reacting with the polymer and modifying its degradation mechanism. To increase the polymer's time to ignition and flashover, halogenated FRs are typically used in synergism with antimony trioxide. Although economically and technically very effective, halogen-based flame retardants also produce obscuring, toxic and corrosive smoke, and are a source of various environmental concerns (Camino and Costa, 1988; Dufton, 1995; Morgan and Gilman, 2013; Kiliaris and Papaspyrides, 2010). The performance of the halogenated FR materials (with a few exceptions due to their diversity) is summarised in Table 5.

Table 5. Pros and cons of halogenated FR materials

Advantages	Disadvantages
⇒ Effective at low dosage ⇒ Little negative effect on the physical properties ⇒ Easy incorporation and processing ⇒ Low-cost materials	⇒ Require synergist ⇒ Toxic and corrosive even during handling and processing ⇒ Obscuring, corrosive and toxic degradation products

2.4.4 Phosphorous-based FR materials

FR materials containing phosphorous (oxidation states: 0, +3 and +5) within their inorganic or organic structure, including phosphates, phosphonates, phospinates, phosphine oxides, phosphates, red phosphorous, etc., are widely used in polymer composites. Some phosphorous compounds can be either vapour phase and/or condensed phase FR, depending on their chemical structure and their interaction with the molten polymer matrix. In the condensed phase they basically catalyse char formation by inhibiting carbon oxidation, i.e. phosphorous participates in the reaction by promoting char formation but is not consumed. Volatile species produced during combustion, such as P_2, PO, PO_2, HPO_2, etc., are responsible for reduction of the flammability in the vapour phase (Dufton, 1995; Levchik and Weil, 2006; Bourbigot and Duquesne, 2007; Laoutid *et al.*, 2009; Morgan and Gilman, 2013).

Phosphorous can also be incorporated into the polymeric material via copolymerisation, as a reactive FR. This procedure is relatively expensive and limiting (in terms of applications) but requires low loading of phosphorous to achieve acceptable flame retardancy (Levchik *et al.*, 1998; Bourbigot and Duquesne, 2007; Laoutid *et al.*, 2009). During degradation, phosphorous-containing FRs have a tendency to react with polar groups (e.g. OH) of the polymer's backbone, producing

thermally stable cross-linked or carbonised structures (Levchik *et al.*, 1998; Laoutid *et al.*, 2009). The main advantages and disadvantages are summarised in Table 6.

Table 6. Pros and cons of phosphorous-based FR materials

Advantages	Disadvantages
⇒ Effective at low dosage (organics) ⇒ Little negative effect on the physical properties ⇒ Easy incorporation and processing ⇒ Low-cost materials ⇒ UV stable (organics)	⇒ Labile and hygroscopic (inorganics) ⇒ Health issues during processing ⇒ Toxic degradation products

2.4.5 Nitrogen-based FR materials

Nitrogen-based FR materials are an old class of FR. The most important organic nitrogen-based FR is melamine (and its derivatives) and ammonium polyphosphate is the most important inorganic additive (Horacek and Grabner, 1996).

Nitrogen-based FR materials are environmentally friendly. Their main applications are melamine for polyurethane flexible foams, melamine cyanurate in nylons, melamine phosphates in polyolefines, melamine and melamine phosphates or dicyandiamide in intumescent paints, guanidine phosphates for textiles and guanidine sulphamate for wallpapers (Horacek and Grabner, 1996). A brief comparative performance of nitrogen-based FRs is given in Table 7.

Table 7. Pros and cons of nitrogen-based FR materials

Advantages	Disadvantages
⇒ Solids – easy incorporation and processing ⇒ Little negative effect on the physical properties ⇒ Low toxicity and smoke evolution ⇒ Environmentally friendly ⇒ Recyclability (high decomposition temperatures) ⇒ Disposable (long-term fertilisers) ⇒ Moderate price	⇒ Corrosive and toxic degradation products (less than halogen-based). but good performance in intumescent systems ⇒ In some cases require synergist (by incorporation of phosphorous)

2.4.6 Nanoparticles

More recent work on the FR of polymeric materials reports the use of nanosized particles. Montmorillonite (MMT) clay, carbon nanotubes (CNT), polyhedral silsesquioxanes (POSS) and graphene are some of the most studied nanosized FR additives.

Well-dispersed nanoparticles are known to enhance the thermal stability and hence the fire resistance of polymeric materials. Thanks to their high aspect ratio, polymer nanocomposites can be prepared with considerably lower filler loading. Actually, the exfoliated and/or intercalated nanoparticles increase the melt viscosity and form a layer that provides a barrier against mass and heat transfer between the polymer melt and the vapour phase. However, some studies have shown that nanoparticles have to be used in combination with other flame-retardant additives in order to meet some required fire performance levels (Laoutid *et al.*, 2009; Tabuani *et al.*, 2012).

The basic distinction of nanoparticles takes into account the presence of nanometric dimensions in a 3D system. Actually, their designation is related to the number of non-nanometric dimensions in a particle. According to Laoutid *et al.* (2009), they can be classified as:

⇒ *Layered nanomaterials or 2D nanoparticles* – with one nanometric dimension and include nanoclays (e.g. MMT, vermiculite) and graphene.

⇒ *Fibrous nanomaterials or 1D nanoparticles* – typically elongated structures with two dimensions at nanoscale. Carbon nanotubes (single-walled, SWNT and multi-walled, MWNT) are the main representative of this group which also includes some clays such as sepiolite.

⇒ *Particulate nanomaterials or 0D nanoparticles* – are basically spherical nanoparticles which are characterised by all three nanosized dimensions. Functionalised POSS and spherical silica are the main representatives of this class (Lichtenhan *et al.*, 1995; Choi *et al.*, 2004).

The good performance of nanosized FR materials is attributed to the good dispersion of the nanoparticles, which leads to the formation of more compact and cohesive char (Laoutid *et al.*, 2009). Dittrich *et al.* (2013) have shown that the FR performance of layered nanoparticles (2D) is superior to that of nanotubes (1D) and spherical nanoparticles (0D).

2.4.7 Intumescent FR materials

Intumescent systems are, basically, physical and additive FRs. They provide radiation shielding and thermal insulation by forming a heat-induced swollen multi-layer barrier (Dufton, 1995; Laoutid *et al.*, 2009; Kind and Hull, 2012).

In general, the formulation of an efficient intumescent system requires three components (Camino and Costa, 1988; Dufton, 1995):

⇒ an acid source (dehydrating agent, e.g. ammonium polyphosphate)

⇒ a carbonising agent (carbonific or char former, e.g. dipentaerythritol)

⇒ a nitrogen blowing agent (spumific, e.g. melamine).

In an intumescent system, it is critical that the gas is released by the blowing agent during the thermal decomposition of the carbonising agent in order to trigger the expansion of the carbonised layers (Laoutid *et al.*, 2009).

2.4.8 Mineral fillers

Natural or synthetic mineral fillers are used as additive FRs with, basically, physical action. Their properties are summarised in Table 8.

During the combustion they influence the thermal degradation and fire performance of the molten polymer by (Laoutid et al., 2009)

⇒ reduction of the combustible content

⇒ modification of the thermal conductivity of the material

⇒ change of the viscosity of the composite material.

Mineral fillers are a fairly cheap, very old and proven technology and are supposed to be environmentally friendly (Morgan and Gilman, 2013). Under fire conditions, they can delay the time to ignition (t_{ign}), slow the initial heat release rate (HRR), lower the smoke production rate (SPR) and reduce overall toxic gas emissions.

In case of fire, mineral fillers replace the flammable polymer fuel with non-flammable inorganic molecules. However, in general, they have a limited fire performance window and cannot reduce the total heat release rate (tHR) if enough constant external heat is applied. On the other hand, for mineral fillers to be effective, high loadings are needed and such loading levels may impair the processability and the mechanical properties of the polymeric material (Hornsby, 1994; Wang *et al.*, 2001; Lv *et al.*, 2005; Berta *et al.*, 2006; Laoutid *et al.*, 2009; Morgan and Gilman, 2013).

Table 8. Properties of common inorganic fillers (Camino and Costa, 1988; Laoutid *et al.*, 2009; Krassowski *et al.*, 2012; Morgan and Gilman, 2013)

Filler	Onset Temp. (°C)	Chemical reaction	Enthalpy, ΔH (kJ kg^{-1})
Aluminium hydroxide (ATH) or bauxite	180–220	$2Al(OH)_3 \rightarrow Al_2O_3 + 3H_2O$	1 050-1 970
Hydromagnesite	220–240 320–350	$3Mg(CO_3)\cdot Mg(OH)_2\cdot 3H_2O \rightarrow Mg_4(CO_3)_3(OH)_2 + 3H_2O$ $Mg_4(CO_3)_3(OH)_2.3H_2O \rightarrow 4MgO + 3CO_2 + 4H_2O$	800
Magnesium hydroxide (MDH)	300–320	$Mg(OH)_2 \rightarrow MgO + H_2O$	1 030
Zinc borate	290–450	$4ZnO\cdot 6B_2O_3\cdot 7H_2O \rightarrow 4ZnO + 4B_2O_3 + 4H_3BO_3 + H_2O$	503
Expandable graphite	210–250		
Urea vermiculite	209 ± 35	*(Proposed in the present work)*	

According to Horrocks and Price (2001), char-forming agents seem to be the best choice and the way forward in developing effective fire-resistant composites.

2.5 ANALYTICAL AND CHARACTERISATION TECHNIQUES

2.5.1 Fourier transform–infrared spectroscopy (FT-IR)

FT-IR is a versatile and commonly used analytical technique. It essentially comprises an IR source, an interference modulator, a sample chamber and an IR detector. In an IR instrument the beam of light from the source is split into two parts, with one of them having a continuous varying phase difference. When the two beams are combined and the interference signal measured and recorded, the detected light provides the interferogram or spectrum of the sample under consideration (Crompton, 2006).

IR spectroscopy is a useful tool for the characterisation of vermiculite and its modified forms. In general, clays and clay minerals can be distinguished by the characteristic O-H, Si-O and Si-O-Si bands at 3800 to 3400 cm^{-1}. The band position and shape are intrinsic to the arrangement within the layers, especially the O-H bending and the Si-O stretching and bending vibrations around 1300–400 cm^{-1} (Farmer, 1971; Farmer, 1974; van der Marel and Beutelspacher, 1976; Raupach, 1988; Badreddine *et al.*, 2002a).

2.5.2 X-ray fluorescence (XRF)

The XRF technique is widely used in material sciences since it is fast, non-destructive and, usually, does not require laborious sample preparation.

Absorbed energy from a primary X-ray source (X-ray tube or radioactive source) can eject sample electrons from inner shells, creating vacancies. So, to re-establish the stable condition, the outer shell electrons have to move into the inner shells, producing characteristic XRF patterns (Fig. 3) (Jenkins, 1988; Wilson, 1994).

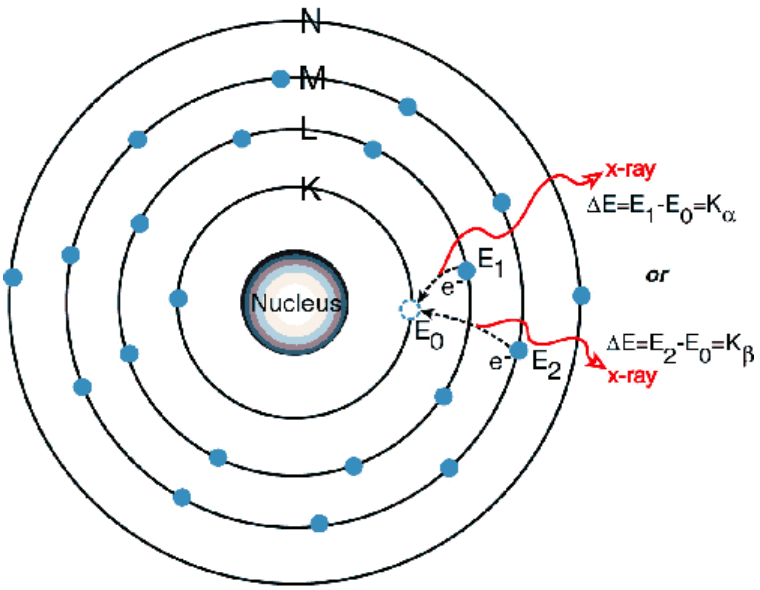

Figure 3. X-ray fluorescence after photoelectric effect with respective production of K_α and K_β X-rays

X-rays possess energy (E) that is a sinusoidal waveform with a typical wavelength (λ). These parameters and the frequency (ν), speed of light (c) and Planck's constant (h) are related by the equation represented by Scheme IX:

$$E = h\nu = \frac{hc}{\lambda}$$

Scheme IX: Planck's energy quantisation law

X-rays are labelled K, L, M or N, according to the destination shell. The suffixes alpha (α), beta (β) or gamma (γ) are added to distinguish X-rays originating from electrons from the different shell levels (Jenkins, 1988; Wilson, 1994).

2.5.3 Thermogravimetric analysis (TGA)

Thermogravimetry is an analytical technique that measures the mass change (loss or gain) of the analyte, due to decomposition, oxidation or dehydration, as a function of temperature, independent of the bonding mode. To determine the composition and/or the thermal stability, a sample can be heated, cooled, or even held at a constant temperature in an certain environment (Haines, 2002; Crompton, 2006).

The results are evaluated and interpreted by thermogravimetric analysis (TGA) and/or by evaluating the respective derivative against temperature (dm/dT), known as derivative thermogravimetry (DTG). DTG also shows the rate at which the mass changes (Brown, 2001; Haines, 2002; Bergaya *et al.*, 2006; Gabbott, 2008).

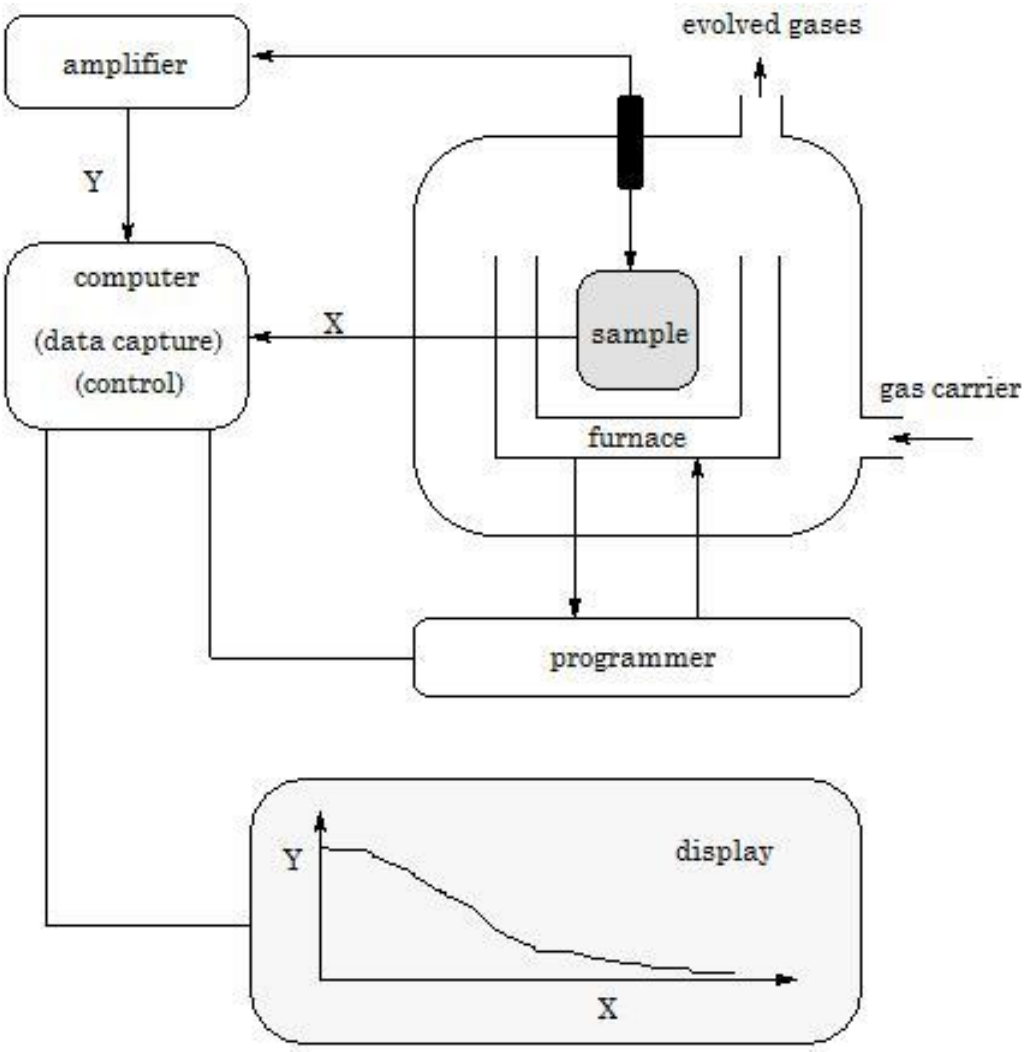

Figure 4. Schematic representation of a TGA set-up (adapted from Brown, 2001).

Modern thermal instruments (TGA, DTA, TMA, DSC, etc.) comprise basically of an electronic balance, furnace, atmosphere control, sample holder, thermocouples, temperature control and a data collection device (Brown, 2001; Haines, 2002; Bergaya *et al.*, 2006). A schematic representation of a TGA instrument is shown in Fig. 4.

2.5.4 *Thermomechanical analysis (TMA)*

TMA or static force-TMA (sf-TMA) is a technique that derives from thermomechanometry. It is a very important tool for studying materials that are to be subjected to a wide variation in temperature during their usage. An illustrative example is food packaging which has to undergo thermal processes such as heating, pasteurisation, freezing, etc. (Brown, 2001; Haines, 2002). In TMA the sample's dimension or length is measured as a function of temperature (heating, cooling or held at a constant temperature) while it is under constant mechanical stress. Usually, the results are evaluated by examining the changes in the thermal expansion coefficients with temperature and/or time (Haines, 2002; Crompton, 2006; Gabbott, 2008).

Modern TMA instruments are designed to measure: (i) penetration; (ii) extension; (iii) flexure; and (iv) torsion (Brown, 2001). For extension measurements, a flat-ended probe is inserted and rested on the top surface of the sample, and a static force is applied. A sensor then measures the movement of the probe (Haines, 2002).

2.5.5 *Differential scanning calorimetry (DSC)*

DSC is an analytical technique that is used to determine composition, chemical and thermal stability, as well as decomposition kinetics. It does not require sample preparation (just a few milligrams of a powder, pellet or fibre) and measures the amount of energy absorbed or released by an analyte during heating, cooling or even at a constant temperature. The heat flow, associated with transitions, provides quantitative and qualitative information about physical or chemical changes related to exothermic or endothermic processes or changes in heat capacity (Crompton, 2006).

The glass transition (Tg), melting temperature (Tm), crystallisation temperature, specific heat, thermal and oxidative stability, and reaction kinetics, etc. can be determined directly, rapidly and accurately by a DSC instrument using appropriate software.

2.5.6 X-ray diffraction (XRD)

The XRD technique has been extensively used to identify and distinguish vermiculite from other clay minerals (e.g. chlorite and smectites). In fact, the definition of vermiculite is based on its ca. 1.45 nm basal spacing for Mg-vermiculite treated with glycerol and on the characteristic 1.0 nm spacing for the K-vermiculite form on heating at 300 °C (Brindley and Brown, 1980; Bergaya *et al.*, 2006). XRD is also used to distinguish the dioctahedral (d_{060} = 0.149–0.150 nm) from the trioctahedral (d_{060} = 0.151–0.153 nm) clay minerals (Brindley and Brown, 1980). It is a versatile and also non-destructive technique that reveals detailed information about the phases contained, as well as their crystallographic features (Cullity, 1978; Moore and Reynolds, 1989).

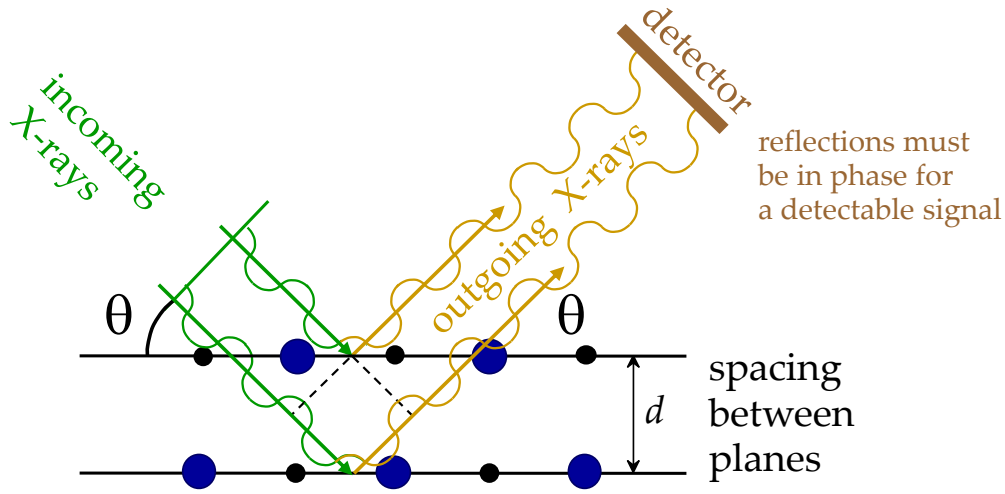

Figure 5. X-ray diffraction by a crystal according to Bragg's law

When the incident wavelength (λ) is of the same order of magnitude as the repeated distance (d) between scattering centres, diffraction can occur. This diffraction phenomenon, known as Bragg's law and represented in Fig. 5, is mathematically described by Scheme X.

$$n\,\lambda = 2\,d\,\sin\theta$$

Scheme X: Bragg's law

where n is an integer (n = 1, 2, ...); d is the interlayer spacing ;θ is the diffraction angle or Bragg's angle; and λ is the wavelength of the incident X-rays.

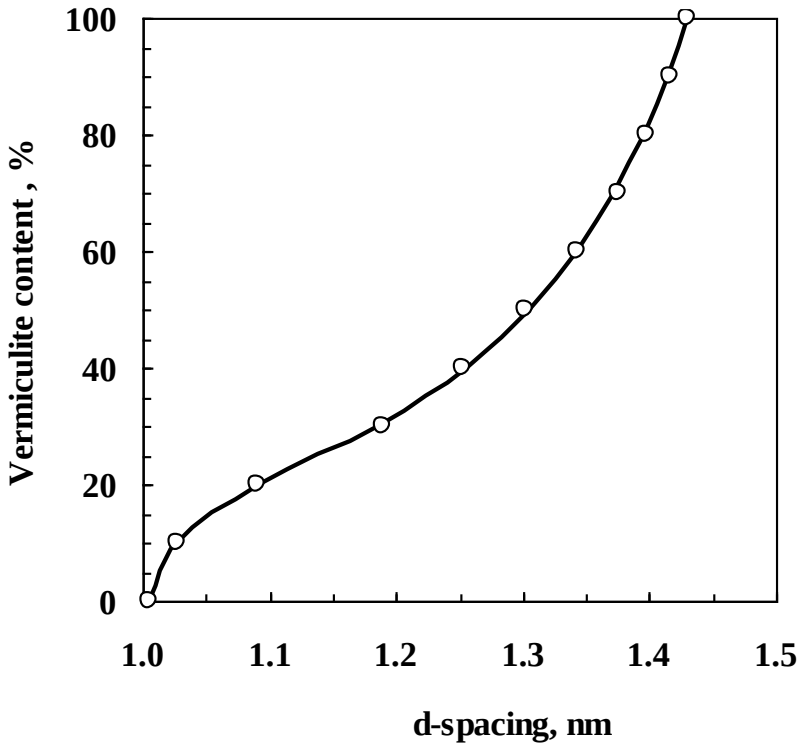

Figure 6. Determination of vermiculite content from the d-spacing (according to Moore and Reynolds, 1989)

By knowing λ and measuring θ, d can be calculated using the relationship shown in Scheme X. Furthermore, in mixtures (as often found in nature) the vermiculite content can be determined by applying the d-spacing estimated using Bragg's law, as shown in Fig. 6 (Moore and Reynolds, 1989).

2.5.7 Scanning electron microscopy (SEM)

Nowadays SEM (along with TEM) is one of the most important characterisation techniques as a result of the huge technological improvements made since its invention and the relatively easy interpretation of data. This technique has also been used by some researchers to study the surface changes in vermiculite resulting from physical or chemical modification.

In a SEM, the electron gun bombards the sample with electrons of a specific wavelength. Deflected electrons, commonly elastically scattered electrons, are collected as signals for imaging. Different topographies and different chemical compositions bring about different signal intensities, thereby giving different contrasts on the SEM screen (Lawes, 1987).

2.5.8 Dynamic mechanical analysis (DMA)

DMA is a mechanical testing method used to measure the elastic (modulus) and viscous (damping) properties of polymeric materials as a function of temperature, time, frequency, stress or a combination of these parameters. As a thermal method, it is also used to study the degradation mechanisms, chemical reactions, etc. of materials (Crompton, 2006;2012).

The polymer processing conditions and end-use performance can also be evaluated according to the rheological changes observed during a DMA experiment. It can be therefore used to evaluate elastomers, viscous thermoset liquids, composite coatings and adhesives, and other materials with viscoelastic behaviour (Crompton, 2006;2012).

2.5.9 Mechanical properties of polymers

The application of a polymeric material depends on a combination of different factors, including its mechanical properties, processability and price. To understand the behaviour of plastic materials and thus infer about the performance of a specific fabricated article (with time, stress and temperature) it is necessary to gather relevant and comprehensive experimental data (Crompton, 2012).

Typical mechanical properties include tensile strength (at yield or at break, MPa), elongation at break (%), strain at yield (%), Izod impact (kJ m^{-1}), modulus of elasticity, etc. Most of them are measured at room temperature but on some modern equipment they can also be determined at different desirable temperatures.

2.5.10 Flammability testing of polymers

Different flammability tests and rating criteria have been developed in research, industry and by regulatory agencies. This diversity of testing and quality control methods derives from the varying nature of fire risk situations (Crompton, 2006). However, substantially, all FR materials can be defeated in large-scale fire situations and the tests run under standard small scale conditions do not necessarily predict the behaviour of the materials under real fire conditions (Weil and Levchik, 2009).

The three most widely used flammability tests are given (Kiliaris and Papaspyrides, 2010):

a) Cone calorimetry

The cone calorimeter is one of the most effective and commonly used bench-scale flammability test methods for polymers. It has been standardised as ASTM E 1354 and ISO 5660. It is efficient, robust and accurate, and is so designated because of the geometric arrangement of the electric heater. The sensing principle is based on the measurement of oxygen consumption in the combustion gases of a specimen under a defined heat flux. Together with oxygen, the gas flow, carbon monoxide and carbon dioxide concentrations are also measured in the exhaust duct. The amount of heat released is proportional to the amount of oxygen consumed throughout polymer combustion and is equal to 13.1 kJ g^{-1}. It is through this relationship and the measurement of the gas flow that most of the fire parameters are calculated (Huggett, 1980; Babrauskas, 1984; Laoutid *et al.*, 2009; Kiliaris and Papaspyrides, 2010).

In a cone calorimeter several fire parameters of a material can be determined and/or calculated simultaneously. They include time to ignition (t_{ign}), heat release rate (HRR), peak of heat release rate (pHRR), total heat released (tHR), mass loss rate (MLR) and smoke production rate (SPR). Among them the HRR (fire driving force) and pHRR (fire propagation), and their mathematical combination, are generally considered the most important parameters for evaluating the flammability of a chosen

polymeric material (Babrauskas, 1984; Babrauskas and Peacock, 1992; Laoutid *et al.*, 2009; Chen *et al.*, 2013; Kiliaris and Papaspyrides, 2010).

b) Underwriters Laboratory Inc. (UL 94)

UL 94 measurements are the most common flammability tests for electronic devices and appliances. They measure the burning times that result from different flame-ignition orientations. The most commonly used is the vertical UL 94 V (vertical bulk test in a small flame for ignitability and flame spread, IEC 60695-11-10), but there are also horizontal tests for bulk and foamed materials, and a radiant panel flame-spread test (Dufton, 1995; Laoutid *et al.*, 2009; Kiliaris and Papaspyrides, 2010). In UL 94 V two sets of five specimens must be tested and, according to the experimental results, the material is classified into the categories V-0, V-1 or V-2, according to the criteria shown in Table 9.

Table 9. UL 94 V classifications at 50 W (U.L.I., 1997; Kiliaris and Papaspyrides, 2010)

Fire classification	**V-0**	**V-1**	**V-2**
Total flaming combustion for each specimen	≤ 10 s	≤ 30 s	≤ 30 s
Total flaming combustion for all 5 specimens of any set	≤ 50 s	≤ 250 s	≤ 250 s
Flaming and glowing combustion after second burner flame application	≤ 30 s	≤ 60 s	≤ 60 s
Cotton ignited by flaming drips from any specimen	No	No	Yes
Glowing or flaming combustion of any specimen to holding clamp	No	No	No

c) Limiting Oxidation Index (LOI)

The LOI test is used to study quantitatively a material's resistance to ignition. It is defined as the minimum fraction of oxygen in a mixture of oxygen and nitrogen that will just support flaming combustion. This relative flammability test has been standardised as ASTM D 2863, ISO 4589 and NF T 51-071 (Tabuani *et al.*, 2012; Kiliaris and Papaspyrides, 2010).

Basically, the LOI test consists of a glass tube in which the specimen is vertically mounted. The ignition source is applied from the top and a slow stream of oxygen/nitrogen mixture is supplied at the bottom. According to the LOI test results, materials are classified as combustible (LOI < 21 vol.%) or self-extinguishing (LOI > 21 vol.%). The higher the LOI, the better the flame-retarding properties of a designated material (Laoutid *et al.*, 2009; Kiliaris and Papaspyrides, 2010).

REFERENCES

Abate, G., Dos Santos, L.B.O., Colombo, S.M., Masini, J.C., 2006. Removal of fulvic acid from aqueous media by adsorption onto modified vermiculite. Applied Clay Science 32, 261-270.

Alexandre, M., Dubois, P., 2000. Polymer-layered silicate nanocomposites: preparation, properties and uses of a new class of materials. Materials Science and Engineering: R: Reports 28, 1-63.

Anthony, J.W., Bideaux, R.A., Bladh, K.W., Nicholis, M.C., 2004. Hydobiotite. Mineralogical Society of America, Chantilly.

Association, T.V., 2000. Vermiculite: Health, safety and environmental aspects.

Babrauskas, V., 1984. Development of the cone calorimeter - A bench-scale heat release rate apparatus based on oxygen consuption. Fire and Materials 8, 81-95.

Babrauskas, V., Peacock, R.D., 1992. Heat release rate: The single most important variable in fire hazard. Fire Safety Journal 18, 255-272.

Badreddine, R., Le Dred, R., Prost, R., 2002a. A far infrared study of K+ ions during K+ ⇄ Ca2+ exchange in vermiculite. Clay Minerals 37, 59-70.

Badreddine, R., Vandormael, D., Fransolet, A.-M., Long, G.J., Stone, W.E.E., Grandjean, F., 2002b. A comparative X-ray diffraction, Mössbauer and NMR spectroscopic study of the vermiculites from Béni Bousera, Morocco and Palabora, Republic of South Africa. Clay Minerals 37, 367-376.

Bailey, G.W., White, J.L., 1964. Soil-Pesticide Relationships, Adsorption and Desorption of Organic Pesticides by Soil Colloids, with Implications Concerning Pesticide Bioactivity. Journal of Agricultural and Food Chemistry 12, 324-332.

Barrer, R.M., Klinowski, J., 1977. Theory of Isomorphous Replacement in Aluminosilicates. Philosophical Transactions of the Royal Society of London. Series A, Mathematical and Physical Sciences 285, 637-676.

Barshad, I., 1948. Vermiculite and its relation to biotite as revealed by base exchange reactions, X-ray analyses, differential thermal curves, and water content. American Mineralogist 35, 225-238.

Barshad, I., 1950. The effect of the interlayer cations on the expansion of the mica type of crystal lattice. American Mineralogist 35, 225-238.

Basset, W.A., 1961. The geology of vermiculite occurrences. Clays and Clay Minerals 10, 61-69.

Baumeister, W., Hahn, M., 1976. An improved method for preparing single crystal specimen supports: H2O2 exfoliation of vermiculite. Micron 7, 247-251.

Bergaya, F., Theng, B.K.G., Lagaly, G., 2006. Handbook of Clay Science. Elsevier, Amsterdam.

Berta, M., Lindsay, C., Pans, G., Camino, G., 2006. Effect of chemical structure on combustion and thermal behaviour of polyurethane elastomer layered silicate nanocomposites. Polymer Degradation and Stability 91, 1179-1191.

Beyer, J., Reichenbach, H.G.V., 1998. Dehydration and rehydration of vermiculites: IV. Arrangements of interlayer components in the 1.43 nm and 1.38 nm hydrates of Mg-vermiculite. Zeitschrift fur Physikalische Chemie 207, 67-82.

Boss, B.D., 1967. Differential thermal analysis of biotitic vermiculite to determine vermiculite content. American Mineralogist 52, 294-298.

Bourbigot, S., Duquesne, S., 2007. Fire retardant polymers: recent developments and opportunities. Journal of Materials Chemistry 17, 2283-2300.

Brindley, G.W., Brown, G., 1980. Crystal Structures of Clay Minerals and Their X-ray Identification. Mineralogical Society.

Brindley, G.W., Zalba, P.E., Bethke, C.M., 1983. Hydrobiotite, a regular 1 : 1 interstratification of biotite and vermiculite layers. American Mineralogist 68, 420-425.

Brown, M.E., 2001. Introduction to Thermal Analysis: Techniques and Applications, 2nd ed. ed. Springer, Dordrecht.

Camino, G., Costa, L., 1988. Performance and mechanisms of fire retardants in polymers—A review. Polymer Degradation and Stability 20, 271-294.

Chen, S., Wang, B., Kang, J., Chen, J., Gai, J., Yang, L., Cao, Y., 2013. Synergistic Effect of Organic Vermiculite on the Flame Retardancy and Thermal Stability of Intumescent Polypropylene Composites. Journal of Macromolecular Science, Part B 52, 1212-1225.

Choi, J., Yee, A.F., Laine, R.M., 2004. Toughening of Cubic Silsesquioxane Epoxy Nanocomposites Using Core–Shell Rubber Particles: A Three-Component Hybrid System. Macromolecules 37, 3267-3276.

Company, R., 2014. Flame retardant thermoplastics.

Connell, J.E., Kendrick, D.A., Marks, G., Parsonage, J.R., Thomas, M.J.K., Vidgeon, E.A., 1994. Synthesis of QMD and QD polyorganosiloxanes from tetrakis(trimethylsiloxy)silane and palabora vermiculite. Journal of Materials Chemistry 4, 399-406.

Connell, J.E., Metcalfe, E., Thomas, M.J.K., 2000. Silicate–siloxane fire retardant composites. Polymer International 49, 1092-1094.

Couderc, P., Douillet, P., 1973. Les vermiculites industrielles: exfoliation, caractéristiques minéralogiques et chimiques. Bulletin de la Societe francaise de ceramique 99, 51-59.

Crompton, T.R., 2006. Polymer Reference Book. Rapra Technology Limited.

Crompton, T.R., 2012. Physical Testing of Plastics. Smithers Rapra.

Cullity, B.D., 1978. Elements of X-ray Diffraction. Assison-Wesley, Reading.

Da Fonseca, M.G., Almeida, R.K.S., Arakaki, L.N.H., Espinola, J.G.P., Airoldi, C., 2006. Vermiculite as a useful host for guest cyclic aliphatic amine intercalation, followed by cation adsorption. Colloids and Surfaces A: Physicochemical and Engineering Aspects 280, 39-44.

Da Silva Jr, U.G., De F. Melo, M.A., Da Silva, A.L.F., De Farias, R.F., 2003. Adsorption of crude oil on anhydrous and hydrophobized vermiculite. Journal of Colloid and Interface Science 260, 302-304.

Das, N.C., Bandyopadhyay, M., 1991. Removal of lead by vermiculite medium. Applied Clay Science 6, 221-231.

Dittrich, B., Wartig, K.-A., Hofmann, D., Mülhaupt, R., Schartel, B., 2013. Carbon black, multiwall carbon nanotubes, expanded graphite and functionalized graphene flame retarded polypropylene nanocomposites. Polymers for Advanced Technologies 24, 916-926.

Dufton, P.W., 1995. Fire - Additives and Materials. Smithers Rapra Technology.

Eaves, D., 2006. Sampling and analysis of crude vermiculite samples for possible asbestiform fibre and quartz content. IOM Consulting Ltd.

Evans, A.M., 1987. An Introduction to Ore Geology, 2nd ed. Blackwell Scientific, Oxford.

Evans, A.M., 1993. Ore geology and industrial minerals: An introduction, 3rd ed. Blackwell Scientific, Oxford.

Farmer, V.C., 1971. The characterization of adsorption bonds in clays by infrared spectroscopy. Soil Science 112, 62-68.

Farmer, V.C., 1974. The Infrared spectra of minerals. Mineralogical Society.

Ferrage, E., Tournassat, C., Rinnert, E., Lanson, B., 2005. Influence of pH on the interlayer cationic composition and hydration state of Ca-montmorillonite: Analytical chemistry, chemical modelling and XRD profile modelling study. Geochimica et Cosmochimica Acta 69, 2797-2812.

Fischer, H., 2003. Polymer nanocomposites: from fundamental research to specific applications. Materials Science and Engineering: C 23, 763-772.

Frank, D., Edmond, L., 2001. Feasibility for identifying mineralogical and geochemical tracers for vermiculite ore deposits. United States Environmental Protection Agency, Seattle, p. 48.

Friedman, S.D., Mckinney, R.W., Ou, C.C., Spotnitz, R.M., Wu, S., 1994. Vermiculite ore concentrate with specified specific density. Google Patents.

Fripiat, J.J., Chaussidon, J., Touillaux, R., 1960. Study of dehydration of montmorillonite and vermiculite by infrared spectroscopy. The Journal of Physical Chemistry 64, 1234-1241.

Gabbott, P., 2008. Principles and Applications of Thermal Analysis. Wiley, Oxford.

Giannelis, E.P., 1996. Polymer layered silicate nanocomposites. Advanced Materials 8, 29-35.

Gier, S., Johns, W.D., 2000. Heavy metal-adsorption on micas and clay minerals studied by X-ray photoelectron spectroscopy. Applied Clay Science 16, 289-299.

Gomes, E.D., Visconte, L.Y., Pacheco, E.a.V., 2009. Thermal characterization of polypropylene/vermiculite composites. Journal of Thermal Analysis and Calorimetry 97, 571-575.

Grim, R.E., 1968. Clay mineralogy. 2nd edition. McGraw Hill.

Gruner, J.W., 1934. The structures of vermiculites and their collapse by dehydration. American Mineralogist 19, 557-575.

Haines, P.J., 2002. Principles of Thermal Analysis and Calorimetry. Royal Society of Chemistry, Cambridge.

Harben, P.W., Bates, R.L., 1990. Industrial minerals: geology and world deposits. Metal Bulletin Plc.

Harland, C.E., 1994. Ion Exchange: Theory and Practice. Royal Society of Chemistry.

Hendricks, S.B., Jefferson, M.E., 1938. Crystal structure of vermiculites and mixed vermiculite-chlorites. American Mineralogist 23, 851-862.

Hindman, J.R., 2006. Vermiculite, in: Kogel, J.E., Trivedi, N.C., Krukowski, S.T. (Eds.), Industrial Minerals & Rocks: Commodities, Markets, and Uses. Society for Mining, Metallurgy, and Exploration, Colorado, pp. 1015-1027.

Holešová, S., Valášková, M., Plevová, E., Pazdziora, E., Matějová, K., 2010. Preparation of novel organovermiculites with antibacterial activity using chlorhexidine diacetate. Journal of Colloid and Interface Science 342, 593-597.

Horacek, H., Grabner, R., 1996. Advantages of flame retardants based on nitrogen compounds. Polymer Degradation and Stability 54, 205-215.

Hornsby, P.R., 1994. The application of magnesium hydroxide as a fire retardant and smoke-suppressing additive for polymers. Fire and Materials 18, 269-276.

Horrocks, A.R., Price, D., 2001. Fire Retardant Materials. CRC Press.

Hougardy, J., Serratosa, J.M., Stone, W., Van Olphen, H., 1970. Interlayer water in vermiculite: thermodynamic properties, packing density, nuclear pulse resonance, and infra-red absorption. Special Discussions of the Faraday Society 1, 187-193.

Hudson, E.A., Terminello, L.J., Viani, B.E., Denecke, M., Reich, T., Allen, P., Bucher, J.J., Shuh, D.K., Edelstein, N.M., 1999. The structure of U6+ sorption complexes on vermiculite and hydrobiotite. Clays & Clay Minerals 47, 439-457.

Huggett, C., 1980. Estimation of rate of heat release by means of oxygen consumption measurements. Fire and Materials 4, 61-65.

Inoue, A., 1984. Thermodynamic study of Na-K-Ca exchange reactions in vermiculite. Clays & Clay Minerals 32, 311-319.

Jiménez De Haro, M.C., Pérez-Rodríguez, J.L., Poyato, J., Pérez-Maqueda, L.A., Ramírez-Valle, V., Justo, A., Lerf, A., Wagner, F.E., 2005. Effect of ultrasound on preparation of porous materials from vermiculite. Applied Clay Science 30, 11-20.

Justo, A., Maqueda, C., Perez-Rodríguez, J.L., Morillo, E., 1989. Expansibility of some vermiculites. Applied Clay Science 4, 509-519.

Justo, A., Pérez-Rodríguez, J.L., Sánchez-Soto, P.J., 1993. Thermal study of vermiculites and mica-vermiculite interstratifications. Journal of Thermal Analysis 40, 59-65.

Kiliaris, P., Papaspyrides, C.D., 2010. Polymer/layered silicate (clay) nanocomposites: An overview of flame retardancy. Progress in Polymer Science 35, 902–958.

Kind, D.J., Hull, T.R., 2012. A review of candidate fire retardants for polyisoprene. Polymer Degradation and Stability 97, 201-213.

Konta, J., 1995. Clay and man: clay raw materials in the service of man. Applied Clay Science 10, 275-335.

Krassowski, D.W., Hutchings, D.A., Qureshi, S.P., 2012. Expandable Graphite Flake as an Additive for a New Flame Retardant Resin. GrafTech.

Kresten, P., Berggren, G., 1978. The thermal decomposition of vermiculite. Thermochimica Acta 23, 171-182.

Langer, R.L., Marlor, A.J., 1981. Intumescent sheet material. Google Patents.

Laoutid, F., Bonnaud, L., Alexandre, M., Lopez-Cuesta, J.M., Dubois, P., 2009. New prospects in flame retardant polymer materials: From fundamentals to nanocomposites. Materials Science and Engineering R: Reports 63, 100-125.

Levchik, S.V., Camino, G., Luda, M.P., Costa, L., Muller, G., Costes, B., 1998. Epoxy resins cured with aminophenylmethylphosphine oxide—II. Mechanism of thermal decomposition. Polymer Degradation and Stability 60, 169-183.

Levchik, S.V., Weil, E.D., 2006. A review of recent progress in phosphorus-based flame retardants. Journal of Fire Sciences 24, 345-364.

Lichtenhan, J.D., Otonari, Y.A., Carr, M.J., 1995. Linear hybrid polymer building blocks: Methacrylate-functionalized polyhedral oligomeric silsesquioxane monomers and polymers. Macromolecules 28, 8435-8437.

Liu, B., Ding, Q., Zhang, J., Hu, B., Shen, J., 2005. Preparation and properties of new EPDM/vermiculite nanocomposites. Polymer Composites 26, 706-712.

Lv, P., Wang, Z., Hu, K., Fan, W., 2005. Flammability and thermal degradation of flame retarded polypropylene composites containing melamine phosphate and pentaerythritol derivatives. Polymer Degradation and Stability 90, 523-534.

Macewan, D.M.C., Ruiz-Amil, A., Brown, G., 1961. The X-ray identification and crystal structures of clay minerals. Mineralogical Society.

Marcos, C., Arango, Y.C., Rodriguez, I., 2009. X-ray diffraction studies of the thermal behaviour of commercial vermiculites. Applied Clay Science 42, 368-378.

Marcos, C., Argüelles, A., Ruiz-Conde, A., Sánchez-Soto, P.J., Blanco, J.A., 2003. Study of the dehydration process of vermiculites by applying a vacuum pressure: Formation of interstratified phases. Mineralogical Magazine 67, 1253-1268.

Mekhamer, W.K., Assaad, F.F., 1999. Thermodynamics of Sr–Mg vermiculite exchange and the effect of PVA on Mg release. Thermochimica Acta 334, 33-38.

Moore, D.M., Reynolds, R.C., 1989. X-ray diffraction and the identification and analysis of clay minerals. Oxford University Press.

Morgan, A.B., Gilman, J.W., 2013. An overview of flame retardancy of polymeric materials: Application, technology, and future directions. Fire and Materials 37, 259-279.

Newman, A.C.D., 1987. Chemistry of clays and clay minerals. Wiley.

Obut, A., Girgin, I., 2002. Hydrogen peroxide exfoliation of vermiculite and phlogopite. Minerals Engineering 15, 683-687.

Okhotnikov, V.B., Babicheva, I.P., Musicantov, A.V., Aleksandrova, T.N., 1989. Thermal decomposition of materials with layered structures: Isothermal dehydration of vermiculite single crystals in vacuum. Reactivity of Solids 7, 273-287.

Palabora Mining Company Limited, M.G.a.M.S., 1976. The geology and the economic deposits of copper, iron, and vermiculite in the Palabora igneous complex; a brief review. Economic Geology 71, 177-192.

Pavlidou, S., Papaspyrides, C.D., 2008. A review on polymer–layered silicate nanocomposites. Progress in Polymer Science 33, 1119-1198.

Peralta, M.M.C., 2009. Tratamento químico de uma vermiculite visando seu uso em compósitos de polipropileno. Universidade de São Paulo, São Paulo.

Pérez-Maqueda, L.A., Balek, V., Poyato, J., Pérez-Rodríquez, J.L., Šubrt, J., Bountsewa, I.M., Beckman, I.N., Málek, Z., 2003. Study of natural and ion exchanged vermiculite by emanation thermal analysis, TG, DTA and XRD. Journal of Thermal Analysis and Calorimetry 71, 715-726.

Plachá, D., Martynková, G.S., Rümmeli, M.H., 2008. Preparation of organovermiculites using HDTMA: Structure and sorptive properties using naphthalene. Journal of Colloid and Interface Science 327, 341-347.

Qiu, Z.-C., Zhang, J.-J., Zhou, Y., Song, B.-Y., Chang, J.-J., Yang, K.-K., Wang, Y.-Z., 2011. Biodegradable poly(p-dioxanone) reinforced and toughened by organo-modified vermiculite. Polymers for Advanced Technologies 22, 993-1000.

Raman, K.V.V., Jackson, M.L., 1963. Vermiculite surface morphology, Proc 12th National Conference on Clays and Clay Minerals, pp. 423-429.

Raupach, M., 1988. Polarized infrared study of anilinium-vermiculite intercalate: II. Frequency shifts and dipole interactions. Journal of Colloid and Interface Science 121, 466-475.

Reichenbach, H.G., Beyer, J., 1994. Dehydration and rehydration of vermiculites: I. Phlogopitic Mg-vermiculite. Clay Minerals 29, 327-340.

Reichenbach, H.G., Beyer, J., 1995. Dehydration and rehydration of vermiculites: II. Phlogopitic Ca-vermiculite. Clay Minerals 30, 273-286.

Reichenbach, H.G., Beyer, J., 1997. Dehydration and rehydration of vermiculites: III. Phlogopitic Sr- and Ba-vermiculite. Clay Minerals 29, 327-340.

Reichle, W.T., 1986. Synthesis of anionic clay minerals (mixed metal hydroxides, hydrotalcite). Solid State Ionics 22, 135-141.

Reynolds Jr., R.C., 1985. NEWMOD©. A computer program for the calculation of one-dimensional diffraction patterns of mixed-layered clays, in: R.C., R.J. (Ed.), 8 Brook Rd., Hanover, NH, USA.

Rosa, M.L., Tankink, A., Hoch, M., 2008. Highly flexible halogen free and flame retardant thermoplastic cable compounds modified with EVM polymers, 57th International Wire & Cable Symposium, Rhode Island, pp. 125-133.

Ruiz Amil, A., Aragon De La Cruz, F., Vila, E., Ruiz Conde, A., 1992. Study of a material from Libby, Montana containing vermiculite and hydrobiotite; intercalation with aliphatic amines. Clay Minerals 27, 257-263.

Rushton, L., 2014. Sampling and analysis of crude vermiculite samples for possible asbestiform fibre and quartz content. IOM Consulting Ltd.

Saehr, D., Le Dred, R., Baron, J., 1992. K+ ⇌ Na+ ion exchanges and availability of two groups of exchange sites in a vermiculite. II. Variability of the equivalent fraction of the two groups. Sciences Geologiques - Bulletin 45, 109-119.

Schartel, B., Hull, T.R., 2007. Development of fire-retarded materials—Interpretation of cone calorimeter data. Fire and Materials 31, 327-354.

Schoeman, J.J., 1989. Mica and vermiculite in South Africa. Journal of The South African Institute of Mining and Metallurgy 89, 1-12.

Schwellnus, C.M., 1938. Vermiculite deposits in the Palabora area, N. E. Transvaal: South Africa. Geol. Serv. Bull. 11, 7-28.

Sinha Ray, S., Okamoto, M., 2003. Polymer/layered silicate nanocomposites: a review from preparation to processing. Progress in Polymer Science 28, 1539-1641.

Stone, M.H., Wild, A., 1978. The reaction of ammonia with vermiculite and hydrobiotite. Clay Minerals 13, 337-350.

Suquet, H., Franck, R., Lambert, J.-F., Elsass, F., Marcilly, C., Chevalier, S., 1994. Catalytic properties of two pre-cracking matrices: a leached vermiculite and a Al-pillared saponite. Applied Clay Science 8, 349-364.

Survey, U.S.G., 1996. Mineral commodity summaries 1996. U.S. Geological Survey, pp. 184-185.

Survey, U.S.G., 2009. Mineral commodity summaries 2009. U.S. Geological Survey, p. 195 p.

Survey, U.S.G., 2010. Mineral commodity summaries 2010. U.S. Geological Survey, p. 193 p.

Survey, U.S.G., 2015. Mineral commodity summaries 2015, p. 196 p.

Symons, M.W., 1999. Method of preparing exfoliated vermiculite for the manufacture of a finished product. Google Patents, South Africa.

Tabuani, D., Bellucci, F., Terenzi, A., Camino, G., 2012. Flame retarded Thermoplastic Polyurethane (TPU) for cable jacketing application. Polymer Degradation and Stability 97, 2594-2601.

Tan, K.H., 1996. Soil Sampling, Preparation, and Analysis. Marcel Dekker, New York.

Thomas Jr., J., Bohor, B.F., 1969. Surface area of vermiculite with nitrogen and carbon dioxide as adsorbates. Clays & Clay Minerals 17, 205-209.

Tjong, S.C., 2006. Structural and mechanical properties of polymer nanocomposites. Materials Science and Engineering: R: Reports 53, 73-197.

Tjong, S.C., Meng, Y.Z., 2003. Impact-modified polypropylene/vermiculite nanocomposites. Journal of Polymer Science Part B: Polymer Physics 41, 2332-2341.

Tomanec, R., Popov, S., Vučinič, D., Lazič, P., 1997. Vermiculite from Kopaonik (Yugoslavia): Characterization and processing. Fizykochemiczne Problemy Mineralurgii 31, 247-254.

U.L.I., 1997. UL94-Test for flammability of plastic materials for parts in devices and appliances. Underwriters Laboratories Inc., Northbrook, IL.

Vaccari, A., 1998. Preparation and catalytic properties of cationic and anionic clays. Catalysis Today 41, 53-71.

Van Der Marel, H.W., Beutelspacher, H., 1976. Atlas of infrared spectroscopy of clay minerals and their admixtures. Elsevier Scientific Pub. Co.

Vidal, O., Dubacq, B., 2009. Thermodynamic modelling of clay dehydration, stability and compositional evolution with temperature, pressure and H2O activity. Geochimica et Cosmochimica Acta 73, 6544-6564.

Wada, T., 1973a. Manufacture of expanded vermiculite employing a urea compound and low temperatures. Google Patents.

Wada, T., 1973b. Method for the expansion of vermiculite. Google Patents.

Walker, G.F., 1959. Diffusion of Exchangeable Cations in Vermiculite. Nature 184, 1392-1393.

Walker, G.F., 1961. Vermiculite minerals, in: Brown, G. (Ed.), The X-ray identification and crystal structures of clay minerals. Mineralogical Society, London, pp. 297-342.

Wang, Q., 2013. Polymer Nanocomposite: A Promising Flame Retardant. Journal of Materials Science and Nanotechnology 1, 2-3.

Wang, Z., Qu, B., Fan, W., Huang, P., 2001. Combustion characteristics of halogen-free flame-retarded polyethylene containing magnesium hydroxide and some synergists. Journal of Applied Polymer Science 81, 206-214.

Weil, E.D., Levchik, S.V., 2009. Flame Retardants for Plastics and Textiles: Practical Applications. Hanser.

Wild, A., Keay, J., 1964. Cation-exchange equilibria with vermiculite. Journal of Soil Science 15, 135-144.

Xu, J., Li, R.K.Y., Xu, Y., Li, L., Meng, Y.Z., 2005. Preparation of poly(propylene carbonate)/organo-vermiculite nanocomposites via direct melt intercalation. European Polymer Journal 41, 881-888.

Yu, X., Wei, C., Ke, L., Hu, Y., Xie, X., Wu, H., 2010. Development of organovermiculite-based adsorbent for removing anionic dye from aqueous solution. Journal of Hazardous Materials 180, 499-507.

Zhu, R., Zhu, L., Zhu, J., Xu, L., 2008. Structure of cetyltrimethylammonium intercalated hydrobiotite. Applied Clay Science 42, 224-231.

CHAPTER 3
CHARACTERISATION OF NEAT PALABORA VERMICULITE

3.1 INTRODUCTION

The Palabora mine in the Limpopo province of South Africa is a major source of commercial vermiculite.

In this interstratified vermiculite from Palabora, the individual flakes are made up of elementary layers of vermiculite and biotite (MacEwan *et al*., 1961; Gast and Klobe, 1971; Newman, 1987). Unlike the potassium ions in biotite, the hydrated interlayer ions (usually Mg^{2+} ions) in vermiculite are easily exchangeable (Newman, 1987). Justo *et al.* (1989), Ou and Bablouzian (1994), Marcos *et al.* (2009) and Hillier *et al.* (2013) have shown that, compared with pure vermiculite, vermiculite-mica interstratified materials feature higher expansion ratios, with the thermal exfoliation also commencing at lower temperatures.

Palabora vermiculite, like other commercial types, also shows considerable variability in both composition and CEC. This is attributed to differences in the composition of the original parent mica and the degree of progress in the chemical changes induced by weathering (Basset, 1961; Frank and Edmond, 2001).

3.2 EXPERIMENTAL

3.2.1 Starting material and methods

Mandoval Vermiculite supplied samples of milled Palabora material of different grades.

The chemical composition was determined by XRF analyses. For major element analysis a milled sample (< 75 μm) of the neat or exchanged material was roasted at 1 000 °C for at least 3 h to oxidize Fe^{2+} and S, and to determine the loss on ignition (L.O.I.). Glass discs were prepared by fusing 1 g of roasted sample and 8 g consisting of 35% $LiBO_2$ and 64.71% $Li_2B_4O_7$ at 1 050 °C. The glass discs were analysed by a PANalytical Axios XRF spectrometer equipped with a 4 kW Rh tube.

FT-IR spectra were recorded using a Perkin Elmer Spectrum RX FT-IR, coupled with a computer using Spectrum v5.0.1 software, with a scan resolution of 2.0 cm^{-1}. A total of 32 interferograms were collected for each sample, applying single-beam radiation. KBr compressed pellets were prepared from a fine powder that was obtained by grinding a mixture of 3–5 mg of sample with 100 mg of dehydrated KBr using a mortar and pestle.

The interlayer composition was studied using the ammonium acetate (NH_4OOCCH_3) method (Schollenberger and Simon, 1945; Barshad, 1954a;b; Tan, 1996). The leached cations were quantitatively determined by inductively coupled plasma–optical emission spectrometer (ICP-OES).

The TGA measurements were performed using the dynamic method on a Mettler Toledo A851 TGA/SDTA instrument. About 15 mg of powder was placed in an open 150 μℓ alumina pan. The temperature was scanned from 25 to 1 000 °C at a rate of 10 °C min^{-1} with air flowing at a rate of 50 mℓ min^{-1}.

For XRD, samples of neat vermiculite were split and a subsample of each was homogenised and milled to a fine powder. The evaluation was done on random and oriented preparations. The neat vermiculite was saturated with Mg prior to the various treatments. All oriented preparations were analysed in an air-dried state, after

ethylene glycol solvation and heat treatment at 550 °C. XRD data were obtained on a BRUKER D8 Advance diffractometer with CoK_{α} radiation, Johansson crystal primary monochromator and LynxEye detector with an active area of 3.7°. Scans from 2 to 70° 2θ for random powder preparations and 2 to 28° 2θ for oriented slides were recorded in step scan mode at a speed of 0.01° 2θ step size/4 s and generator settings of 40 kV and 40 mA. Mineral identification was based on the BRUKER DIFFRAC^{Plus} - EVA evaluation program using the International Centre for Diffraction Data (ICDD) Inorganic/Organic Database. Phase concentrations were determined by the Rietveld quantitative method with DIFFRAC^{Plus} – TOPAS software and an estimated accuracy of ± 1%. Refinement of the diffraction data was done using the same program.

Images of the vermiculite were obtained on a JSM-840 SEM equipped with Orion 6.60.4 software. For these studies the flakes were mounted on adhesive carbon tape. The temperature-driven dynamic exfoliation process was also studied under a SEM (FEI QUANTA 200 ESEM) fitted with a heating stage. The samples were placed inside a crucible and mounted in the heating stage. They were viewed at 200x magnification. The pressure was 0.5 kPa, voltage 20 kV, spot size 6–7 and a working distance of 16–20 mm. The temperature was ramped at 20 °C min^{-1}.

3.3 RESULTS AND DISCUSSION

3.3.1 Macroscopic appearance

The different grades of vermiculite studied, superfine (1.0 mm) and micron (0.5 mm), ostensibly differ in flake size only. The flakes are mostly brownish with the colour intensity increasing with increases in the thickness of the flakes (or more rigorously with the number of stacked layers). They tend to become golden when the layers are expanded, by heat or by intercalation of large molecules (Figs 7 and 8).

Closer inspection of individual flakes (Fig. 9) revealed numerous surface defects (striations, voids and folds), as well as edge damage. Granular impurities were visible in between the flakes and on the surface of the aggregates. The latter might have been caused by the process of milling the mineral.

The images in Figs 7 and 8 also show the appearance of Palabora vermiculite flakes before and after exfoliation at 800 °C respectively.

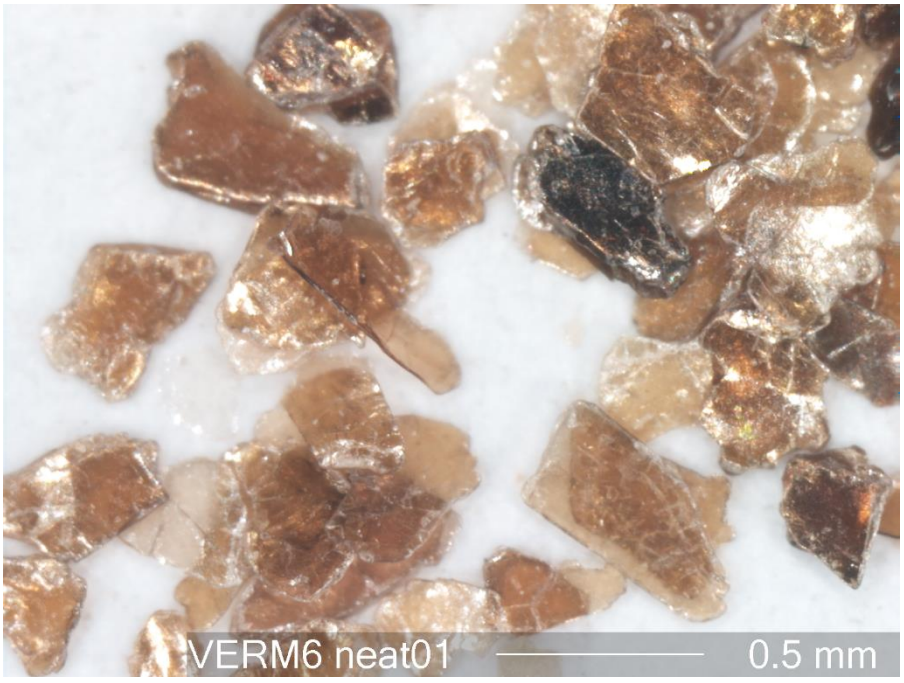

Figure 7. Micrograph of neat micron-grade Palabora vermiculite flakes

Figure 8. Micrograph of heat-expanded Palabora vermiculite flakes

Both Figs 8 and 9 reveal the asymmetric growth of the concertina-like structure and the high variability of the size of the gap between the separated sheets comprising the expanded "worms".

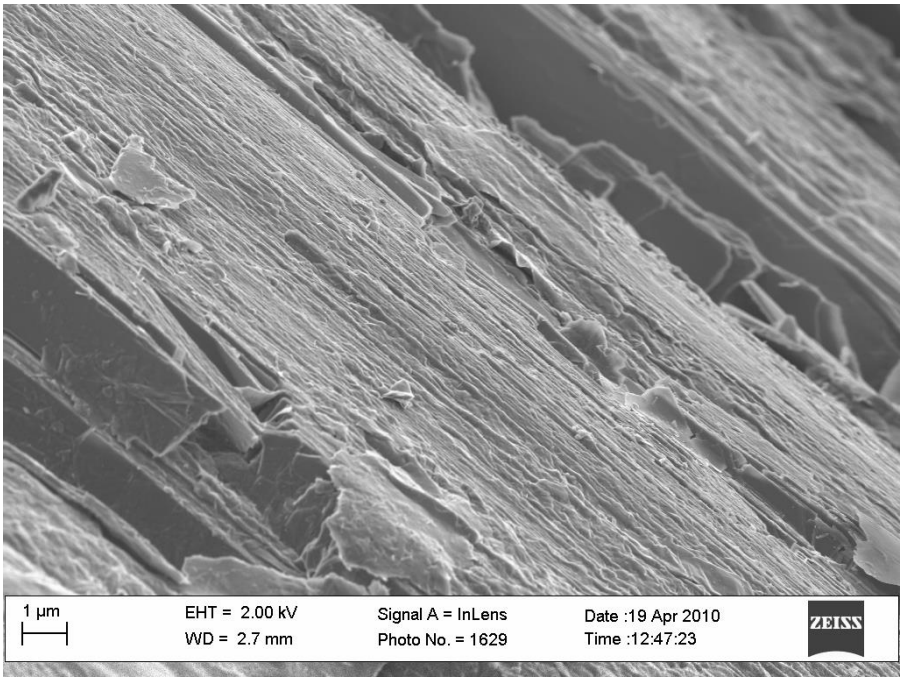

Figure 9. SEM image of neat vermiculite

Careful study of video recordings of the expansion process conducted in the hot stage of an environmental scanning electron microscope (ESEM) confirmed the heterogeneous or mosaic-like nature of individual Palabora vermiculite flakes. Expansion occurred intermittently over a wide temperature range (Appendix IV). The expansion of vermiculite occurred in stages at different positions along the flake thickness (Fig. 8). It is remarkable that significant expansion still occurred despite the low pressure of only 0.5 kPa in the ESEM chamber.

The particle size distribution for the superfine-grade vermiculite shows an apparent bimodal distribution (Fig. 10) and it is not materially affected by ion exchange with inorganic cations (e.g. Na-exchanged form). The material consisted essentially of high-aspect-ratio flakes.

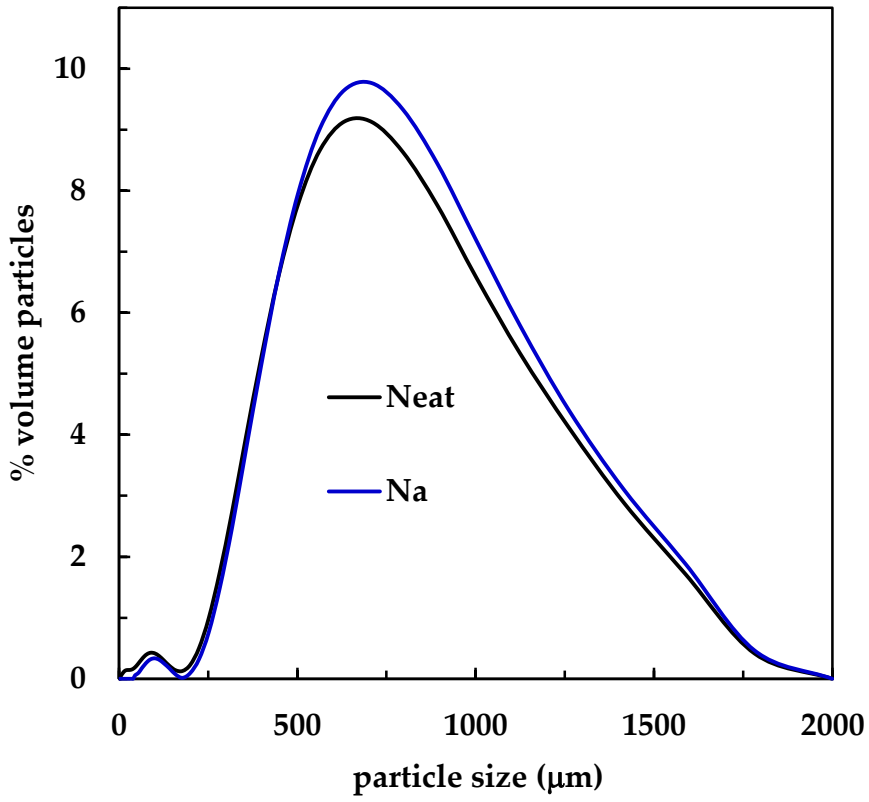

Figure 10. Typical particle size distribution of superfine-grade vermiculite

3.3.3 *Mineralogical composition*

Table 10. XRD-derived mineralogical composition of Palabora vermiculite.

Mineral phase	Mass (wt.%)	Assigned reflections (nm)
Vermiculite	15.88	1.43
Mica/Vermiculite interstratifications	72.10	2.55, 1.24, 1.19
Mica (biotite/phlogopite)	6.13	1.01
Apatite	2.73	
Dolomite	2.61	

The crude material diffraction trace shows typical Palabora vermiculite features. The broad reflection at 2θ = 4.03° (2.55 nm), the intense reflections at 2θ = 8.28° (1.24 nm) and at 2θ = 8.77° (1.19 nm) are indicative of the presence of interstratified phases. The reflection at 2θ = 7.20° (1.43 nm) is consistent with the double-layer Mg-vermiculite phase. The weak reflection at 2θ = 10.20° (1.01 nm) is from the mica (biotite or phlogopite) (Mathieson, 1958; Newman, 1987; Ruiz Amil *et al.*, 1992; Pérez-Maqueda *et al.*, 2003). Fig. 11 a) and b) show the XRD patterns.

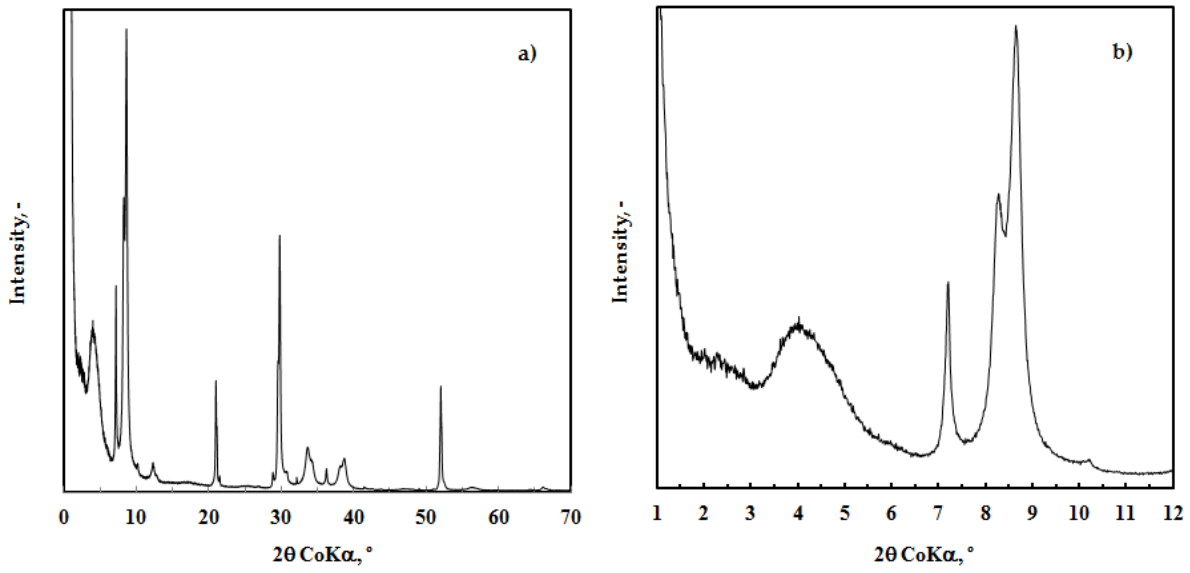

Figure 11. XRD patterns of neat vermiculite. a) Full range and b) small 2Θ, °.

Essentially, Palabora vermiculite is composed of three main phases: mica/vermiculite interstratifications, (pure) vermiculite and mica (either phlogopite or biotite). The main mineral impurities found via XRD analysis were dolomite [$CaMg(CO_3)_2$] and apatite [$Ca_5(PO_4)_3(F,Cl,OH)$].

3.3.4 Chemical composition

The average chemical composition of Palabora vermiculite (in form of the corresponding oxides) is shown in Table 11. As expected, these results reveal high contents of Al, Si and Mg and Ca consistent with the fact that vermiculite is an aluminosilicate. Ca^{2+} and some of the Mg^{2+} are the main interlayer cations.

The XRF results also indicate that Palabora vermiculite is not pure since the content of potassium oxide (K_2O) is higher than 0.35% (Inoue, 1984; Marcos *et al.*, 2009). Cardile and Slade (1987), Schoeman (1989), Badreddine *et al.* (2002), Marcos *et al.* (2009) and Marcos and Rodríguez (2010) also found that Palabora vermiculite has, comparatively, an unusually high level of iron.

The iron ions and aluminium ions are the main magnesium isomorphous substitutes in the octahedral sites. There is also considerable silica replacement in the tetrahedral sites (Cardile and Slade, 1987).

The presence of phosphorus (combined with calcium) is attributed to apatite contamination. The neat material contains very little organic material, shown by the low L.O.I. which also relates to the diverse forms of water and hydroxyl groups in the crystalline structure.

Table 11. Chemical composition of Palabora vermiculite

SiO_2	TiO_2	Al_2O_3	Fe_2O_3 (t)	MnO	MgO
39.74	0.88	8.36	7.06	0.05	22.70

CaO	Na_2O	K_2O	P_2O_5	Cr_2O_3	L.O.I.	Total
5.72	0.01	4.81	2.81	0.02	7.83	100.0

The unknown quantities in Scheme XI were determined by fitting the formulae to the XRF data for the other elements using atom balances. In this calculation it was assumed that titanium and manganese occupied the tetrahedral and octahedral positions respectively. Neglecting the presence of these impurities made little difference to the calculations.

$$0.60\,(Mg_{2.60}Fe^{2+}_{0.60})[Si_{3.2}Al_{0.78}Fe^{3+}_{0.02}]O_{10}(OH)_2K^{+}_{0.49}$$
$$+0.40(Mg_{2.60}Fe^{2+}_{0.60})[Si_{3.2}Al_{0.78}Fe^{3+}_{0.02}]O_{10}(OH)_2Mg^{2+}_{0.20}.nH_2O$$

Scheme XI: Structural formula of neat vermiculite consistent with the XRF data

The composition estimated from the XRF data suggest 60% biotite and 40% vermiculite are present, with a CEC value of about 98 mEq/100 g.

The ammonium acetate method was also used to explore the interlayer composition of the neat vermiculite. This procedure showed tangible results compared with the XRF results. It was shown that the exchangeable Mg^{2+} ions are negligible in comparison with the structural Mg^{2+} and thus the difference after exchange is not easily detectable by XRF. However, after extraction with ammonium acetate it was possible to differentiate between them.

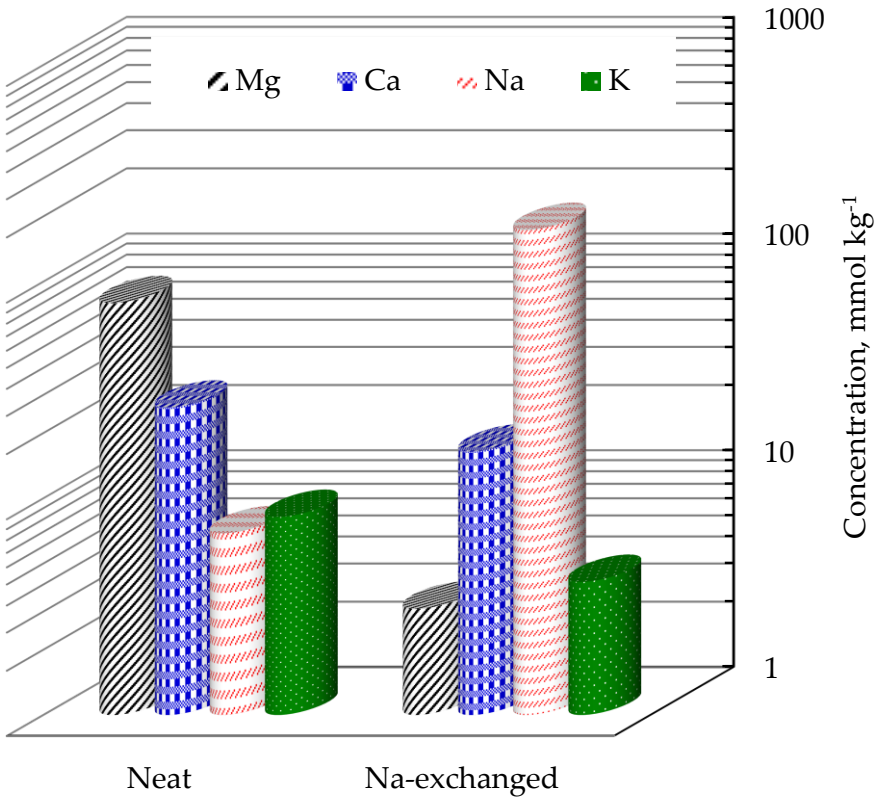

Figure 12. Change in interlayer composition of neat vermiculite after exchange with NaCl

Vermiculite's interlayer space originally contains both Mg^{2+} and Ca^{2+}, in addition to some K^{+} ions. The extraction data (Fig. 12) indicate almost quantitative replacement of the exchangeable Mg^{2+} ions, e.g. by using Na^{+} ions. Some Ca^{2+} and K^{+} ions (associated with other mineral phases) are not easily exchangeable but are extractable and detectable by the ammonium acetate method (Barshad, 1948; MacEwan *et al.*, 1961; Newman, 1987).

The FT-IR spectrum of neat vermiculite shows a strong band at 3420–3446 cm^{-1}, ascribed to the O–H stretching vibration of the hydration water and bound silanol groups. Other strong bands are observed at around 1641–1646 cm^{-1}. They are due to the O–H bending vibrations of the hydration water molecules. At 995–999 cm^{-1} there is a strong band attributed to the Si–O–Si and Si–O–Al stretching vibrations (Hougardy *et al.*, 1970; Farmer, 1974; van der Marel and Beutelspacher, 1976).

3.3.5 Thermal decomposition

Vermiculite's mass loss commences below 100 °C and occurs in several steps (Fig. 13).

Most of the mass loss occurs in the first stage (dehydration of unbound water, below 150 °C) and in the final temperature ranges (dehydroxilation, above 520 °C).

The total mass loss, at 1 000 °C, is around 7–8 wt.%. This compares with a total expected mass loss of 10 wt.%, with interlayer water contributing 6.5 mass %, for the structure indicated in Scheme XI, with the assumption that n = 4.

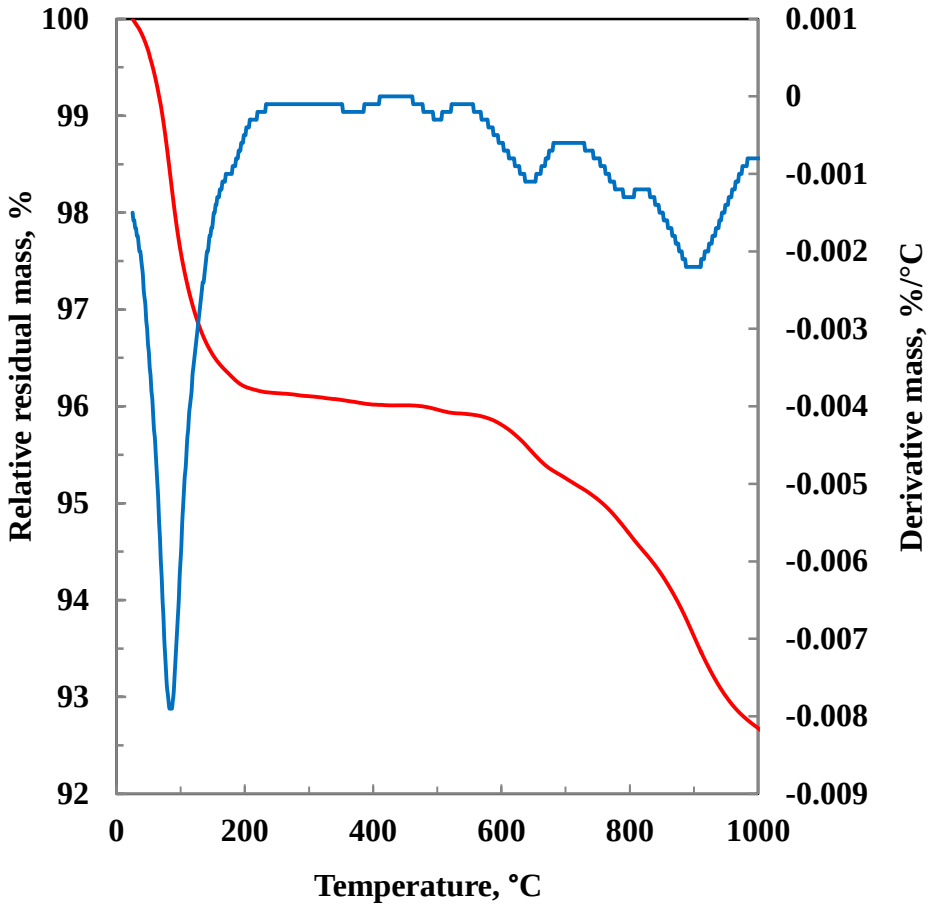

Figure 13. Thermal degradation of neat vermiculite

3.4 CONCLUSIONS

Palabora vermiculite was studied by SEM, XRF, FT-IR, ICP-OE, XRD and TGA. Commercial Palabora vermiculite apparently differs in flake size only. The flakes show visible surface defects and edge damage caused by the milling process.

The mineral structure was confirmed by saturating the neat material with magnesium ions, and analysing it in the air-dried state, after ethylene glycol solvation and after heat treatment at 550 °C. Palabora vermiculite is composed of mica/vermiculite interstratifications, vermiculite and mica. Dolomite and apatite are also found as mineral impurities. Magnesium is the main interlayer and exchangeable cation. Unusually high levels of iron and non-exchangeable potassium ions were detected in the samples.

The expanded flakes exhibit variability in the size of the gap between the separated sheets and an asymmetric, heterogeneous or mosaic-like growth of the concertina-like structure which comprises the expanded "worms".

Ion exchange of vermiculite with inorganic salts does not affect its macroscopic appearance nor destroy its crystalline structure. The preservation of the trioctahedral unit cell structure was confirmed by the presence of the d_{060} clay mineral reflection at 1.53 nm.

*

REFERENCES

Badreddine, R., Vandormael, D., Fransolet, A.-M., Long, G.J., Stone, W.E.E., Grandjean, F., 2002. A comparative X-ray diffraction, Mössbauer and NMR spectroscopic study of the vermiculites from Béni Bousera, Morocco and Palabora, Republic of South Africa. Clay Minerals 37, 367-376.

Barshad, I., 1948. Vermiculite and its relation to biotite as revealed by base exchange reactions, X-ray analyses, differential thermal curves, and water content. American Mineralogist 35, 225-238.

Barshad, I., 1954a. Cation exchange in micaceous minerals: I. Replaceability of the interlayer cations of vermiculite with ammonium and potassium ions. Soil Science Society of America Journal 77, 463-472.

Barshad, I., 1954b. Cation exchange in micaceous minerals: II. Replaceability of ammonium and potassium from vermiculite, biotite and montmorillonite. Soil Science Society of America Journal 78, 57-76.

Basset, W.A., 1961. The geology of vermiculite occurrences. Clays and Clay Minerals 10, 61-69.

Cardile, C.M., Slade, P.G., 1987. Structural study of a benzidine-vermiculite intercalate having a high tetrahedral-iron content by 57Fe Mössbauer spectroscopy. Clays and Clay Minerals 35, 203-207.

Farmer, V.C., 1974. The Infrared spectra of minerals. Mineralogical Society.

Frank, D., Edmond, L., 2001. Feasibility for identifying mineralogical and geochemical tracers for vermiculite ore deposits. United States Environmental Protection Agency, Seattle, p. 48.

Gast, R.G., Klobe, W.D., 1971. Sodium-lithium exchange equilibria on vermiculite at 25 ° and 50 °C. Clays and Clay Minerals 19, 311-319.

Hillier, S., Marwa, E.M.M., Rice, C.M., 2013. On the mechanism of exfoliation of 'Vermiculite'. Clay Minerals 48, 563-582.

Hougardy, J., Serratosa, J.M., Stone, W., Van Olphen, H., 1970. Interlayer water in vermiculite: thermodynamic properties, packing density, nuclear pulse resonance, and infra-red absorption. Special Discussions of the Faraday Society 1, 187-193.

Inoue, A., 1984. Thermodynamic study of Na-K-Ca exchange reactions in vermiculite. Clays & Clay Minerals 32, 311-319.

Justo, A., Maqueda, C., Perez-Rodríguez, J.L., Morillo, E., 1989. Expansibility of some vermiculites. Applied Clay Science 4, 509-519.

Macewan, D.M.C., Ruiz-Amil, A., Brown, G., 1961. The X-ray identification and crystal structures of clay minerals. Mineralogical Society.

Marcos, C., Arango, Y.C., Rodriguez, I., 2009. X-ray diffraction studies of the thermal behaviour of commercial vermiculites. Applied Clay Science 42, 368-378.

Marcos, C., Rodríguez, I., 2010. Expansion behaviour of commercial vermiculites at 1000°C. Applied Clay Science 48, 492-498.

Mathieson, A.M., 1958. Mg-vermiculite: A refinement of the crystal structure of the 14.36 Å phase. American Mineralogist 43, 216-227.

Newman, A.C.D., 1987. Chemistry of clays and clay minerals. Wiley.

Ou, C.C., Bablouzian, L., 1994. Intumescent sheet material. Google Patents.

Pérez-Maqueda, L.A., Balek, V., Poyato, J., Pérez-Rodríquez, J.L., Šubrt, J., Bountsewa, I.M., Beckman, I.N., Málek, Z., 2003. Study of natural and ion exchanged vermiculite by emanation thermal analysis, TG, DTA and XRD. Journal of Thermal Analysis and Calorimetry 71, 715-726.

Ruiz Amil, A., Aragon De La Cruz, F., Vila, E., Ruiz Conde, A., 1992. Study of a material from Libby, Montana containing vermiculite and hydrobiotite; intercalation with aliphatic amines. Clay Minerals 27, 257-263.

Schoeman, J.J., 1989. Mica and vermiculite in South Africa. Journal of The South African Institute of Mining and Metallurgy 89, 1-12.

Schollenberger, C.J., Simon, R.H., 1945. Determination of exchange capacity and exchangeable bases in soil-ammonium acetate method. Soil Science 59, 13-24.

Tan, K.H., 1996. Soil Sampling, Preparation, and Analysis. Marcel Dekker, New York.

Van Der Marel, H.W., Beutelspacher, H., 1976. Atlas of infrared spectroscopy of clay minerals and their admixtures. Elsevier Scientific Pub. Co.

CHAPTER 4
INORGANIC MODIFICATION OF PALABORA VERMICULITE

4.1 INTRODUCTION

Ou and Yang (1987) and Ou (1992) investigated the delamination and dispersion of vermiculite flakes in water. Swelling of the vermiculite was facilitated by citrate ions or anionic chelating agents and the delamination was effected by shear forces. Stable dispersions were obtained that could be used to prepare films and coatings.

Thomas Jr. and Bohor (1969), Couderc and Douillet (1973) and Justo *et al.* (1989) studied ion-exchanged vermiculites. They noticed that Mg-vermiculite retained coordinated water more powerfully at comparable elevated temperatures than other vermiculites. Reichenbach and Beyer (1994) concurred that some ion-exchanged vermiculites, without well-defined WLHS, are less thermally stable than Mg-vermiculite. Recently da Fonseca *et al.* (2005) investigated the ion exchange of vermiculite with heavy cations. They concluded that the extension of each exchange at the solid/liquid interface was dependent on the reaction time, pH and concentration.

Urea is stabilised for agricultural purposes by intercalation into clays. This can be done by grinding and mixing of montmorillonite with molten urea (Park *et al.*, 2004; Abramova *et al.*, 2007; Kim *et al.*, 2011). However, the low degradation temperature of urea and the preference for ligand water over urea in water–metal complexes solutions pose problems (Park *et al.*, 2004). Urea acts as a monodentate ligand for metal cations coordinating via the oxygen atom of the carbonyl group through ion-dipole interactions (Mortland, 1966; Orlova *et al.*, 1985; Theophanides and Harvey, 1987). According to Mortland (1966), the urea bonding mechanism in clays depends on the nature of the interlayer cation. In Fe-montmorillonite and Al-montmorillonite, FT-IR

spectra indicate that the urea carbonyl oxygen is protonated. This implies ion-dipole interactions between urea complexes and montmorillonite. In Mg-, Ca-, Li-, Na-, and K-montmorillonite, urea is bonded to the metal ion by coordination and possibly by ionisation of the N-H bond.

Abramova *et al.* (2007) found that some interlayer cations with low polarising ability (e.g. K^+, Rb^+, Cs^+ and NH_4^+) are not suitable for the preparation of clay-urea complexes. Cations with a high polarising ability (e.g., Al^{3+} or Fe^{3+}) or transition metals (e.g., Co^{2+}, Ni^{2+} or Cu^{2+}) readily form urea coordination complexes, even in the interlayer space of the clay. In the latter case, urea coordinates directly to the metal ion, while in the former case the urea is protonated and linked to the interlayer cation via a water bridge. Brigatti *et al.* (2005) found only partial intercalation of urea-aluminium and urea-chromium complexes into vermiculite from water at 25 °C. Interestingly, attempts to prepare such complexes at 60 °C were unsuccessful.

On heating, urea and urea metal-complexes decompose and polymerise simultaneously, releasing gaseous products (Schaber *et al.*, 2004). The actual product spectrum depends on the heating rate, final temperature and pressure, etc. The evolved gases contain ammonia, carbon dioxide and nitrogen oxides. Solid products include cyanuric acid, cyanic acid and biuret (Orlova *et al.*, 1985; Stradella and Argentero, 1993; Chen and Isa, 1998; Brigatti *et al.*, 2005).

The present interest was to modify vermiculite so that it can provide a fire-retardancy effect in polymers similar to that achieved with expandable graphite (Krassowski *et al.*, 2012). "The right place at the right time" flame-retardant principle dictates that there should be a near-perfect match between the exfoliation onset temperature of the expandable filler and the decomposition onset temperature of the host polymer. This means that the exfoliation onset temperature of ordinary commercial vermiculite is much too high for common polymers. It can be lowered by suitable chemical modifications under diverse conditions (Wada, 1973a;b; Baumeister and Hahn, 1976; Langer and Marlor, 1981; Muiambo and Focke, 2012).

4.2 EXPERIMENTAL

4.2.1 Starting material

Mandoval vermiculite supplied the micron-grade (0.5 mm) sample of Palabora material. Urea and the metal chlorides of magnesium, iron and aluminium were sourced from Merck Chemicals, SA.

4.2.2 Ion-exchange reaction of vermiculite

Selected metal-urea complexes were prepared in a closed 500 mℓ vessel under constant agitation (200 rpm in an orbital shaker) for 2 h. The metal chloride to urea molar ratio was set at 1:6. Washed vermiculite was added and the ion-exchange reaction (between the cationic complex and the interlayer cation) was allowed to proceed for 15 days. The complexes, in the reaction mixture, amounted to exactly 150% CEC. The urea complex-modified vermiculites were rinsed with distilled water and allowed to air dry. The metal-exchanged vermiculites were prepared using the same procedure. All steps were executed at room temperature (Gast and Klobe, 1971; Brigatti *et al.*, 2005).

4.2.3 Characterisation of inorganically modified vermiculites

FT-IR spectra of inorganically modified vermiculites were recorded using a PerkinElmer Spectrum RX FT-IR apparatus. The elemental composition of the vermiculites was determined by XRF.

Samples subjected to chemical analysis were milled into a fine powder (< 75 μm). The carbon and sulphur contents were determined on an Eltra CS 800 analyser. The instrument was calibrated using the Euronorm-CRM 484-1 Whiteheart malleable iron, Euronorm-CRM 058-2 sulphur steel and Euronorm-CRM 086-1 carbon steel standards, while instrument stability was monitored using the Council for Geoscience laboratory in-house soil reference standards. The detection limits for carbon and sulphur were 0.017% and 0.009% respectively.

4.3 RESULTS AND DISCUSSION

The treatment with various salts and urea complexes did not materially affect the macroscopic appearance of the material.

4.3.1 Elemental analysis

The modified vermiculites showed an expected increase in the amount of exchanger cations, confirming the success of the ion-exchange process under the conditions considered.

Table 12. Normalised XRF composition analysis of neat vermiculite, metal-exchanged forms and the corresponding metal-urea complexes

Sample	Neat	Mg-urea	Mg	Al-urea	Al	Fe-urea	Fe
SiO_2	39.74	39.83	39.60	42.73	41.32	39.26	40.52
TiO_2	0.88	1.11	1.05	0.95	1.15	1.11	1.12
Al_2O_3	8.36	9.54	10.18	10.93	10.80	9.81	9.62
Fe_2O_3 (t)	7.06	9.70	8.13	8.42	10.10	10.60	11.15
MnO	0.05	0.06	0.06	0.05	0.06	0.06	0.06
MgO	22.70	22.10	24.24	22.90	22.41	21.54	21.50
CaO	5.72	3.94	3.42	1.58	1.38	1.87	2.99
Na_2O	0.01	0.27	<0.01	0.20	0.22	0.22	0.24
K_2O	4.81	4.79	5.08	4.23	4.42	4.42	4.37
P_2O_5	2.81	1.39	1.17	0.11	0.00	0.65	1.12
Cr_2O_3	0.02	0.06	0.03	0.05	0.06	0.05	0.05
L.O.I.	7.83	7.23	7.03	7.84	8.06	10.40	7.26
Total	**100.0**	**100.0**	**100.0**	**100.0**	**100.0**	**100.0**	**100.0**

The XRF results reported in Table 12 indicate that the potassium content was not significantly affected by ion exchange with other metal cations or metal-urea

complexes. This indicates that the K^+ cations present in the neat vermiculite were associated primarily with the biotite layers, i.e. they were non-exchangeable.

Magnesium ions make up the trioctahedral sheets and they were the main interlayer cations in the neat material. Consequently, the Mg^{2+} samples and those treated with magnesium-urea complex did not show a noteworthy increase in the magnesium content. However, factors such as XRF-method sensitivity and inhomogeneous composition of the flakes also contribute to some extent to some of the discrepancies observed.

Significant substitution of the interlayer Ca^{2+} cations occurred when Al^{3+}, Fe^{3+} and their respective urea complexes were intercalated. Nevertheless, a considerable amount of Ca^{2+} ions remained in the Mg-vermiculite and Mg(urea)-vermiculite samples. This persistence probably stems from the unaffected dolomite [$CaMg(CO_3)_2$] and apatite [$Ca_5(PO_4)_3(F,Cl,OH)$] phases present in Palabora vermiculite.

The carbon and sulphur elemental analysis results are reported in Table 13. As expected, there was almost no sulphur present, and the carbon content increased with the intercalation of the urea complexes. Based on the vermiculite CEC (98 mEq/100 g), the urea content corresponded to less than one urea molecule coordinated per metal ion present in the interlayer space.

Table 13. Carbon and sulphur content of the neat and modified vermiculite forms

Sample		Mg-urea	Al-urea	Fe-urea	Mg	Al	Fe
C	(wt.%)	0.45	0.32	0.65	0.04	0.04	0.04
S	(wt.%)	0.01	0.01	0.01	0.01	0.01	0.01
Urea*	(wt.%)	2.3	1.6	3.3	-	-	-
Urea*	(mmol)/100 g	37.5	26.4	54.5	-	-	-

*Estimated from the measured carbon content.

Low urea intercalation levels were also indicated for the urea-modified montmorillonite clay studied by Abramova et al. (2007) and for samples subjected to washing (Park et al., 2004). The interlayer urea:metal ratio was almost 0.6 for Fe-urea

(60% CEC), while for Mg-urea and Al-urea it was about 0.3. The higher urea content found for Fe-urea is consistent with the higher loss on ignition (L.O.I.) determined from the XRF results.

4.3.2 TGA

The TGA curves for the unaltered material, the metal-exchanged vermiculites and their respective urea-modified forms are shown in Fig. 14 to Fig. 18.

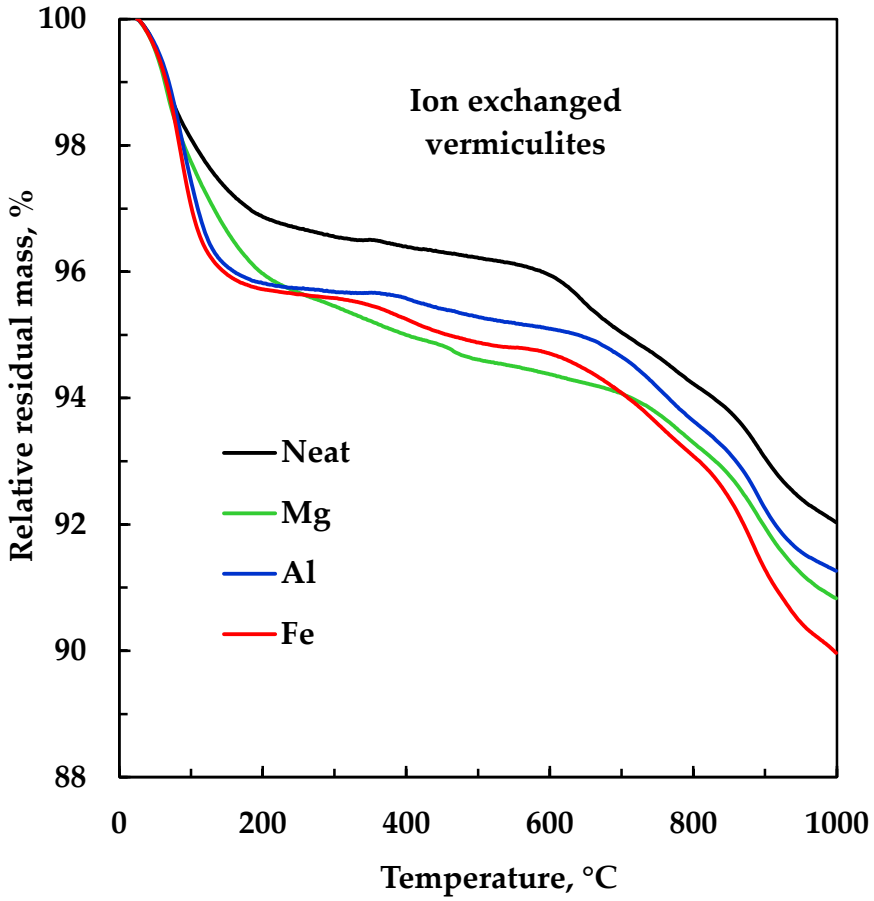

Figure 14. Thermal behaviour of neat vermiculite and its metal ion exchanged forms

Mass loss commenced below 100 °C and occurred in several steps. The total mass loss recorded at 1 000 °C was limited to 8–11 wt.% for all samples. Significant mass loss occurred in the first stage. This represents the loss of physisorbed (unbound) water and some of the water present in the galleries.

The crude material showed a mass loss of 2.7 wt.% at 150 °C. Up to this temperature the vermiculites modified with Mg^{2+}, Al^{3+} and Fe^{3+} cations showed a greater mass loss than the crude material, but for the corresponding urea complexes it was less.

The same trend held for the total mass loss measured for the samples. The mass loss above 500 °C is attributed to dehydroxylation of the clay sheets.

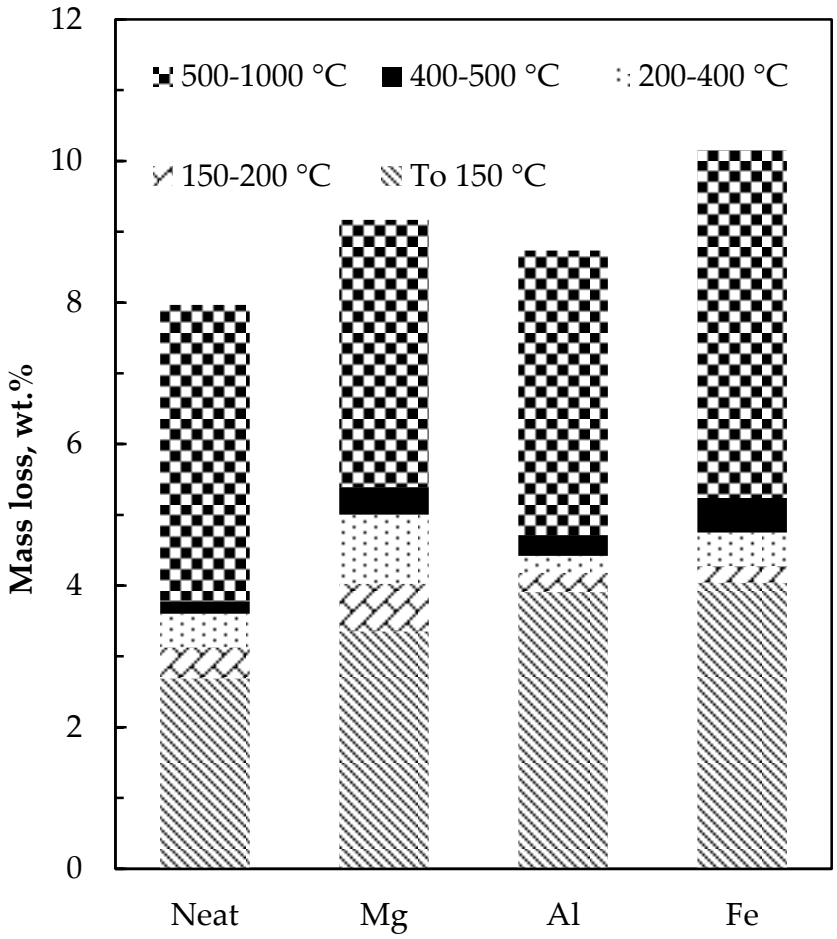

Figure 15. TGA mass loss of neat vermiculite and its metal-exchanged forms at selected temperature intervals. The black bands correspond to the exfoliation temperature range.

As will be shown, all metal-exchanged samples expanded in the temperature range 400 to 500 °C. On the other hand, the expansion occurred between 200 and 250 °C for the urea-modified versions.

Surprisingly, the observed mass loss in the temperature range where expansion occurred was relatively small, usually significantly less than 1 wt.%. The vermiculite modified by the urea complexes of Mg, Al and Fe showed mass losses of 0.4, 0.3 and 0.6 wt.% respectively. This may be compared with 0.2 wt.% for the crude material, between 200 and 250 °C (Figs 14–18).

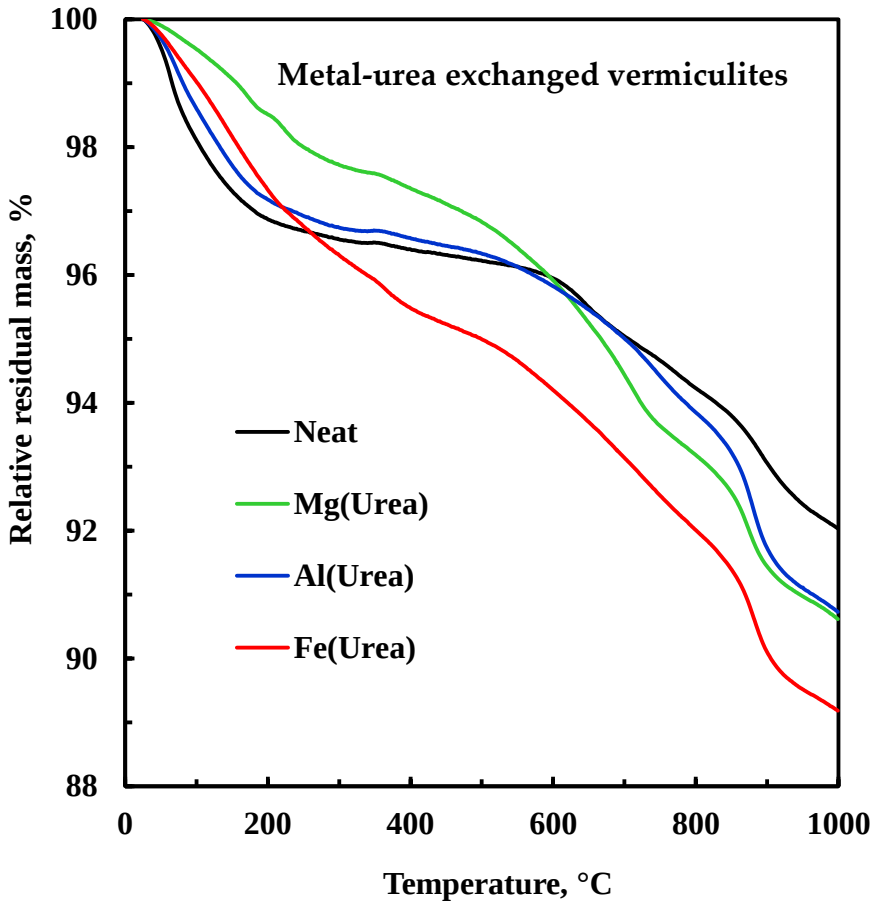

Figure 16. Thermal behaviour of neat vermiculite and its metal-urea complexes

The expansion may be driven by the release of both water and volatile urea degradation products in this temperature range. Brigatti *et al.* (2005) studied Al-urea complexes intercalated in vermiculite. They reported the release of H_2O and NH_3 below 150 °C, and of CO_2 and HNCO at about 200 °C.

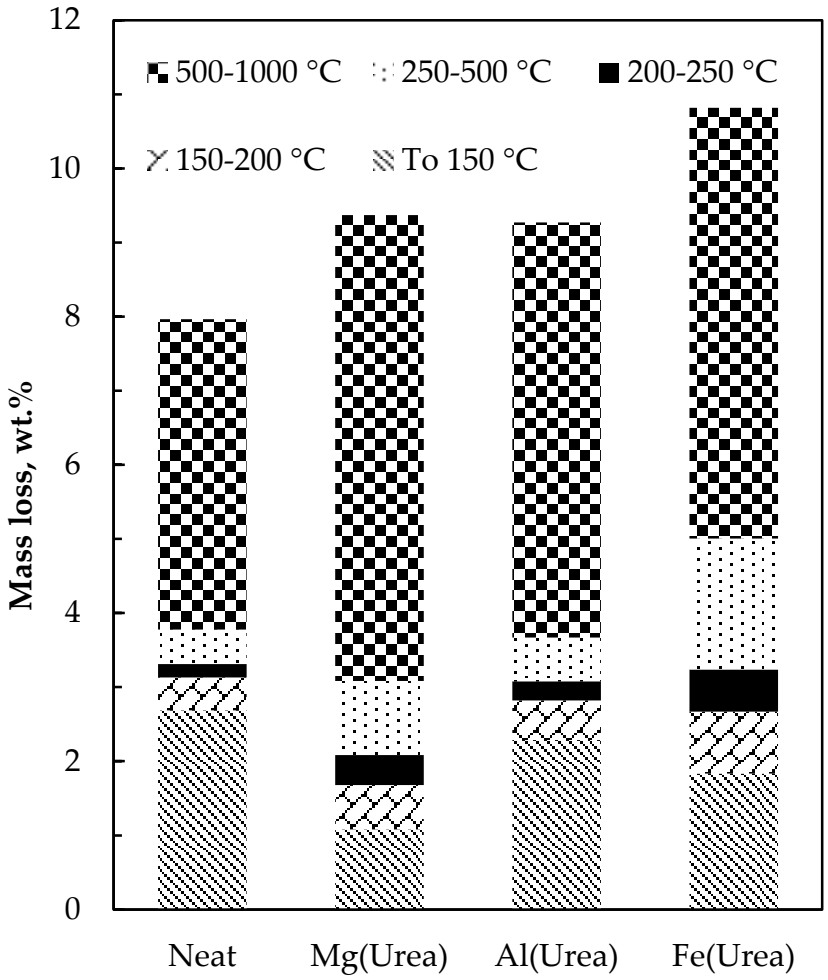

Figure 17. TGA mass loss of neat vermiculite and the corresponding metal urea complexes at selected temperature intervals. Most of the exfoliation occurred between 200 °C and 250 °C.

4.3.3 XRD

Fig. 18 presents XRD diffractograms for neat Palabora vermiculite (in essence the magnesium form) and its metal-exchanged forms. The broad reflection at 2θ = 4.03° (2.55 nm), and the intense reflections at 2θ = 8.28° (1.24 nm) and 2θ = 8.77° (1.19 nm) are indicative of the presence of interstratified phases. The 2θ = 7.20° (1.43 nm) reflection is consistent with the Mg-vermiculite phase. The 1.01 nm reflection is from the mica (biotite or phlogopite) and it is present even after urea complexation (Mathieson, 1958; Newman and Brown, 1987; Ruiz Amil *et al.*, 1992; Pérez-Maqueda *et al.*, 2003).

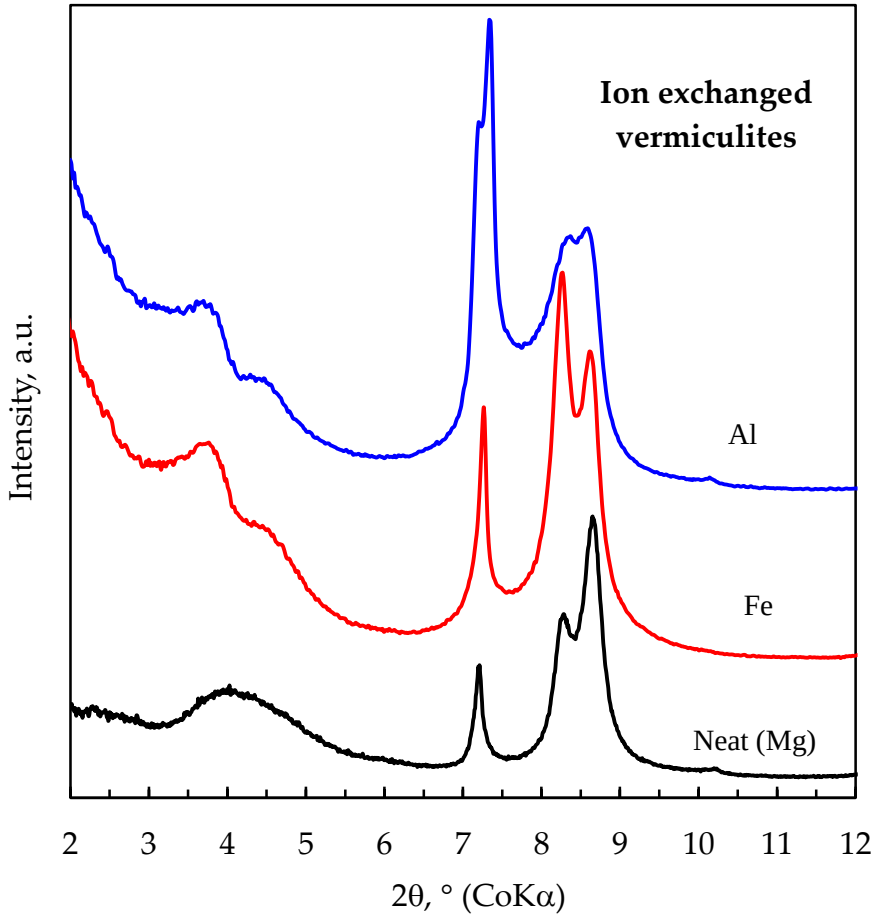

Figure 18. X-ray diffractograms for neat Palabora vermiculite and its metal-exchanged forms

In the metal urea complexes (Fig. 19), the main reflection at 2θ = 4.03° (2.55 nm) has shifted to lower 2θ values and increased in intensity. It has assumed the following values: 2θ = 3.76° (2.72 nm), 2θ = 3.73° (2.75 nm) and 2θ = 3.68° (2.79 nm) respectively for the Fe^{3+}, Al^{3+} and Mg^{2+} complexes. In the Al^{3+} and Mg^{2+} complexes the reflection at 2θ ≈ 8.77° (1.19 nm) becomes more prominent at the expense of the reflection at 2θ ≈ 8.20° (1.25 nm).

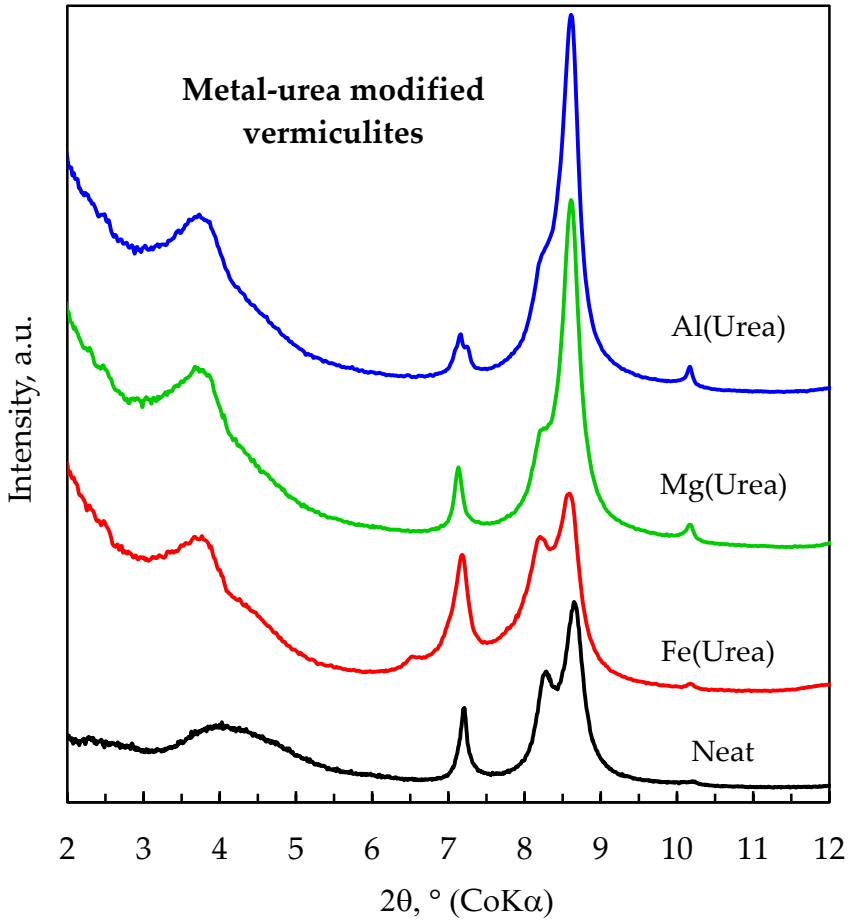

Figure 19. X-ray diffractograms for neat Palabora vermiculite and its metal-urea complexes

4.4 CONCLUSIONS

The treatment of vermiculite with urea complexes of Mg-, Al-, and Fe-salts resulted in the incorporation of urea into the interlayers of the clay. This did not affect the macroscopic appearance nor destroy the crystalline structure of the clay. Indications are that the interlayer cations were coordinated to both urea and water molecules. Below 150 °C, these compounds showed lower mass loss than the neat vermiculite. In all these cases the K^+ ions from the biotite layers were neither replaced nor complexed by urea.

The change in the interlayer chemical environment did not favour the adsorption of more unbound water molecules. However, compared with the neat material, the urea-modified Mg^{2+}, Al^{3+} and Fe^{3+} vermiculites showed increased mass loss in the exfoliation temperature ranges (200–250 °C). This is attributed to the release of both water and urea degradation products.

REFERENCES

Abramova, E., Lapides, I., Yariv, S., 2007. Thermo-XRD investigation of monoionic montmorillonites mechanochemically treated with urea. Journal of Thermal Analysis and Calorimetry 90, 99-106.

Baumeister, W., Hahn, M., 1976. An improved method for preparing single crystal specimen supports: H2O2 exfoliation of vermiculite. Micron 7, 247-251.

Brigatti, M.F., Laurora, A., Malferrari, D., Medici, L., Poppi, L., 2005. Adsorption of [Al(Urea)6]3+ and [Cr(Urea)6]3+ complexes in the vermiculite interlayer. Applied Clay Science 30, 21-32.

Chen, J.P., Isa, K., 1998. Thermal Decomposition of Urea and Urea Derivatives by Simultaneous TG/(DTA)/MS. Journal of the Mass Spectrometry Society of Japan 46, 299-303.

Couderc, P., Douillet, P., 1973. Les vermiculites industrielles: exfoliation, caractéristiques minéralogiques et chimiques. Bulletin de la Societe francaise de ceramique 99, 51-59.

Da Fonseca, M.G., De Oliveira, M.M., Arakaki, L.N.H., Espinola, J.G.P., Airoldi, C., 2005. Natural vermiculite as an exchanger support for heavy cations in aqueous solution. Journal of Colloid and Interface Science 285, 50-55.

Gast, R.G., Klobe, W.D., 1971. Sodium-lithium exchange equilibria on vermiculite at 25 ° and 50 °C. Clays and Clay Minerals 19, 311-319.

Justo, A., Maqueda, C., Perez-Rodríguez, J.L., Morillo, E., 1989. Expansibility of some vermiculites. Applied Clay Science 4, 509-519.

Kim, K.S., Park, M., Lim, W.T., Komarneni, S., 2011. Massive intercalation of urea in montmorillonite. Soil Science Society of America Journal 75, 2361-2366.

Krassowski, D.W., Hutchings, D.A., Qureshi, S.P., 2012. Expandable Graphite Flake as an Additive for a New Flame Retardant Resin. GrafTech.

Langer, R.L., Marlor, A.J., 1981. Intumescent sheet material. Google Patents.

Mathieson, A.M., 1958. Mg-vermiculite: A refinement of the crystal structure of the 14.36 Å phase. American Mineralogist 43, 216-227.

Mortland, M.M., 1966. Urea complexes with montmorillonite: an infrared absorption study. Clay Minerals 6, 143-156.

Muiambo, H.F., Focke, W.W., 2012. Ion exchanged vermiculites with lower expansion onset temperatures. Molecular Crystals and Liquid Crystals 555, 65-75.

Newman, A.C.D., Brown, G., 1987. The chemical constitution of clays. Longman Scientific & Technical Mineralogical Society.

Orlova, V.T., Kudinov, I.B., Kosterina, V.I., Semendyaeva, N.K., Lepeshkov, I.N., 1985. Thermal stability of urea complexes of magnesium nitrate and magnesium monophosphate. Journal of Thermal Analysis 30, 1047-1051.

Ou, C.C., 1992. Swelling and delamination by treating with anionic chelating agent. Google Patents.

Ou, C.C., Yang, J.C., 1987. Citrate swelling agents. Google Patents.

Park, M., Kim, C.Y., Lee, D.H., Choi, C.L., Choi, J., Lee, S.R., Choy, J.H., 2004. Intercalation of magnesium-urea complex into swelling clay. Journal of Physics and Chemistry of Solids 65, 409-412.

Pérez-Maqueda, L.A., Balek, V., Poyato, J., Pérez-Rodríquez, J.L., Šubrt, J., Bountsewa, I.M., Beckman, I.N., Málek, Z., 2003. Study of natural and ion exchanged vermiculite by emanation thermal analysis, TG, DTA and XRD. Journal of Thermal Analysis and Calorimetry 71, 715-726.

Reichenbach, H.G., Beyer, J., 1994. Dehydration and rehydration of vermiculites: I. Phlogopitic Mg-vermiculite. Clay Minerals 29, 327-340.

Ruiz Amil, A., Aragon De La Cruz, F., Vila, E., Ruiz Conde, A., 1992. Study of a material from Libby, Montana containing vermiculite and hydrobiotite; intercalation with aliphatic amines. Clay Minerals 27, 257-263.

Schaber, P.M., Colson, J., Higgins, S., Thielen, D., Anspach, B., Brauer, J., 2004. Thermal decomposition (pyrolysis) of urea in an open reaction vessel. Thermochimica Acta 424, 131-142.

Stradella, L., Argentero, M., 1993. A study of the thermal decomposition of urea, of related compounds and thiourea using DSC and TG-EGA. Thermochimica Acta 219, 315-323.

Theophanides, T., Harvey, P.D., 1987. Structural and spectroscopic properties of metal-urea complexes. Coordination Chemistry Reviews 76, 237-264.

Thomas Jr., J., Bohor, B.F., 1969. Surface area of vermiculite with nitrogen and carbon dioxide as adsorbates. Clays & Clay Minerals 17, 205-209.

Wada, T., 1973a. Manufacture of expanded vermiculite employing a urea compound and low temperatures. Google Patents.

Wada, T., 1973b. Method for the expansion of vermiculite. Google Patents.

CHAPTER 5
ORGANIC INTERCALATION OF PALABORA VERMICULITE

5.1 INTRODUCTION

Intercalation is a diffusion process in which guest species are reversibly inserted into the crystalline lattice of a host species, resulting in a material with distinctly different properties. This reaction is affected by the pH of the media, as well as the particle size of the clay. Intercalation in water is a well-known and preferential technique for preparing organoclays (Newman, 1987; LeBaron *et al.*, 1999; Utracki, 2004; de Paiva *et al.*, 2008).

The intercalation process can be partial (<100% CEC), complete (100% CEC) or even excessive (>100% CEC), according to the surfactant loading amount (Zhu *et al.*, 2008). The structure of the organo-clays is basically influenced by the clay's structure, the surfactant structure and the surfactant loading amount (Vaia *et al.*, 1994; He *et al.*, 2006). Most importantly, appropriate clays for polymer layered silicate nanocomposites (PLSNs) must have 50 < CEC < 200 and the intercalants must bond strongly to the clay platelets and also interact strongly with the polymer matrix (Utracki, 2004).

Therefore the intercalation of long-chain organic molecules (alkylammonium or alkylphosphonium) aims to reduce the interfacial tension between the hydrophilic clay layers and the (usually) hydrophobic polymer matrix. During the course of the reaction, the adjacent 2:1 clay layers expand in a systematic way due to the release of the native and relatively smaller hydrated inorganic cations (Na^+, Mg^{2+}, Ca^{2+}, etc.) to accommodate the much larger and favoured organic molecules (surfactants).

The use of surfactants with two or more long chains favours the formation of a more exfoliated nanocomposite than those with a single long chain (Hotta and Paul,

2004). Shah (2007) emphasised that the use of a two-tail modified organo-clay can lead to the formation of more highly exfoliated nanocomposites than a one-tailed organo-clay, when both have nearly the same non-polar properties. So the polyolefin matrices give better exfoliation with organo-clays modified by a surfactant with two or more long alkyl tails, which are non-polar (Hotta and Paul, 2004; Cui *et al.*, 2007).

In a later stage, and as precursors of polymer nanocomposites, clay's hydrophobicity and the expanded layers might enable further diffusion of the polymer chains into the clay galleries. This will eventually lead to the co-intercalation of the polymer chains into the clay galleries or delamination (exfoliation) and dispersion of the clay layers into the polymer matrix (Lagaly, 1986; Newman, 1987; Fornes *et al.*, 2002; Williams-Daryn and Thomas, 2002; Sinha Ray and Okamoto, 2003; Simha Martynková *et al.*, 2007; de Paiva *et al.*, 2008; Theng, 2012).

Organo-clays find application in several fields and therefore have become an important research topic in science and industry. The preparation of organo-vermiculites for different purposes requires treatment with various organic cations. Most of the studies related to the intercalation of vermiculite employed temperatures higher than ambient, apart from other mechanical stratagems. Alkylammonium vermiculite complexes were prepared at 70 °C in an oven (Serratosa *et al.*, 1970); at 50 °C with a shaker (Abate *et al.*, 2006), and at 70 °C in a centrifuge and dried at 40 °C (Simha Martynková *et al.*, 2007). Zhu *et al.* (2008) stirred the suspensions at 50 °C and dried them at 80 °C. Nevertheless, da Fonseca *et al.* (2005), da Fonseca *et al.* (2006) performed cation exchange (with heavy metal ions) and intercalation (with cyclic aliphatic amines) at 25 °C.

The extent to which Palabora vermiculite can be intercalated with alkylammonium ions of differing chain lengths and structures was assessed. In this investigation an attempt was made to determine how readily four different surfactants could be intercalated into neat and Na-exchanged vermiculites. Their effect on the basal spacing and on the expansion onset temperature was also evaluated.

5.2 EXPERIMENTAL

5.2.1 Starting materials and suppliers

The surfactants were obtained from Merck Chemicals. The micron-grade (0.5 mm) sample of Palabora material was from Mandoval.

5.2.2 Intercalation reaction

Vermiculite features a high layer charge density and has a relatively larger flake size and hence bigger lateral dimensions than conventional smectites. The intercalation reaction was carried out using an SPO-MP15 shaker for 15 days at room temperature. A longer contact time and frequency (200 rpm) were chosen due to the very slow rate of exchange (Inoue, 1984; Skipper *et al.*, 1991; Burnside *et al.*, 1999; Tatsuya and Komarneni, 1999).

Three sets of experiments were performed. Firstly, neat vermiculite (with magnesium and calcium as exchangeable cations) was reacted with various surfactants.

For the second set of reactions an attempt was made to replace the magnesium with sodium cations before the intercalation with the organic cations took place (Serratosa *et al.*, 1970; Williams-Daryn and Thomas, 2002; Utracki, 2004). For both sets of experiments, 30 g of vermiculite was weighed and added to enough of the surfactant solution so that there would be a 50% excess of the ions, based on a CEC of 98 mEq/100 g.

In the third approach the aim was to evaluate vermiculite's structure at different surfactant loadings. So a double-chain 10-carbon-long surfactant (DC10) was intercalated with neat vermiculite from 25 to 200%CEC.

The quantitative removal of the excess of the surfactant was tested by precipitating the reaction of the chloride and bromide anions with an aliquot of supernatant solution containing Ag+ cations ($AgNO_3$).

$$Ag^{+}_{(aq)} + Cl^{-}_{(aq)} \longrightarrow AgCl_{(s)} \text{ (white)} \qquad K_{ps} = 1{,}8.10^{-10}$$

Scheme XII: Reaction of Ag+ and Cl- ions with formation of a white precipitate

$$Ag^{+} + Br^{-}_{(aq)} \longrightarrow AgBr_{(s)} \text{ (pale yellow)} \qquad K_{ps} = 5{,}4.10^{-13}$$

Scheme XIII: Reaction of Ag+ and Br- ions with formation of a pale yellow precipitate

5.2.3 Characterisation of organo-vermiculites

TGA was performed by the dynamic method on a Mettler Toledo A851 TGA/SDTA instrument.

XRD data were obtained on a PANalytical X-pert Pro powder diffractometer instrument.

Images of neat and Na-exchanged vermiculite were obtained on a JSM-840 scanning electron microscope equipped with Orion 6.60.4 software.

5.3 RESULTS AND DISCUSSION

5.3.1 TGA

Fig. 20 reports the mass loss curves of neat vermiculite and its organo-vermiculites, intercalated with different surfactants, at 150% CEC loading. Mass loss started below 100 °C. However, the decomposition onset temperatures for all organo-vermiculites were above 200 °C. Generally, the total mass loss increased with increasing surfactant molecular weight. Additional thermal events were recorded in the organo-vermiculites, but neat vermiculite exhibited only two typical steps.

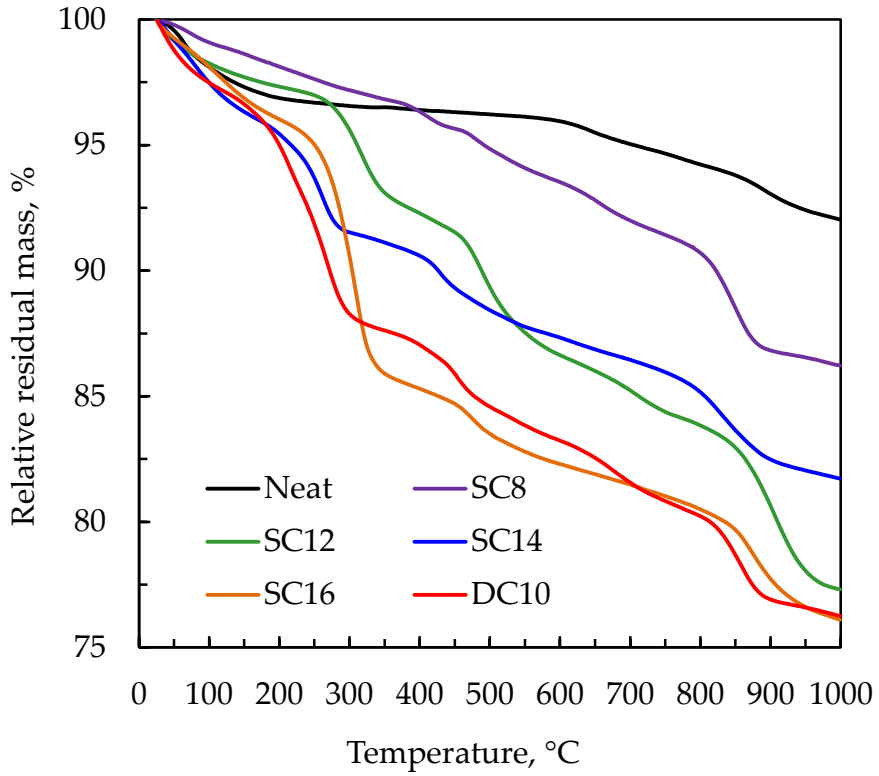

Figure 20. TGA curves of neat vermiculite and its organo-vermiculites

Compared with the neat material, the organo-vermiculites featured lower mass loss below 150 °C. This was an indication that less physisorbed (unbound) water was present in the galleries. Therefore, compared with the neat material, the organo-vermiculites appear to be more thermally stable at low temperatures. This fact is consistent with a change in the character of the internal surface from hydrophilic to more hydrophobic. However, between 200 and 500 °C, the thermal degradation of the

organo-vermiculites proceeded in several, more intense steps due to the degradation of the surfactants.

The organic content and the corresponding d-spacing data are summarised in Table 14. By measuring the total mass loss at 1 000 °C, the amount of the intercalated organics was estimated. It was assumed that most of the interlayer water had been driven off by 150 °C.

Table 14. Organic content and d-spacing of organo-vermiculites

Surfactant	Structure	Organic content, wt.%		d_{001}, nm	
		Neat	Na	Neat	Na
Octylammonium chloride	SC8	6.81	8.18	3.0	3.0
Dodecylpyridinium chloride	SC12	14.25	16.89	3.7	3.3
Tetradecyl-trimethylammonium bromide (Cetrimide BP)	SC14	10.89	13.81	3.9	4.3
Hexadecyltrimethyl-ammonium bromide (CTAB)	SC16	17.48	18.67	4.5	4.5
N,N'-didecyldimethylammonium chloride	DC10	17.11	14.83	4.4	4.4

Fig. 21 reports the TGA results for neat vermiculite and DC10 organo-vermiculites prepared with different surfactant/vermiculite ratios. The volatilisation/decomposition onset temperatures for all DC10-vermiculites were above 200 °C. From 200 to 500 °C, the decomposition of the intercalated surfactant proceeded in different steps.

At a high surfactant concentration level, the variation in residual mass with the amount of surfactant added to the reaction mixture was insignificant. The small variations suggest that the degree of intercalation reached a plateau value above 150% CEC. These TGA results also clearly indicate that the degree of intercalation corresponded approximately to that expected for the 100% CEC for the present

preparation method. This indicates that the intercalation in vermiculite is limited to ion exchange and that the DC10 molecules are held in the interlayer galleries by electrostatic forces, as also suggested by Lagaly (1986).

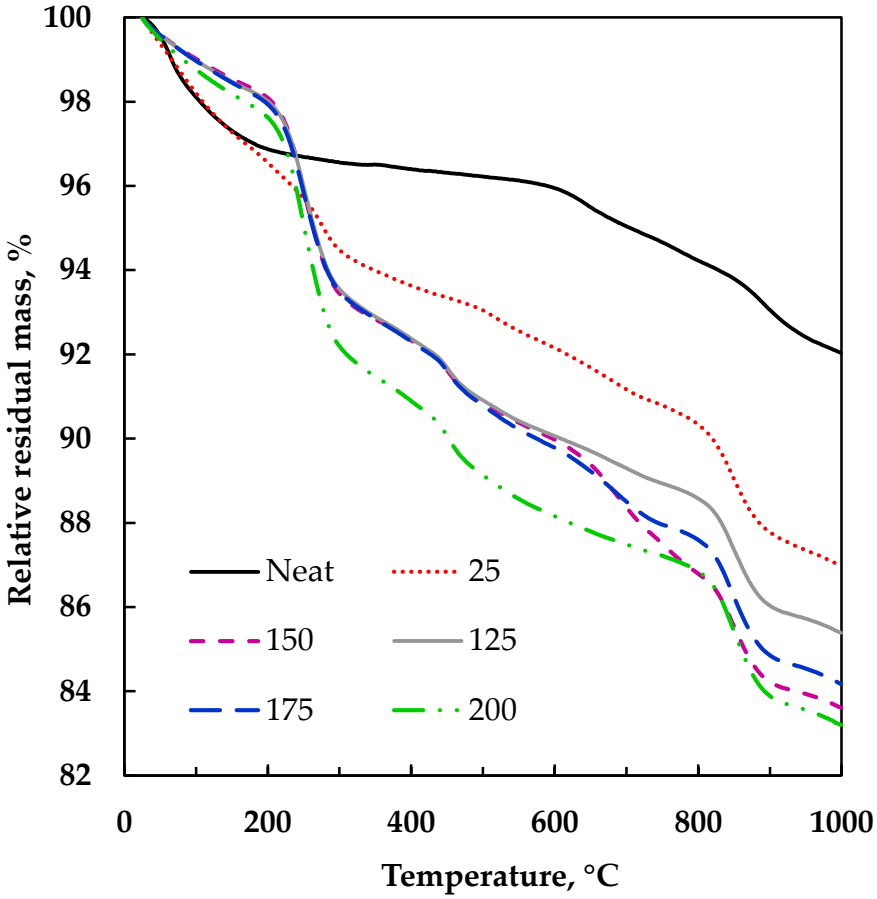

Figure 21. Thermal degradation of different DC10 intercalated vermiculites

5.3.2 XRD

Fig. 22 shows the XRD wide-angle X-ray scattering (WAXS) patterns for samples prepared in this study. The broad reflection at 2θ = 4.03° (2.55 nm) for the neat vermiculite changed into a sharp reflection at a lower 2θ° for the intercalated material. Considering the organo-vermiculites prepared from the neat material, the basal spacings were the following: 3.0, 3.7, 3.9, 4.6 and 4.4 nm, respectively, for SC8, SC12, SC14, SC16 and DC10.

The increase in the d-spacing is proportional to the chain length (molar weight) and confirms successful intercalation of the surfactant into the vermiculite galleries. The persistence of the broad reflection at ca. 2θ = 10.20° (1.01 nm), despite surfactant intercalation, suggests that exchange of the K^+ ions associated with the mica did not occur. This is in agreement with findings by Zhu *et al.* (2008).

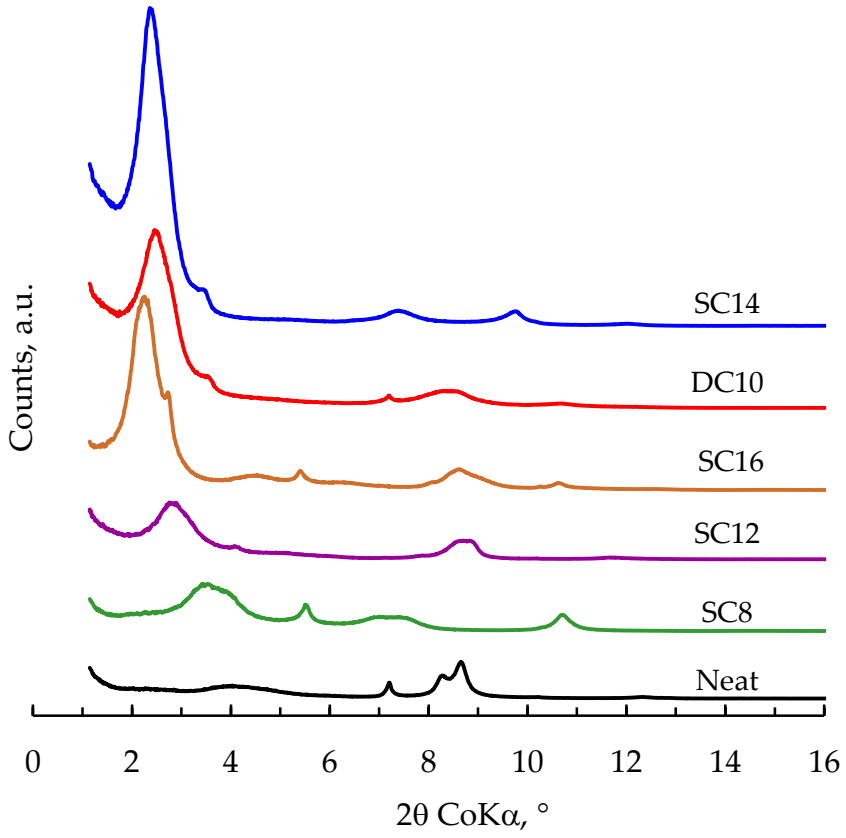

Figure 22. XRD plots of neat vermiculite and its intercalated organo-vermiculite, prepared using different surfactants

DC10 was selected to assess vermiculite's structure and behaviour at different surfactant loadings (Fig. 23). The surfactant:vermiculite ratio used during synthesis did affect the XRD patterns of the resulting materials. The d-spacing values increased with increasing surfactant:vermiculite ratio up to ca. 100% CEC. Zhu *et al.* (2008) ascribed the steep increase of the d-spacing, even at very low surfactant loading, to layer-by-layer replacement. Actually, the intercalated surfactants surround the previously absorbed surfactants, rather than the remaining inorganic cations.

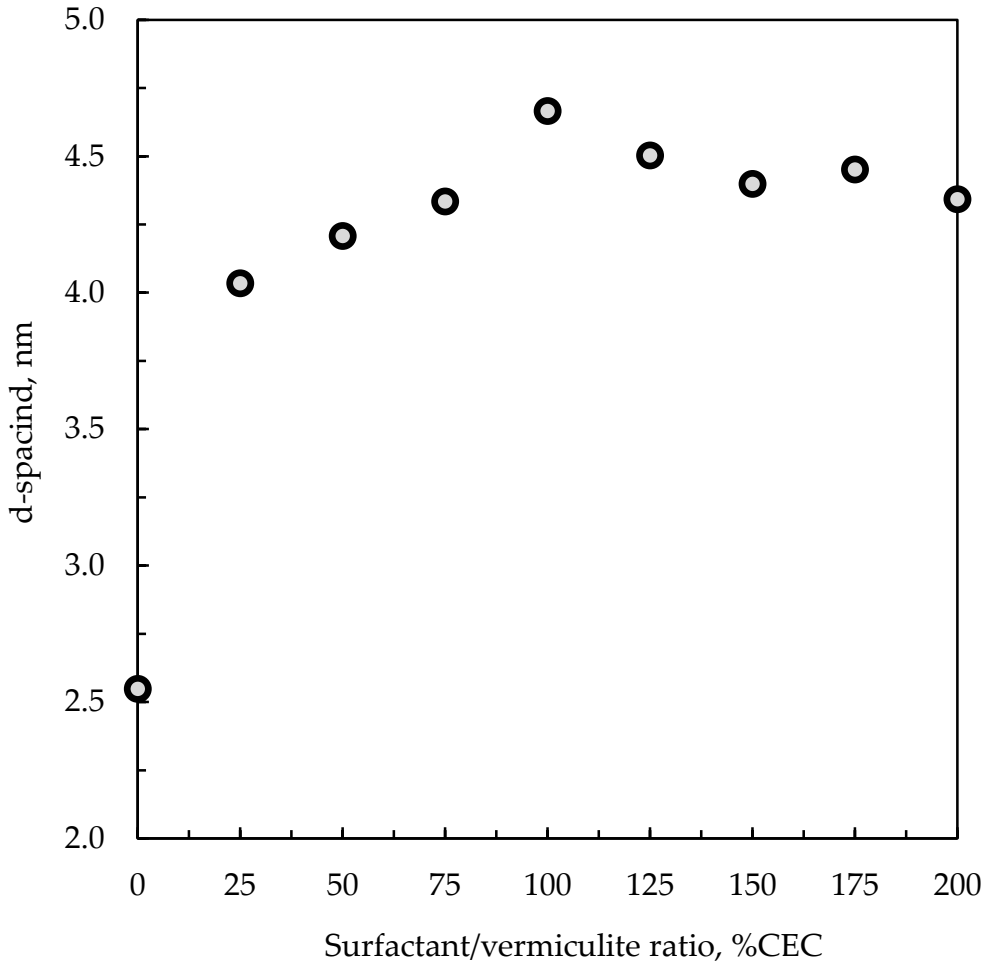

Figure 23. Vermiculite's d-spacing as function of DC10/vermiculite ratio.

Beyond the 100% CEC level, the variation in d-spacing with the amount of surfactant added to the reaction mixture was negligible. The d-spacing assumed an average value of 4.4 nm regardless of the surfactant:vermiculite ratio. This suggests that the excess added to the reaction mixture was not intercalated into the vermiculite galleries because of the clay's high charge density (Zhu *et al.*, 2008).

5.3.3 FT-IR

Fig. 24 shows the FT-IR spectra of the neat vermiculite and the organo-modified materials. The characteristic vermiculite vibration bands are noticeable at: 3420–3446 cm^{-1} (O–H stretching), 1641–1646 cm^{-1} (O–H bending), 995–1000 cm^{-1} (Si–O–Si and Si–

O–Al stretching) and 456 cm^{-1} (Si–O–Mg structural bending) (Hougardy *et al.*, 1970; Farmer, 1974; van der Marel and Beutelspacher, 1976).

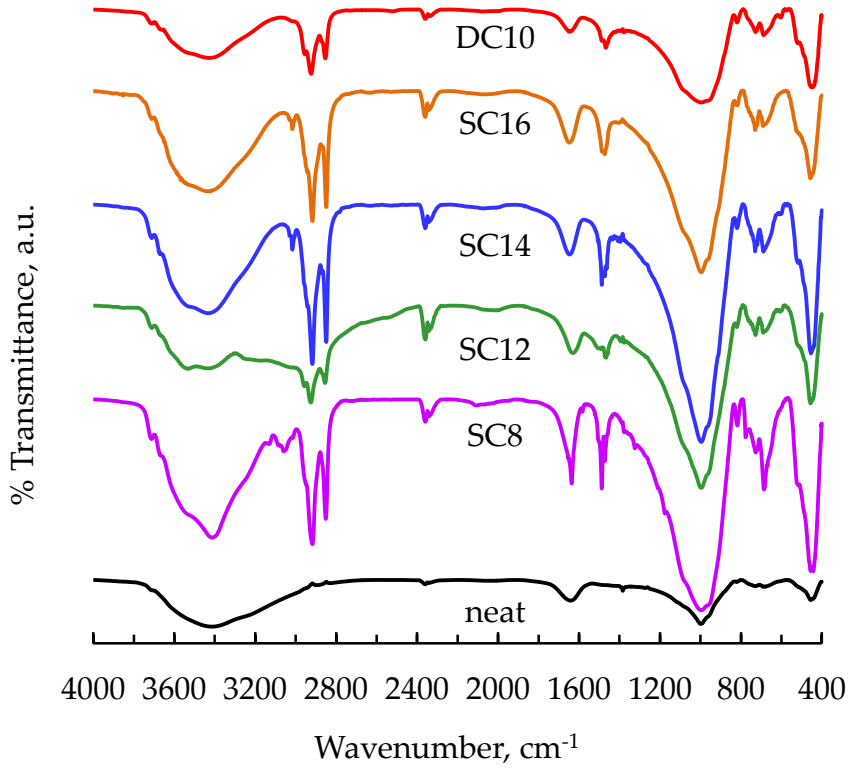

Figure 24. FT-IR spectra of (neat) vermiculite and its organo-modified forms, intercalated with different surfactants.

For the organo-vermiculite, the surfactant's typical strong aliphatic absorption bands are present at 2923 cm^{-1}, $\nu_{as}(CH_2)$, and at 2853 cm^{-1}, $\nu_{s}(CH_2)$, assigned to the CH_2 asymmetric and symmetric stretching vibrations, respectively. CH_2 bending mode, $\delta(CH_2)$, was also observed at 1468 cm^{-1}, suggesting partially ordered interchain interactions (Vaia *et al.*, 1994; Hongping *et al.*, 2004).

Furthermore, all organo-vermiculites prepared with single-chain surfactants exhibited the characteristic CH_3–N head-group asymmetric stretching band [$\nu_{as}(CH_3$–N)] at around 3017 cm^{-1}.

These spectra for the organo-vermiculites were consistent with the aliphatic nature of the intercalated surfactants and, in harmony with the XRD results, confirmed the successful intercalation of the surfactants into vermiculite's galleries.

5.4 CONCLUSIONS

The intercalation of organo-vermiculite was successful to almost the same extent as neat Mg-vermiculite and was restricted to the ion-exchange level (contrary to smectite's behaviour). The maximum degree of intercalation corresponds approximately to that expected for the 150% CEC.

The d-spacing values were proportional to the surfactant's chain length and increased with increasing surfactant:vermiculite ratio up to ca. 100% CEC. The XRD results showed slightly different patterns for both intercalated samples, but without considerable difference, in terms of d-spacing, which increased with increasing surfactant:vermiculite ratio and assumed an average value of 4.4 nm. This sharp reflection suggested expansion of the height of the vermiculite silicate layers in an ordered way. The persistence of the broad mica reflection despite surfactant intercalation indicated that exchange of the K^+ ions by organic molecules did not occur.

Organo-vermiculite's mass loss started below 100 °C and the decomposition onset temperatures were above 200 °C. The total mass loss increased with increasing surfactant molecular weight. The change in the internal surface character from hydrophilic to hydrophobic was attested by the presence of less physisorbed water. On the other hand, the FT-IR spectra for the organo-vermiculites was consistent with the aliphatic nature of the intercalated surfactants.

Later (Section 6.3.1) it is shown that the intercalation of the DC10 surfactant resulted in a lowering of vermiculite's exfoliation onset temperature from ca. 450 °C to ca. 350 °C, with the highest expansion ratio among all analysed surfactants. It is surmised that the decomposition of the intercalated surfactant generated the blowing agents.

REFERENCES

Abate, G., Dos Santos, L.B.O., Colombo, S.M., Masini, J.C., 2006. Removal of fulvic acid from aqueous media by adsorption onto modified vermiculite. Applied Clay Science 32, 261-270.

Burnside, S.D., Wang, H.-C., Giannelis, E.P., 1999. Direct Polymer Intercalation in Single Crystal Vermiculite. Chemistry of Materials 11, 1055-1060.

Cui, L., Ma, X., Paul, D.R., 2007. Morphology and properties of nanocomposites formed from ethylene-vinyl acetate copolymers and organoclays. Polymer 48, 6325-6339.

Da Fonseca, M.G., De Oliveira, M.M., Arakaki, L.N.H., Espinola, J.G.P., Airoldi, C., 2005. Natural vermiculite as an exchanger support for heavy cations in aqueous solution. Journal of Colloid and Interface Science 285, 50-55.

Da Fonseca, M.G., Wanderley, A.F., Sousa, K., Arakaki, L.N.H., Espinola, J.G.P., 2006. Interaction of aliphatic diamines with vermiculite in aqueous solution. Applied Clay Science 32, 94-98.

De Paiva, L.B., Morales, A.R., Valenzuela Díaz, F.R., 2008. Organoclays: Properties, preparation and applications. Applied Clay Science 42, 8-24.

Farmer, V.C., 1974. The Infrared spectra of minerals. Mineralogical Society.

Fornes, T.D., Yoon, P.J., Hunter, D.L., Keskkula, H., Paul, D.R., 2002. Effect of organoclay structure on nylon 6 nanocomposite morphology and properties. Polymer 43, 5915-5933.

He, H., Frost, R.L., Bostrom, T., Yuan, P., Duong, L., Yang, D., Xi, Y., Kloprogge, J.T., 2006. Changes in the morphology of organoclays with HDTMA+ surfactant loading. Applied Clay Science 31, 262-271.

Hongping, H., Ray, F.L., Jianxi, Z., 2004. Infrared study of HDTMA + intercalated montmorillonite. Spectrochimica Acta - Part A: Molecular and Biomolecular Spectroscopy 60, 2853-2859.

Hotta, S., Paul, D.R., 2004. Nanocomposites formed from linear low density polyethylene and organoclays. Polymer 45, 7639-7654.

Hougardy, J., Serratosa, J.M., Stone, W., Van Olphen, H., 1970. Interlayer water in vermiculite: thermodynamic properties, packing density, nuclear pulse resonance, and infra-red absorption. Special Discussions of the Faraday Society 1, 187-193.

Inoue, A., 1984. Thermodynamic study of Na-K-Ca exchange reactions in vermiculite. Clays & Clay Minerals 32, 311-319.

Lagaly, G., 1986. Interaction of alkylamines with different types of layered compounds. Solid State Ionics 22, 43-51.

Lebaron, P.C., Wang, Z., Pinnavaia, T.J., 1999. Polymer-layered silicate nanocomposites: an overview. Applied Clay Science 15, 11-29.

Newman, A.C.D., 1987. Chemistry of clays and clay minerals. Wiley.

Serratosa, J.M., Johns, W.D., Shimoyama, A., 1970. I.R. study of alkyl-ammonium vermiculite complexes. Clays & Clay Minerals 18, 107-113.

Simha Martynková, G., Valášková, M., Čapková, P., Matějka, V., 2007. Structural ordering of organovermiculite: Experiments and modeling. Journal of Colloid and Interface Science 313, 281-287.

Sinha Ray, S., Okamoto, M., 2003. Polymer/layered silicate nanocomposites: a review from preparation to processing. Progress in Polymer Science 28, 1539-1641.

Skipper, N.T., Soper, A.K., Mcconnell, J.D.C., 1991. The structure of interlayer water in vermiculite. The Journal of Chemical Physics 94, 5751-5760.

Tatsuya, T., Komarneni, S., 1999. Alkali metal and alkaline earth metal ion exchange with Na-4-mica prepared by a new synthetic route from kaolinite. Journal of Materials Chemistry 9, 2475-2479.

Theng, B.K.G., 2012. Formation and Properties of Clay-polymer Complexes. Elsevier.

Utracki, L.A., 2004. Clay-Containing Polymeric Nanocomposites, Volumes 1-2. Smithers Rapra Technology.

Vaia, R.A., Teukolsky, R.K., Giannelis, E.P., 1994. Interlayer Structure and Molecular Environment of Alkylammonium Layered Silicates. Chemistry of Materials 6, 1017-1022.

Van Der Marel, H.W., Beutelspacher, H., 1976. Atlas of infrared spectroscopy of clay minerals and their admixtures. Elsevier Scientific Pub. Co.

Williams-Daryn, S., Thomas, R.K., 2002. The intercalation of a vermiculite by cationic surfactants and its subsequent swelling with organic solvents. Journal of Colloid and Interface Science 255, 303-311.

Zhu, R., Zhu, L., Zhu, J., Xu, L., 2008. Structure of cetyltrimethylammonium intercalated hydrobiotite. Applied Clay Science 42, 224-231.

CHAPTER 6
THERMAL EXPANSION BEHAVIOUR OF VERMICULITE

6.1 INTRODUCTION

When heated rapidly to elevated temperatures, vermiculite flakes expand in a vermicular, i.e. worm-like, manner (Walker, 1961; Wada, 1973b; Friedman *et al.*, 1994). The expansion direction is perpendicular to the cleavage planes in a concertina-like fashion. The expansion and partial splitting of the structure are due to sheet exfoliation forced by the explosive release of interlayer water and its transformation into vapour (Baumeister and Hahn, 1976; Justo *et al.*, 1989; Obut and Girgin, 2002). It is conventional to call this expansion "exfoliation", even though the individual sheets that made up the original flake remain attached to each other. During exfoliation the bulk volume can increase by up to 30 times the original volume (Walker, 1951).

It is common understanding that the blowing agent in the neat (mainly Mg^{2+}) vermiculite and other metal-modified vermiculites (e.g. with Li^{+}, Na^{+}, K^{+}, Ca^{2+}, Ba^{2+}) is the interlayer water. The exfoliation is achieved when the inner steam pressure is higher than the forces holding the layers together. For neat vermiculite the exfoliation onset temperature is above 450 °C; in industry, temperatures exceeding 800 °C are employed for the manufacture of exfoliated natural vermiculite.

The exfoliation of vermiculite can also be realised by the release of oxygen generated by the degradation of interlayer hydrogen peroxide (Groves, 1939). Vermiculite's exfoliation only occurs when the force generated by the inner vapour or gas pressure overcomes the ionic bonding forces between the layers (Hillier *et al.*, 2013). Thermomechanical analysis of neat and Na-exchanged vermiculite revealed that the expansion behaviour varied considerably from flake to flake (Muiambo *et al.*, 2010).

Hillier *et al.* (2013) recently offered a plausible and convincing mechanism for the thermal exfoliation of vermiculite. They believe that intra-particle heterogeneities in the form of mosaic-like intergrowths of vermiculite, hydrobiotite and mica play a key role. A contiguous layer traversing a flake may be a vermiculite layer in one place and mica elsewhere. Furthermore, there may be internal boundaries where the nature of the vermiculite interlayer (with hydrated exchangeable cations) changes into a brucite-like interlayer hydroxide of chlorite. Both types of defect prevent complete sheet exfoliation and also act as internal physical barriers that prevent easy escape of the water vapour. The consequence is a build-up of internal pressure that generates forces that inevitably cause exfoliation when they exceed the interlayer bonding forces. The model explains why interstratified vermiculite has the greatest capacity for expansion, why smaller flakes expand less than larger ones, as well as the asymmetry of the exfoliated worm-like (vermiform) particles.

Previous studies have shown that the onset of explosive exfoliation coincides with reaching the 1-WLHS. Furthermore, the event is associated with only a minor loss of water (Muiambo and Focke, 2012). Marcos *et al.* (2003) found that magnesium cations have a very strong affinity for water. Even under vacuum, the dehydration stops at the 1-WLHS, even at temperatures up to 120 °C.

The degree of expansion of vermiculite depends on the flake size, the nature of the interlayer cations, the presence or absence of interstratified phases, the heating rate and the terminal temperature (Justo *et al.*, 1993; Marcos *et al.*, 2009; Muiambo *et al.*, 2010; Huo *et al.*, 2012). For some applications, e.g. intumescent fire barriers, lower exfoliation onset temperatures are desirable (Wada, 1973a;c; Baumeister and Hahn, 1976; Langer and Marlor, 1981; Muiambo *et al.*, 2010). Lowering the exfoliation onset temperature of vermiculite was the prime objective of this study.

6.2 EXPERIMENTAL

TMA experiments were carried out to broadly describe vermiculite and its modified forms.

Thermal expansion measurements were conducted on a TA instruments Q400 thermomechanical analyser. A single flake was sandwiched between the flat surface probe and the bottom surface of a 150 μℓ alumina pan. The flake expansion behaviour was measured under a suitably chosen applied force.

In the dynamic scan experiments the temperature was scanned from 30 °C to 800 °C in nitrogen at a scan rate of 20 °C/min. When the objective was to follow free expansion of the flakes, the lowest possible force (0.001 N) was applied. The thickness of the tested flakes ranged from 30 μm to 467 μm, with an average thickness of 174 μm. The flake expansion behaviour was measured with a flat-tipped standard expansion probe under a small preloaded force, i.e. 0.001 N. The expansion relative to the original flake thickness is reported.

Various heating and cooling protocols, in a nitrogen atmosphere, as well as varying the applied force, were explored. This included recompression of the expanded flake and soaking it in distilled water (added to the alumina pan) in attempts to rehydrate the flake over a period of 48 h. The expansion, compression, rehydration and re-expansion experiments were carried out basically using the following protocol: the sample was first heated to 450 °C and the expansion recorded. The sample was then allowed to cool down to 50 °C. The response to a cyclically applied force progressively increasing in strength was then studied.

6.3 RESULTS AND DISCUSSION

6.3.1 TMA of organo-vermiculites

Palabora vermiculite expands abruptly at above 450 °C and contracts slightly after complete expansion and on cooling. The contraction or negative expansion is also observable during the release of unbound water, at temperatures below 100 °C (Fig. 25 and Fig. 26).

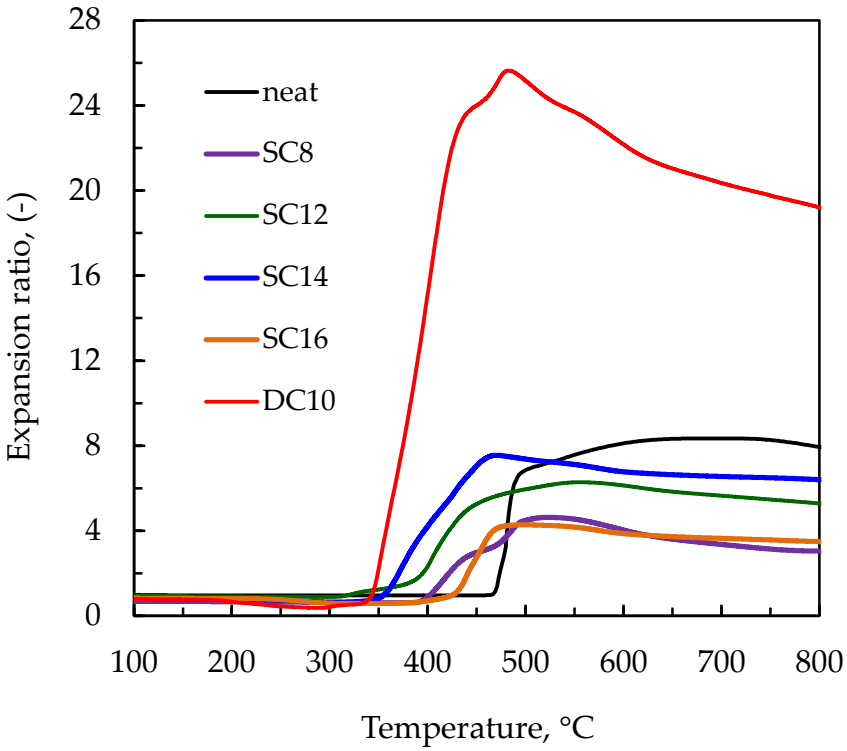

Figure 25. TMA plots of neat vermiculite and its organo-vermiculites prepared at a surfactant:vermiculite ratio of 150% of CEC

Fig. 25 shows the TMA results of neat vermiculite and organo-vermiculites prepared with different surfactants. The free expansion curves, obtained at an initial force of 0.01 N and with constant temperature ramping (Fig. 25), showed a rather abrupt rise at the expansion onset temperature, followed by a more gradual expansion over a temperature range of several hundred degrees Celsius.

Intercalation of long-chain surfactants, at 150% CEC, also resulted in a lowering of the vermiculite's exfoliation onset temperature, but to a different extent. No

relationship between the surfactant's structure and its exfoliation onset temperature or expansion ratio could be found. It was surmised that the intercalated surfactant's decomposition products (low molecular weight organic species) acted as blowing agents and caused the expansion on heating.

DC10 organo-vermiculite showed a reasonable decrease in the exfoliation onset temperature from ca. 450 °C to ca. 350 °C. Interestingly, it also showed the best flake expansion ratio (25 times, in contrast to 8 times in the neat vermiculite), despite the fact that it contained less water in the galleries due to its hydrophilic character.

Comparison of the TGA and TMA data shows that the rapid expansion is associated with only a very low mass loss and that it occurs only after a considerable portion (ca. 50%) of the intercalant has already been lost. This result is unexpected and implies that the mechanism responsible for the expansion of organo-modified vermiculites needs further clarification.

6.3.2 TMA of inorgano-vermiculites

In Tables 15 and 16 and Figs 26 - 34 a summary of the TMA results for neat vermiculite, its ion-exchanged forms and the corresponding urea-modified materials is shown.

Table 15. Summary of TMA expansion ratio results. The results pertain to single flakes using an applied force of 0.001 N.

	Expansion ratio, -			
Vermiculite form	**Minimum**	**Maximum**	**Average**	**Std. Dev.**
Multivalent	5.3	8.6	7.1	1.3
Urea-modified	5.0	14.7	8.3	3.0
Sodium-exchanged	6.1	8.6	7.4	0.9

The data in Table 15 indicate that the maximum expansion ratio is not affected by the type of modification. However, the expansion onset temperature does depend on the nature of the modification (Table 16).

Water is considered the exclusive blowing agent for neat vermiculite and for the samples that did not contain urea (Hillier et al., 2013). According to the TGA data (Figs 14 to 17), during expansion there is a related release of less than 1 wt.% of water.

Table 16. Expansion onset temperature of different vermiculites

Expansion onset temperature, °C				
Vermiculite form	**Minimum**	**Maximum**	**Average**	**Std. Dev.**
Multivalent	440	467	456	11
Urea-modified	174	290	209	35
Sodium-exchanged	232	304	272	21

Fig. 26 shows an overlay of the TMA expansion curve for Mg(urea)-vermiculite and the TGA mass loss curve for neat urea. Urea starts to decompose well below 200 °C, releasing ammonia and water vapour which act as the blowing agents. The TMA curve suggests that the intercalated urea shows a slightly higher thermal stability.

Abramova et al. (2007) previously studied the thermal decomposition of intercalated urea-clay complexes. They found that the thermal degradation products are distinctly influenced by the nature of the interlayer cation. The lower expansion onset temperature of the urea-modified vermiculites is attributed to the low thermal stability of urea.

mmol

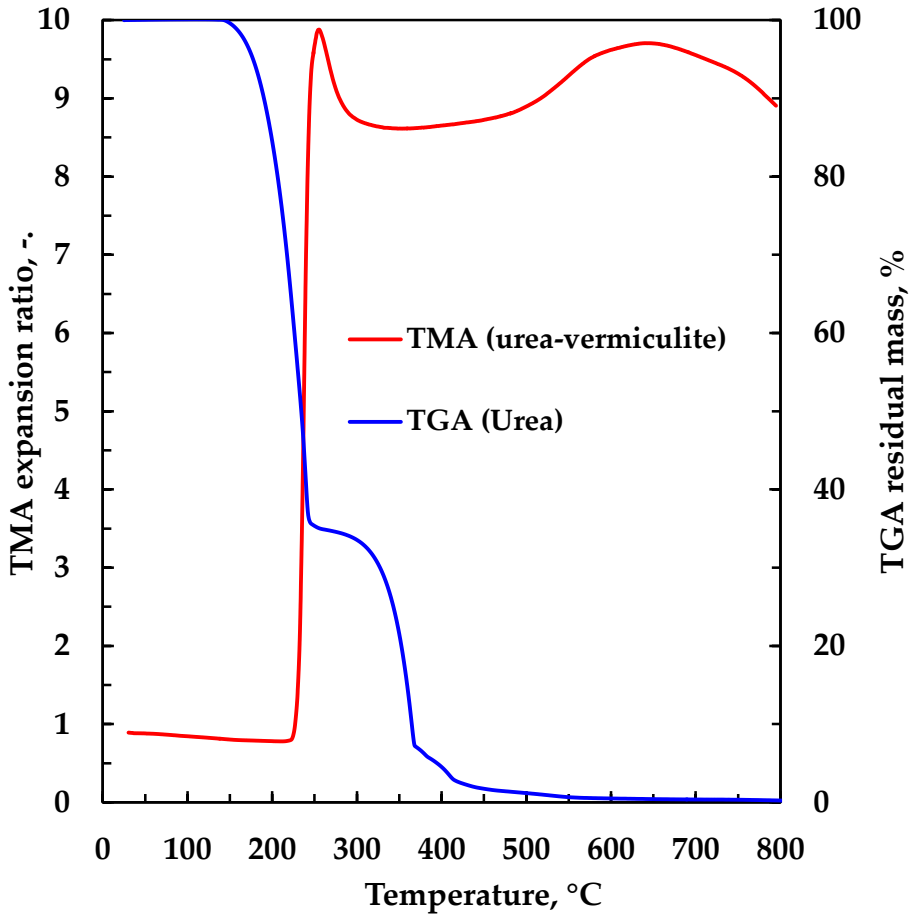

Figure 26. TGA plot of pure urea and TMA graph of urea-vermiculite.

Fig. 27 shows that ion exchange with Mg^{2+}, Al^{3+} or Fe^{3+} cations did not materially change the exfoliation onset temperature nor the maximum expansion ratio of the vermiculite. This was the case despite the fact that the water content had increased (according to the TGA results in Section 4.4). This detail highlights the fact that not all the water released before the exfoliation plays a role in the exfoliation phenomenon. Similar results were found in previous studies of vermiculite modified with ammonium, alkaline and alkaline earth metals (Muiambo and Focke, 2012).

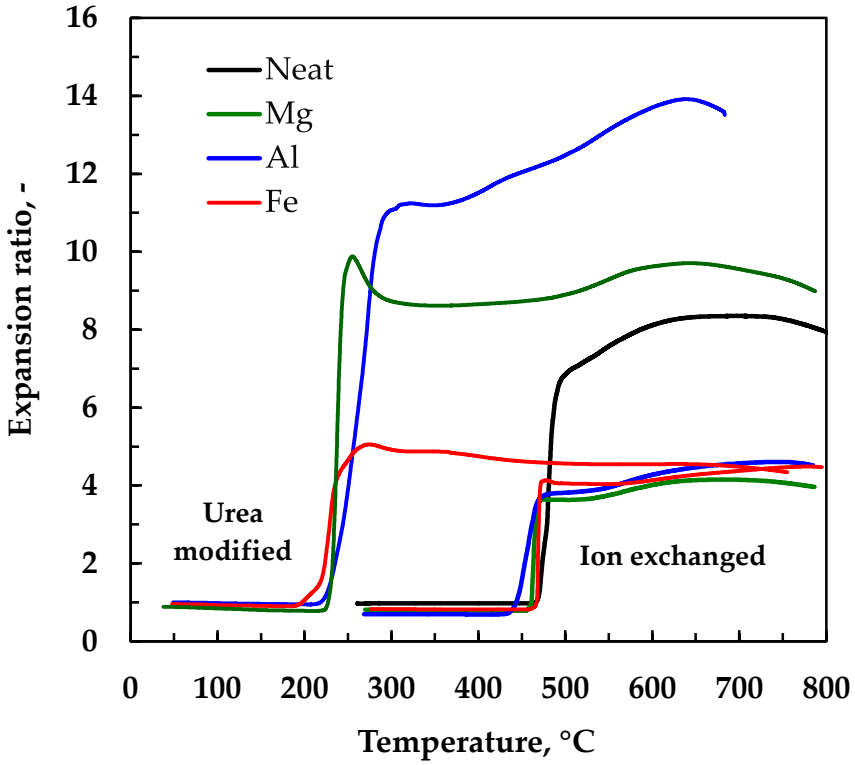

Figure 27. Comparison of the thermal expansion behaviours of neat Palabora vermiculite and its multivalent ion-exchanged versions with the corresponding urea-modified forms. Single flakes were heated up to 800 °C at 20 °C min^{-1} under an applied force of 0.001 N in a nitrogen atmosphere.

Previously it was found that exchanging the magnesium in the interlayers with sodium reduces the expansion onset temperature of neat vermiculite by about 165 °C (Muiambo et al., 2010). The present urea-modified forms feature an even lower expansion onset temperature (209 ± 35 °C), which is within the intumescent systems activation temperature range (Morgan and Gilman, 2013).

a) Isothermal expansion

The expansion of inorganic vermiculites is characterised by an induction time before a sigmoidal expansion occurs.

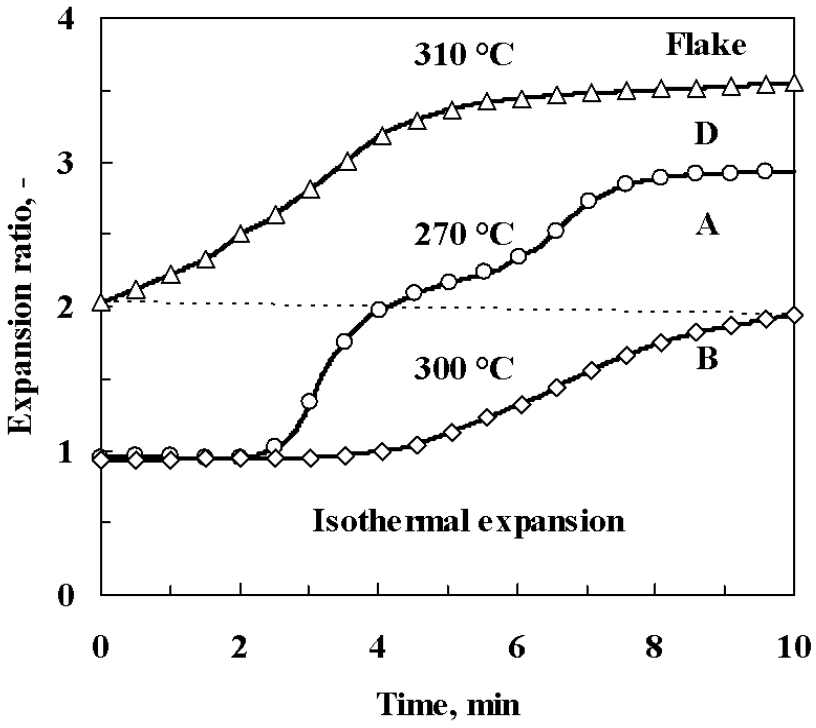

Figure 28. TMA characterisation of the isothermal expansion of Na-exchanged vermiculite, at selected temperatures

Fig. 28 shows the effect of the stepped-temperature-increase protocol on the expansion behaviour of Na-vermiculite. It reveals considerable variability in the behaviour of the individual flakes. Notably, significant expansion occurred during the isothermal periods. This is indicated by the staircase-like expansion as a function of time. The expansion of Flake "A" commenced at the first isothermal hold temperature of 270 °C. Remarkably, in at least two of these curves, the expansion was characterised by an induction time before a sigmoidal expansion occurred. It is assumed that water is continuously lost as time proceeds during the isothermal period. The observed time delay then suggests that expansion was triggered when a critical water content level was reached inside the interlayer space.

The expansion of Flake "A", at the hold temperature of 270 °C, actually took place in two distinct steps. This can be explained by assuming that the composition of the flakes is not homogeneous along the c-axis, i.e. that the vermiculite content varies with distance along the c-axis (flake thickness).

b) Effect of flake thickness on expansion ratio

Some variability in the onset temperature as well as in the expansion ratio of the individual flakes of the same sample was observed in most of the vermiculites analysed.

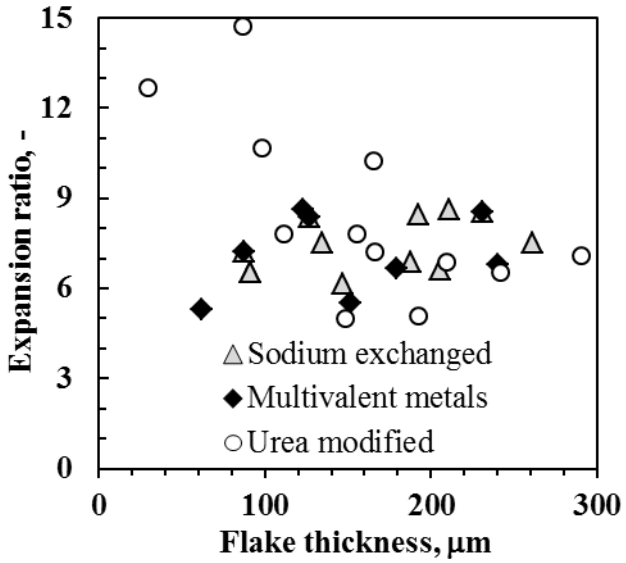

Figure 29. The relationship between the flake thickness and the maximum expansion ratio measured at an applied force of 0.001 N

Fig. 29 shows that there is no correlation between the flake size and the expansion ratio for the three types of vermiculite considered. More scattered data were observed when the clay had been modified with different multivalent metal-urea complexes. This variance in the expansion ratio of metal-urea complexes can be explained by the different compositions of the complexes, essentially their urea content.

c) Effect of strength of applied force on the degree of expansion

Fig. 30 demonstrates the effect of the strength of applied force on the degree of expansion. The curves represented at (A) correspond to Mg(urea)-modified vermiculite (onset at 220 °C) and at (B) to neat vermiculite (onset at 475 °C), as a function of different applied forces.

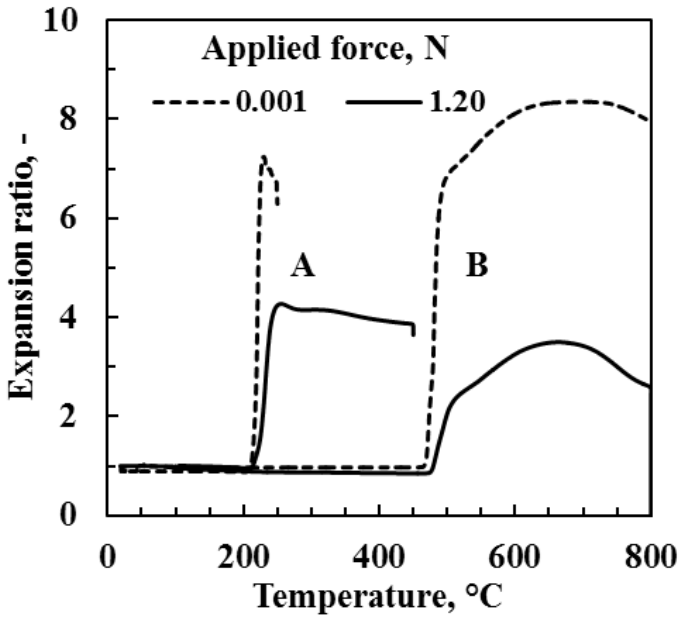

Figure 30. Thermomechanical expansion of (A) Mg(urea)-modified vermiculite and (B) neat vermiculite as a function of different applied forces

Although the expansion onset behaviour of individual flakes showed considerable scatter (also observed when applying same force), indications are that flake expansion (at onset) was reduced when higher forces were applied during the expansion experiments.

d) Reversibility of vermiculite's expansion

The results of an expansion, compression, rehydration and re-expansion experiment on a Mg(urea)-vermiculite sample are reported in Figs 31 and 32. The experimental protocol was as follows: the sample was first heated to 450 °C and the expansion recorded. The sample was then allowed to cool down to 50 °C. The response to a cyclically applied force increasing progressively in strength was studied in the course of the experiment.

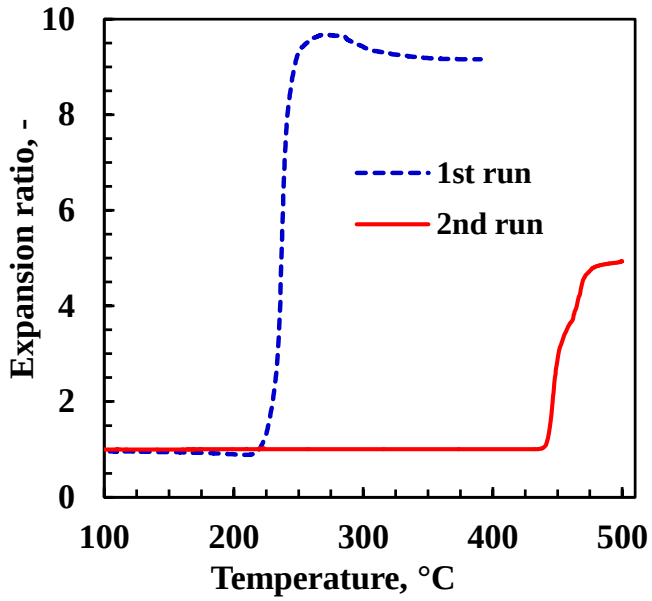

Figure 31. Recovery of the capacity of expansion. 1st run: heating a single Mg-urea-modified vermiculite flake to 450 °C under an applied force of 0.001 N. 2nd run: re-heating the same rehydrated vermiculite flake to 500 °C after it had been allowed to cool down, been recompressed and soaked for 48 h in distilled water.

Nearly full compression to the original thickness was achieved after the final load of 0.64 N had been applied. The compressed flake was then removed and soaked in distilled water for 48 h. Thereafter it was reloaded into the TMA and the experiment was repeated. The only difference was that the temperature was now scanned up to 500 °C. Note that Fig. 31 clearly shows that the presence of urea reduces the exfoliation onset temperature: In the second run water is the sole blowing agent and the exfoliation temperature is significantly higher and consistent with the behaviour of neat vermiculite.

Fig. 31 depicts the expansion behaviour as a function of the scanning time, starting from the lowest temperature. The expansion curve (1st run) exhibited the expected onset at around 215 °C, due to the release of urea and its volatile degradation products. After rehydration (48 h), the same flake showed thermomechanical behaviour similar to that of the neat or Mg-vermiculite (2nd run), i.e. it displayed an

increase in the expansion onset temperature to around 428 °C (2nd run). This illustrates the reversibility of vermiculite's expansion properties and also confirms that neat vermiculite's interlayer environment was successfully modified with urea molecules. Comparable results were obtained with metal-vermiculite flakes, except that the onset temperatures differed.

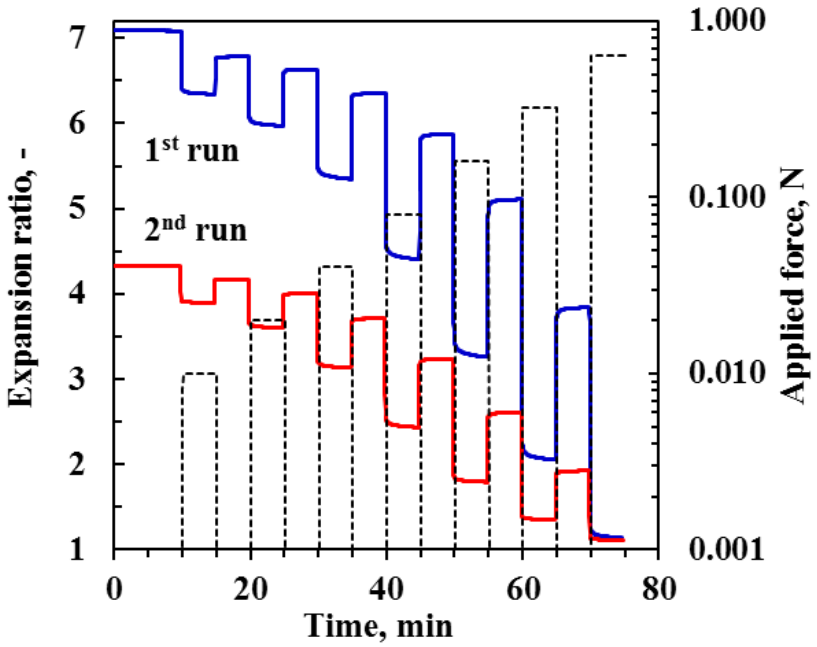

Figure 32. The effect of different TMA applied forces on the compression of the same vermiculite flake described in Fig. 15. The measurements were done at 50 °C. The applied force was doubled after each compression cycle.

Fig. 32 shows the effect of progressively applying, stepwise, an increased force using the TMA, followed by a reduction to a small force of 0.001 N. After each step increase in the applied force there is a rapid decrease in the flake height, followed by a much slower reduction over time. When the force is reduced, the sample height recovers, but not fully. In addition, a rapid recovery is followed by a slower increase in height. This implies that the expanded worm-like flake behaves like a spring, showing both hysteresis and slight creep behaviour.

These observations can be explained in terms of the model postulated by Hillier *et al.* (2013) as follows. The expanded vermicular form comprises numerous partially delaminated sheets stacked on top of each other. Probably the rapid expansion caused most, if not all, of these sheets to become mechanically deformed and distorted, i.e. bent, twisted, warped, buckled, etc. The mosaic-like defect patterns keep the whole structure together in a state of static equilibrium.

However, when a large mechanical force is applied, the distorted sheets are flattened out and the original flake dimensions are approached. The original vermiculite structure is almost fully recovered when the compacted particle is equilibrated with water as it recovers the ability to expand again.

When a smaller force is applied, only some of the warped sheets revert to the straightened state. The fraction flattened depends on the force that is applied. This explains the hysteresis observed in Figs 32 to 35: an expanded flake does not recover its fully expanded height once a force has been applied. Furthermore, the extent of the recovery decreases as the compression force increases.

e) Effect of a cyclically applied force on expansion and compression

When a TMA constant force (0.5 N) is cyclically applied to an expanded vermiculite flake (at 50 °C), it shrinks slightly (Fig. 33). When the force is released, it tends to recover from the deformation, but not fully.

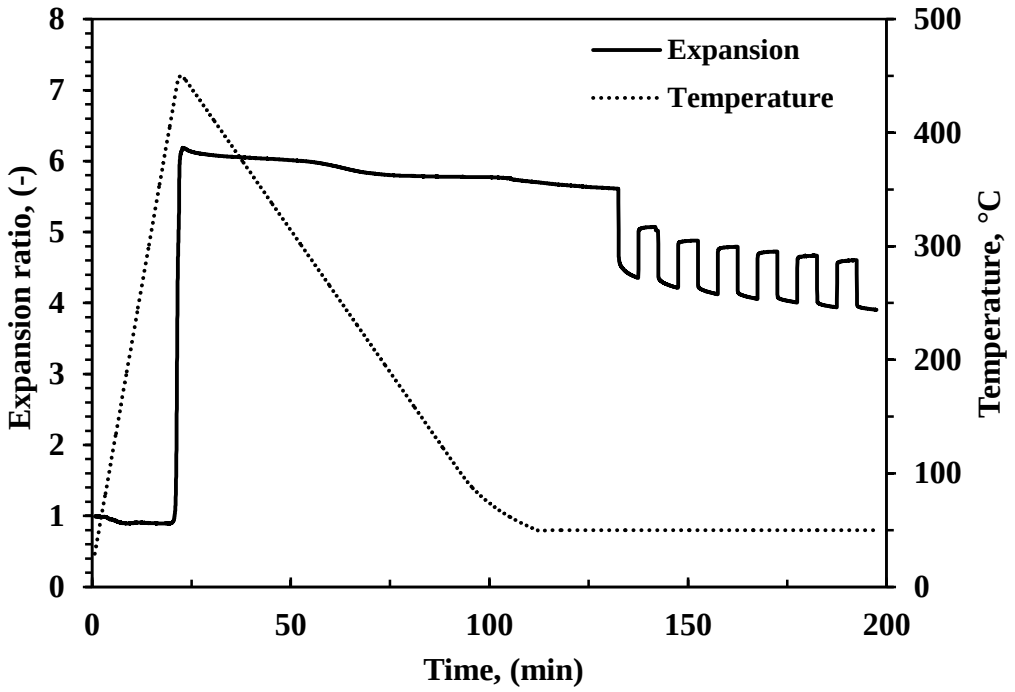

Figure 33. Effect of the TMA applied constant force (0.5 N) on the expansion and compression behaviour of the expanded (at 450 °C) neat vermiculite flakes

Fig. 34 shows neat vermiculite's behaviour when subjected to three equal cycles (0–200 min, 200–400 min and 400–600 min). When the TMA applied force is exponentially increased, the creeping is even more evident (from 150 to 200 min) and at 0.64 N the expanded flake eventually reverts to its initial dimension (just before 200 min). However, if the same flake is again subjected to an identical heating cycle (from 200 to 240 min), it does not expand substantially and it retains its initial expanded dimension as soon as the applied force is released. The very same behaviour is observed during the third cycle (from 400 to 600 min).

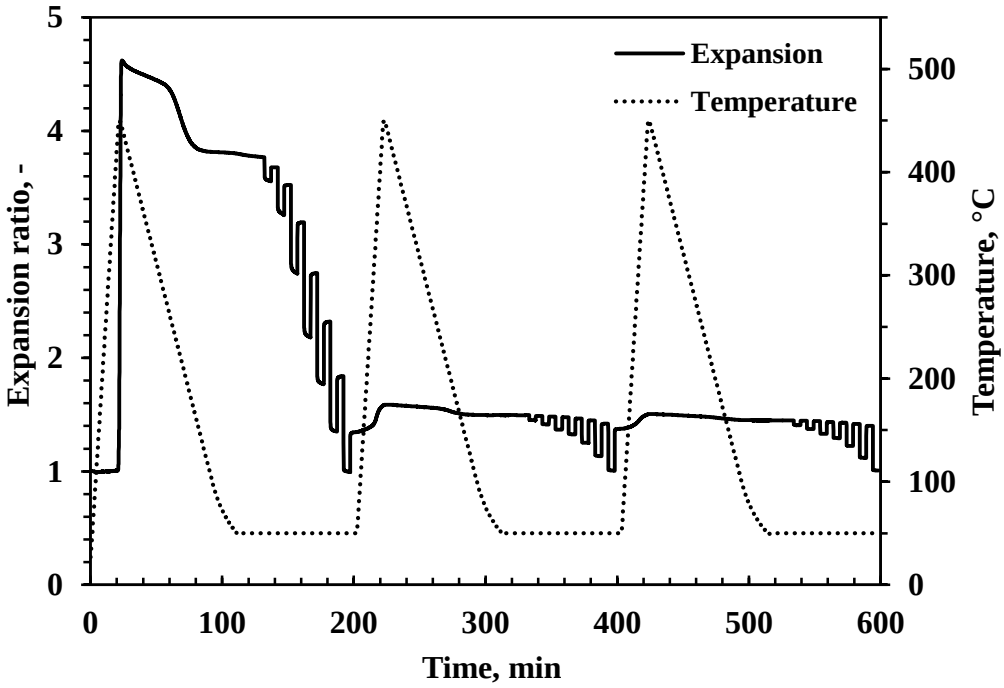

Figure 34. Effect of different TMA applied forces (at 50 °C) on the expansion and compression behaviour of the expanded (at 450 °C) Mg(urea)-vermiculite flakes

These results suggest that these experimental conditions could not allow vermiculite flakes to rehydrate spontaneously (from the environment) after expansion at 450 °C and on cooling. So, the initial dimension and structure could not be recovered and as consequence the extension of expansion could not be fully reversed as well. Nevertheless, a residual and similar spring behaviour was observed in the subsequent cycles.

The expansion:compression ratio of the expanded vermiculite flakes was also studied as a function of the applied force after expansion at 800 °C (Fig. 35).

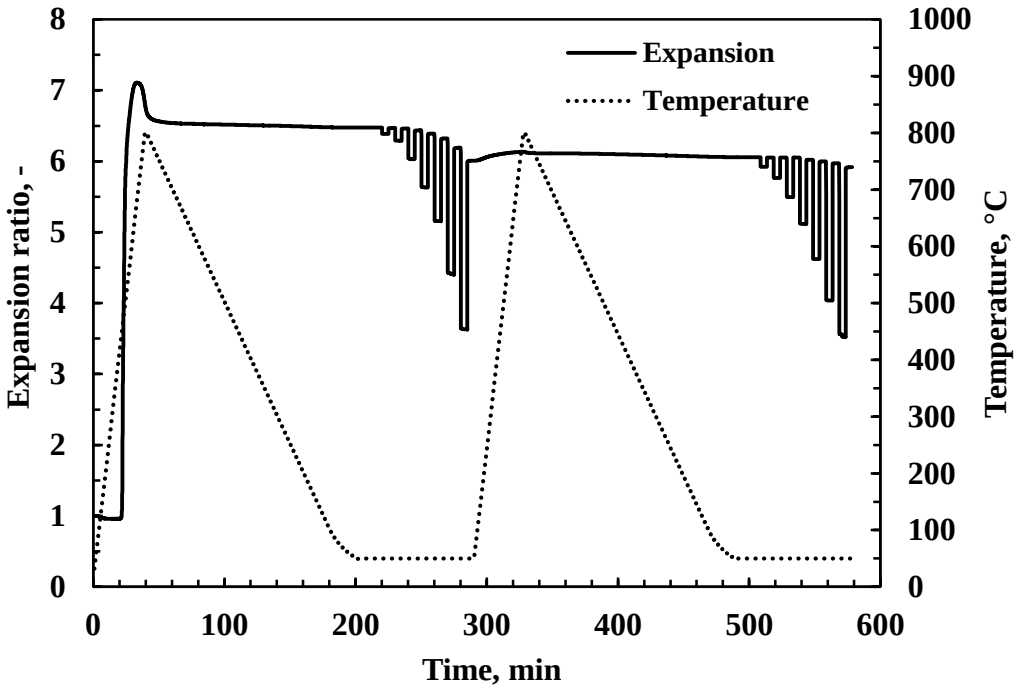

Figure 35. Effect of different TMA applied forces (at 50 °C) on the expansion and compression behaviour of the fully expanded (at 800 °C) neat vermiculite flakes

After the first expansion, at 800 °C, the force required to compress the flakes is relatively low compared with the following cycles. Actually, from the second expansion, the force required to compress vermiculite flakes to a certain magnitude is quite similar. A constant force of as high as 1.0 N is necessary to compress a single expanded flake to its original c-axis dimensions (see also Appendix VII).

6.4 CONCLUSIONS

The expansion behaviour of Palabora vermiculite modified by intercalation of organic surfactants and by ion exchange, in the presence or absence of urea, was studied.

The maximum expansion ratio was independent of the flake thickness and the nature of the modification. Ion exchange with Mg^{2+}, Al^{3+} and Fe^{3+} did not materially affect the macroscopic appearance, the expansion ratio and the expansion onset temperature. However, co-intercalation of urea did reduce the expansion onset temperature of vermiculite, from above 450 °C to within the intumescent systems activation temperature range (209 ± 35 °C). This is attributed to the low thermal stability of the intercalated urea which decomposes and releases ammonia and water vapour as blowing agents. Mg^{2+} and Al^{3+} complexes showed a remarkably better exfoliation ratio, respectively 10 and 11.5 times the initial flake dimension.

Ion-exchanged vermiculites also showed spring-like behaviour with hysteresis. The original flakes were almost perfectly flat, but after expansion the individual sheets assumed a buckled arrangement. The preservation of the mosaic-like flaws during modification provided the needed bonding between the sheets. Adjacent sets of sheets could still snap back to the initial flattened and more stable state when subjected to a compressive force. When the compressive force was removed, only part of the expansion could be recovered.

Application of a compressive force sufficient to compact an expanded (at temperatures up to 450 °C) vermiculite flake to the original dimensions, followed by equilibration with liquid water, did result in reconstitution into vermiculite flakes that showed the usual exfoliation behaviour.

At low compressive forces the vermicular structure shows spring-like behaviour (with hysteresis), which can be explained in terms of the vermiculite model postulated by Hillier *et al.* (2013). The expansion of vermiculite flakes can be viewed as a bifurcation of potential equilibrium states. In the original particle the flakes are almost

perfectly flat. In the secondary expanded state the individual sheets comprising a flake assume a buckled configuration. Overall, the structure is stabilised by the system of mechanical interconnects which prevents complete expansion or exfoliation/delamination. Ultimately, it is the mosaic-like flaws present in the original particle that provide the bonding that holds the sheets together. Individual sheets or, more likely, neighbouring sets of such sheets can snap back to the initial flattened and more stable state when subjected to a compressive force. Since the nature of the buckling varies among sheets, whether they will buckle will depend on the strength of the applied compression force. This explains why only part of the expansion is recovered when the compressive force is removed.

REFERENCES

Abramova, E., Lapides, I., Yariv, S., 2007. Thermo-XRD investigation of monoionic montmorillonites mechanochemically treated with urea. Journal of Thermal Analysis and Calorimetry 90, 99-106.

Baumeister, W., Hahn, M., 1976. An improved method for preparing single crystal specimen supports: H2O2 exfoliation of vermiculite. Micron 7, 247-251.

Friedman, S.D., Mckinney, R.W., Ou, C.C., Spotnitz, R.M., Wu, S., 1994. Vermiculite ore concentrate with specified specific density. Google Patents.

Groves, R.C., 1939. Exfoliation of Vermiculite by Chemical Means. Nature 144, 554-554.

Hillier, S., Marwa, E.M.M., Rice, C.M., 2013. On the mechanism of exfoliation of 'Vermiculite'. Clay Minerals 48, 563-582.

Huo, X., Wu, L., Liao, L., Xia, Z., Wang, L., 2012. The effect of interlayer cations on the expansion of vermiculite. Powder Technology 224, 241-246.

Justo, A., Maqueda, C., Perez-Rodríguez, J.L., Morillo, E., 1989. Expansibility of some vermiculites. Applied Clay Science 4, 509-519.

Justo, A., Pérez-Rodríguez, J.L., Sánchez-Soto, P.J., 1993. Thermal study of vermiculites and mica-vermiculite interstratifications. Journal of Thermal Analysis 40, 59-65.

Langer, R.L., Marlor, A.J., 1981. Intumescent sheet material. Google Patents.

Marcos, C., Arango, Y.C., Rodriguez, I., 2009. X-ray diffraction studies of the thermal behaviour of commercial vermiculites. Applied Clay Science 42, 368-378.

Marcos, C., Argüelles, A., Ruiz-Conde, A., Sánchez-Soto, P.J., Blanco, J.A., 2003. Study of the dehydration process of vermiculites by applying a vacuum pressure: Formation of interstratified phases. Mineralogical Magazine 67, 1253-1268.

Morgan, A.B., Gilman, J.W., 2013. An overview of flame retardancy of polymeric materials: Application, technology, and future directions. Fire and Materials 37, 259-279.

Muiambo, H.F., Focke, W.W., 2012. Ion exchanged vermiculites with lower expansion onset temperatures. Molecular Crystals and Liquid Crystals 555, 65-75.

Muiambo, H.F., Focke, W.W., Atanasova, M., Der Westhuizen, I.V., Tiedt, L.R., 2010. Thermal properties of sodium-exchanged palabora vermiculite. Applied Clay Science 50, 51-57.

Obut, A., Girgin, I., 2002. Hydrogen peroxide exfoliation of vermiculite and phlogopite. Minerals Engineering 15, 683-687.

Wada, T., 1973a. Manufacture of expanded vermiculite employing a urea compound and low temperatures. Google Patents.

Wada, T., 1973b. Method for the expansion of vermiculite. Google Patents.

Wada, T., 1973c. Method for the expansion of vermiculite. Google Patents.

Walker, G.F., 1961. Vermiculite minerals, in: Brown, G. (Ed.), The X-ray identification and crystal structures of clay minerals. Mineralogical Society, London, pp. 297-342.

CHAPTER 7
MODIFIED VERMICULITE/POLYMER COMPOSITES

7.1 ORGANO-VERMICULITE/LLDPE COMPOSITES

7.1.1 Introduction

Linear low-density polyethylene (LLDPE) is one of the most widely used commodity polymers. It is in high demand due to its low cost and the ready availability of the ethylene building block. LLDPE is used in a wide variety of applications, which include wire and cable insulation, pipes, plastic bags and wraps, containers, covers and lids, toys, etc. It has good chemical resistance, mechanical durability, low toxicity, good electrical insulation and easy processability (Li *et al.*, 2009; Intratec, 2013).

Vermiculite-polymer nanocomposites with improved mechanical properties, as well as good flame-retardant and intumescent properties, are discussed in the literature, although less frequently than other clay minerals (montmorillonite, hectorite and saponite) which are relatively less abundant and much more expensive (Liu *et al.*, 2005; Gomes *et al.*, 2009; Qiu *et al.*, 2011). On the other hand, vermiculite-polyethylene (PE) or polypropylene (PP) nanocomposites are also much less studied due to the non-polar chemical structure of the olefin chain. Furthermore, the relatively high crystallinity of LLDPE also obstructs homogeneous distribution of filler additives (Dufton, 1995).

Some tangible results were obtained using maleic anhydride grafted polyethylene (PE-g-MA), maleic anhydride grafted polypropylene (PP-g-MA), maleic anhydride grafted ethylene vinyl acetate (EVA-g-MA) or low molecular weight oxidised polyethylene (OxPE) as compatibilisers (Tjong *et al.*, 2002; Tjong and Meng, 2003; Hotta and Paul, 2004; Chrissopoulou *et al.*, 2005; Lee *et al.*, 2005; Durmuş *et al.*, 2007; Rosa *et al.*, 2008; Li *et al.*, 2009; Valášková *et al.*, 2009). However, some other

publications also considered compositions without any additive (Tjong *et al.*, 2002; Valášková *et al.*, 2009; Valášková *et al.*, 2013).

DC10 (prepared and characterised as described in Chapter 5) was chosen for the preparation of polymer composites. It is easily prepared from a liquid surfactant, its organo-vermiculite has a reasonable (17%) organic content, a d-spacing around 4.4 nm, a lowered expansion onset temperature and the best expansion ratio among the surfactants considered. DC10 therefore has the best combination of both organic content and interlayer space enlargement, which can provide good insertion of non-polar polymer chains (Utracki, 2004). It was used without any additional compatibiliser in an attempt to improve the properties of LLDPE composites. The aim was to enlarge the application range of this commodity polymer in an environmentally friendly and cost-effective manner.

7.1.2 Experimental

Rotomoulding grade HR411 (density 0.939 g/cm^3), 1-hexene random copolymer-based LLDPE was supplied by Sasol Polymers (South Africa).

For the preparation of the composites the melt processing technique was used involving a co-rotating twin-screw extruder with intermeshing kneader elements and a forward transport action. This technique is already the standard approach to the preparation of polymer-layered silicate nanocomposites. It is the simplest, most economically favourable method for industrial applications, is very flexible regarding formulation and requires only equipment (e.g. for extrusion or injection moulding) already in use for commercial purposes (Paul and Robeson, 2008; Kiliaris and Papaspyrides, 2010). The DC10 organo-vermiculite was dried in an air circulating oven at 80 °C overnight. It was then mixed manually with LLDPE powder and a 20 wt.% vermiculite masterbatch was loaded into the compounder and extruded. The masterbatch strands were cooled in water, air dried, pelletised and then milled into a fine powder in a Pallmann 300 Series pulveriser, under liquid nitrogen. Four subsequent batches, with the following nominal vermiculite concentrations (wt.%),

were prepared: 10.0, 7.5, 5.0 and 2.5. All batches were prepared following the same procedures and parameters: temperature profiles from 100 to 190 °C and motor speed at 50 rpm.

TGA was performed by the dynamic method on a Mettler Toledo A851 TGA/SDTA instrument. For TGA, a sample of about 15 mg was placed in an open 150 µl alumina pan. The temperature was scanned from 25 to 1 000 °C at a rate of 10 °C min^{-1} with air or nitrogen flowing at a rate of 50 mℓ min^{-1}.

Crystallisation and melting behaviour were assessed on a Mettler Toledo DSC instrument. Samples of about 5 mg were placed in aluminium pans with a small hole in the lid. The samples were heated (and cooled) from – 40 °C to 220 °C at a scan rate of 10 °C min^{-1}. The heating and cooling runs were carried out under nitrogen flowing at 50 mℓ min^{-1}.

XRD data were obtained on a PANalytical X-pert Pro powder diffractometer instrument. The instrument features variable divergence and receiving slits and an X'celerator detector using Fe filtered with CoK_α radiation ($\lambda = 0.17901$ nm). Refinement of diffraction data, phase identification and data manipulation were done using X'Pert High Score Plus software.

Type IV ASTM specimens for mechanical tests were prepared using an Engel 3040 injection moulding machine. The temperature profiles, from the hopper to the nozzle, ranged from 190 to 200 °C. A clamping force of 350 kN was applied and the stroke was 22 mm. The tensile properties of LLDPE and its composites were studied using a Lloyds Instruments LRX Plus, at room temperature, according to ASTM D638-M standard. The cross-head speed was set at 5 mm min^{-1}. Five Type IV specimens of each composition were tested; the average values and the standard deviations are reported.

A dynamic mechanical analysis (DMA) of the injection moulded samples was done using a Perkin-Elmer 8000 dynamic mechanical analyser, in a single cantilever bending mode. The frequency was set to 1 Hz; the temperature was scanned at 2 °C min^{-1} and ranged from – 80 °C to 120 °C.

The injection moulded specimens were cryogenically fractured in liquid nitrogen. The composites were coated three times with carbon under argon gas using a Polaron Equipment Ltd E5200 automatic sputter coater. The fracture surface and the interfacial adhesion morphology of the fractured specimens were examined by field emission SEM (JEOL 5400).

The ISO 5660-1 standard was followed in performing the cone calorimeter tests using a Dual Cone Calorimeter (Fire Testing Technology (UK) Ltd). Three specimens of each composition were tested. The sheet dimensions were 100 mm × 100 mm × 3 mm. The specimens were placed on aluminium foil and exposed, separated horizontally, to an external heat flux of 35 kW m^{-2}. This heat flux was chosen on the basis of the study conducted by Wang *et al.* (1988). They studied polymer sheets 3 mm to 10 mm thick at heat fluxes of 25, 35 and 50 kW m^{-2}. They found that the time to ignition varied linearly with the inverse of the cone calorimeter heat flux. Furthermore, the minimum heat flux for ignition of sheets in this thickness range was found to be about 19 kW m^{-2}. A hold-down frame was used to minimise the swelling and consequent interference from intumescence. The exhaust gas flow rate was set at 24 ℓ s^{-1}. The heat released was calculated from the oxygen consumption. The time to ignition was manually set from the computer's keyboard. The mass loss rate, and the heat release rate and its peak value were obtained directly from the Fire Testing Technology "ConeCalc" software.

7.1.3 Results and discussion

a) TGA and DSC

The thermal decomposition behaviour in air of LLDPE and of the vermiculite composites is compared in Fig. 36. As expected, the neat LLDPE volatilised completely. The onset temperature was ca. 259 °C and the maximum rate was observed at T_{max} = 444 °C.

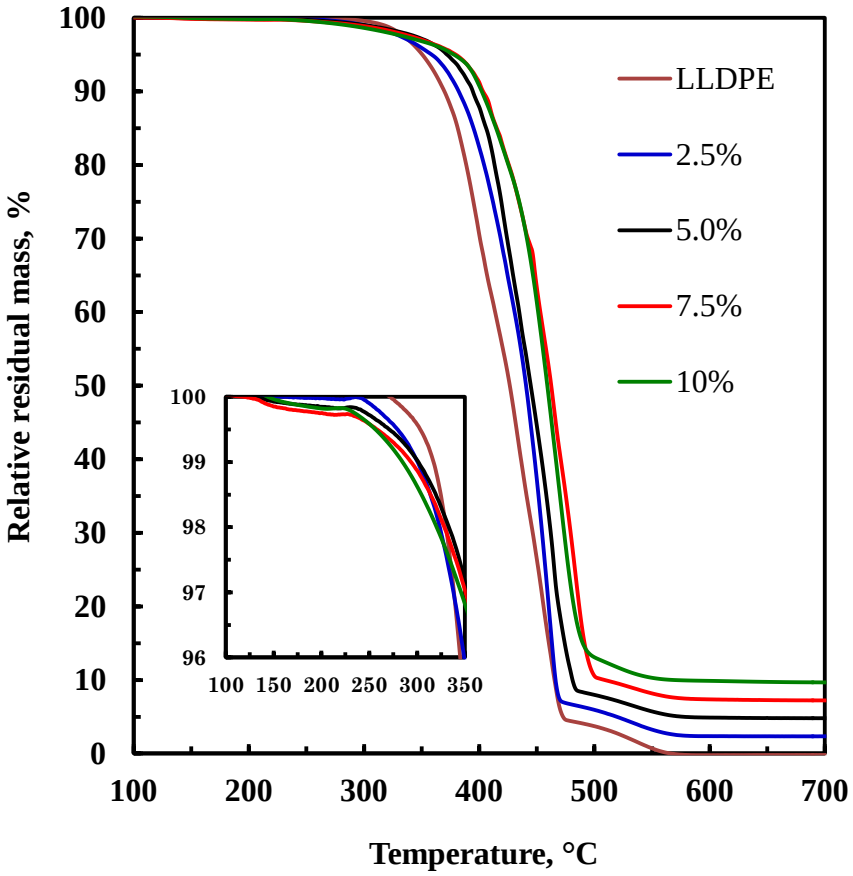

Figure 36. Effect of organo-vermiculite content on thermal degradation of LLPDE composites, in air.

From Fig. 36 one can clearly see that the organo-vermiculite had two distinctive actions on the thermal stability of the composites. At lower temperatures (inset) the organo-vermiculite catalysed the degradation, while at relatively high temperatures it

acted as a mass transfer or heat shield barrier, improving the apparent thermal stability (Zhao *et al.*, 2005).

The composites showed multi-stage decomposition and a residue remained even at 700 °C. All composites showed better thermal stability, with respect to the degradation onset temperature, in both air and nitrogen (not shown) atmospheres. At the point when 50% mass loss of the total had occurred, there was a 10% shift in the temperature from 420 to 459 °C, up to the maximum temperature of 700 °C. The quantity of the residue at 700 °C equalled or exceeded the nominal organo-vermiculite content.

Table 17. DSC and DTG data of LLDPE and its organo-vermiculite composites

Clay, wt.%	**0**	**2.5**	**5.0**	**7.5**	**10.0**
$\Delta H_{crystal}$ ($J.g^{-1}$)	95.9	110.3	87.8	90.5	87.3
Tm (°C)	126	127	127	127	127
Tc (°C)	115	116	116	116	116
T_{max} (°C)	444	458	462	464	468
Residual mass	0	2.5	4.9	9.6	21.2

The thermal properties of the composites determined by DSC and some TGA results are summarised in Table 17. The melting temperature (Tm) of LLDPE was not significantly influenced by the presence of the organo-vermiculite and seems to be independent of clay loading. The melting enthalpy ($\Delta H_{crystal}$) also followed the same trend. For the neat polymer and for the composites, the degree of crystallinity was found to be around 30%, considering the theoretical value of 293 J g^{-1} for 100% crystalline polyethylene (Mathot, 1984). Interestingly, the crystallisation onset temperature (Tc) increased by the same magnitude in the presence of the organo-vermiculite.

b) XRD

The WAXS results presented in the Fig. 37 indicate that the LLDPE composites did not show any organo-vermiculite or even vermiculite features. The original flakes (0.5 mm size) were "destroyed" during processing, suggesting exfoliation or intercalation of vermiculite layers into the LLDPE matrix. However, even after extrusion and injection moulding of the composites, a hump at higher 2θ angles suggests the preservation of some crystal features of the mica phase.

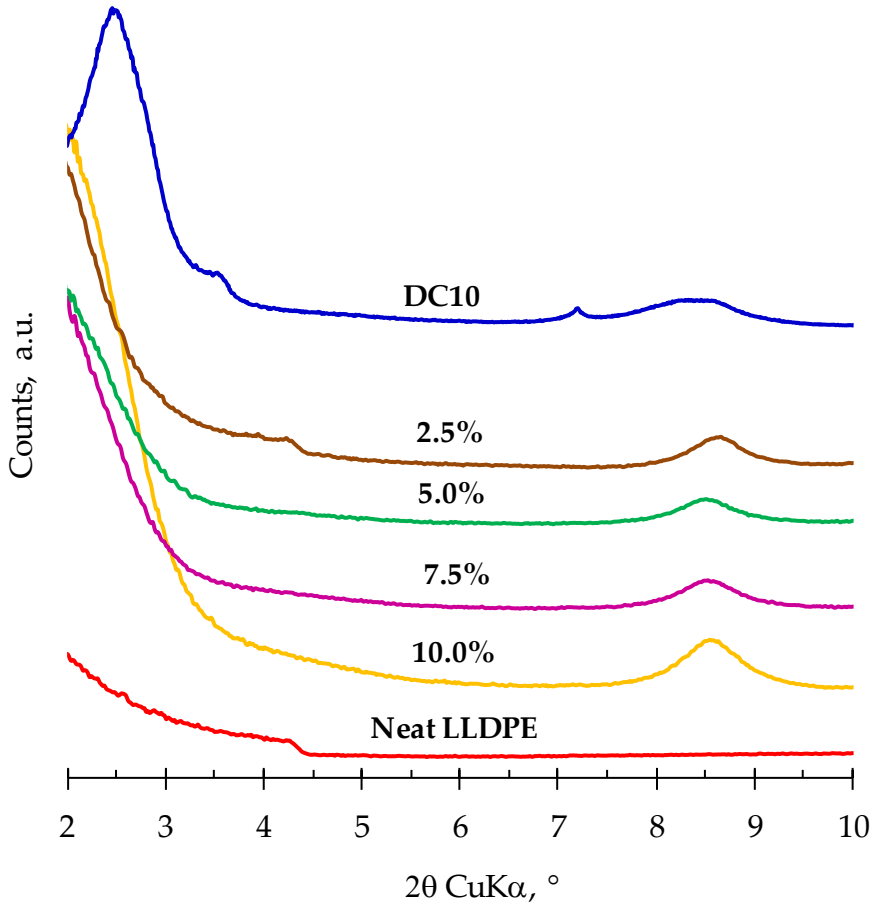

Figure 37. XRD plots of neat LLDPE and its organo-vermiculite composites with different concentrations (wt.%)

The presence of both exfoliated (organo-vermiculite) and non-exfoliated (mica phase detected by XRD) phases in the composites is due to the nature of the starting material, the clay modification procedure and the experimental conditions.

c) Melt rheology

The organoclay dispersion in the LLDPE phase and the structural morphology were assessed by melt rheology at three different temperatures (140, 160 and 180 °C). The results are shown in Figs 38 and 39.

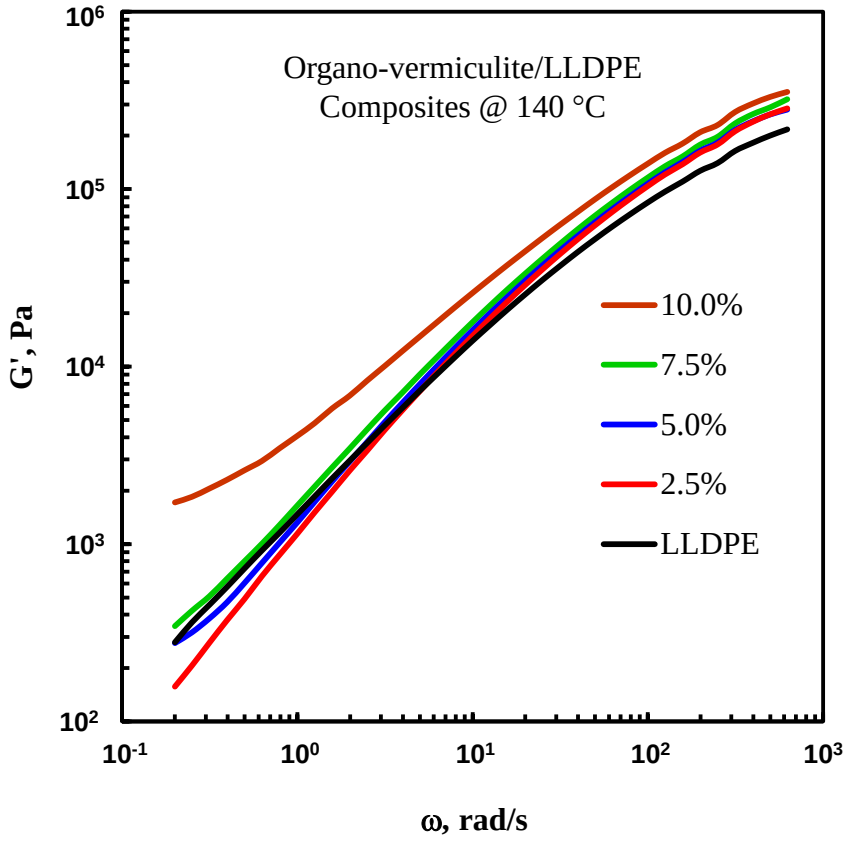

Figure 38. Rheological behaviour of organo-vermiculite/LLDPE composites at 140 °C

Improvement in the storage modulus (G') and dynamic viscosity (η*) from neat LLDPE to its composites was observed. The magnitude of G' and η* was dependent on the organo-vermiculite content, mainly at lower frequencies. This similar performance in G' and η* may indicate poor interaction between the polymer matrix and the clay layers, as also reported by (Durmus *et al.*, 2007). However, the 10% organo-vermiculite showed better low-frequency improvement and exhibited viscoelastic (shear-thinning) behaviour.

When the organo-vermiculite content was decreased, the magnitude of G' also dropped and a more Newtonian behaviour was observed. Lower G' values than those of the neat LLDPE could also be attributed to the presence of exuded surfactant (with low melt viscosity) in the matrix, at experimental temperatures.

On the other hand, the presence of unmodified biotite layers (micro phase) may also be playing a significant role (see also SEM images in Appendix IX).

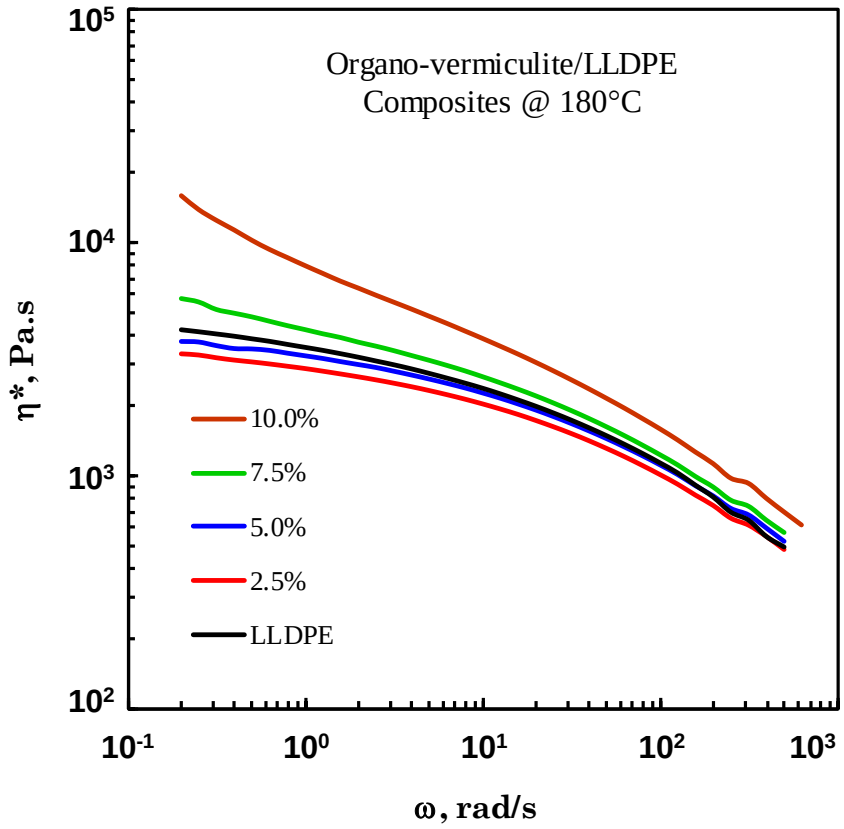

Figure 39. Dynamic viscosity (η*) of organo-vermiculite/LLDPE composites at 180 °C

d) Mechanical properties

The tensile mechanical properties of LLDPE and its organo-vermiculite composites are listed in Table 18.

All samples exhibited an elastic region and neck propagation after yielding. The present results do not show a linear relationship between clay content and mechanical properties. With incorporation of the organo-vermiculite, the tensile strength assumed an average value of 17 MPa, corresponding to an improvement of about 50%.

By contrast, the strain at yield was dramatically reduced, basically due to the poor compatibility between the non-polar LLDPE chains and the polar unmodified biotite layers (Alexandre and Dubois, 2000). However, an increase of 100% in the Young's modulus was also observed, regardless of the amount of the organo-vermiculite content, in the region of 2.5–10 wt.%.

Table 18. Mechanical properties of LLDPE and LLDPE/organo-vermiculite composites

Organo-vermiculite, wt.%	Tensile strength, MPa	Young's modulus, MPa	Strain at yield, %	Strain at break, %
0	11.4 ± 0.3	109 ± 25	39.1 ± 1.6	732 ± 156
2.5	17.1 ± 0.4	203 ± 13	18.6 ± 1.7	509 ± 40
5.0	16.9 ± 0.1	205 ± 5	19.0 ± 3.1	639 ± 17
7.5	17.3 ± 0.2	212 ± 14	17.9 ± 3.0	917 ± 50
10.0	17.4 ± 0.2	239 ± 21	17.5 ± 2.0	482 ± 13

e) *DMA*

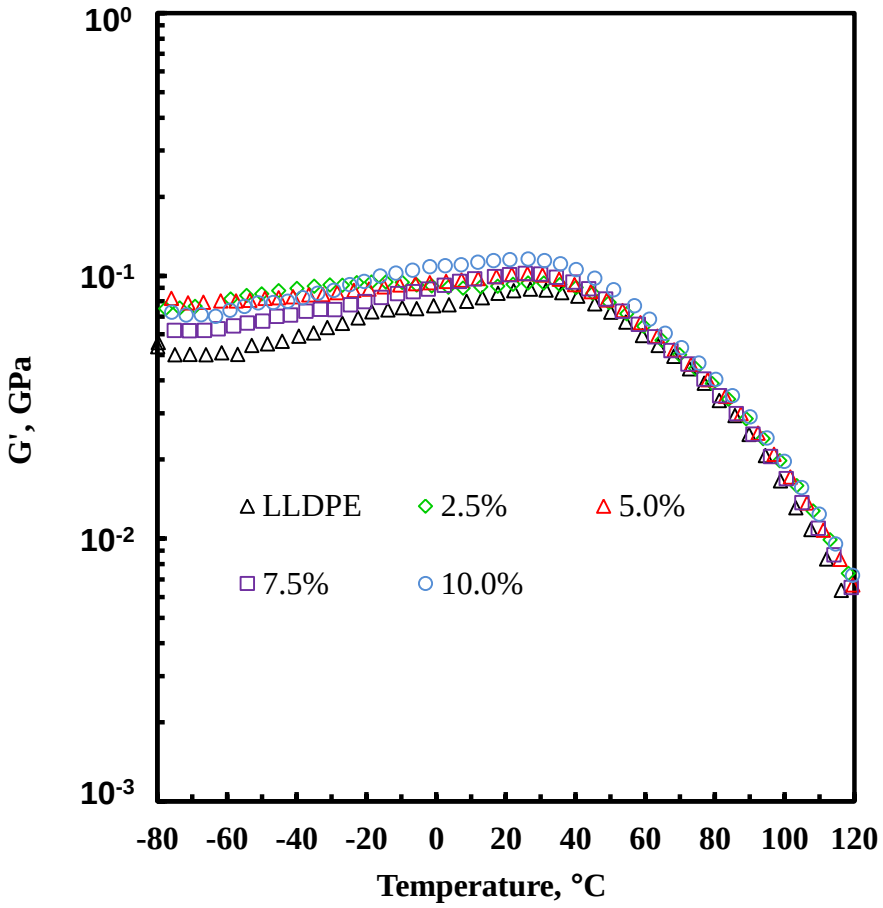

Figure 40. Storage modulus (G′) for LLDPE and its organo-vermiculite composites, at constant frequency (1 Hz)

Figs 40 and 41 show the temperature dependence of the storage modulus (G′) and loss factor (tan δ), respectively. The magnitude of improvement in G′ was noticeable at lower temperatures (still well above Tg, which was too low to measure at present), but the reinforcement effect was not dependent on the organo-vermiculite content.

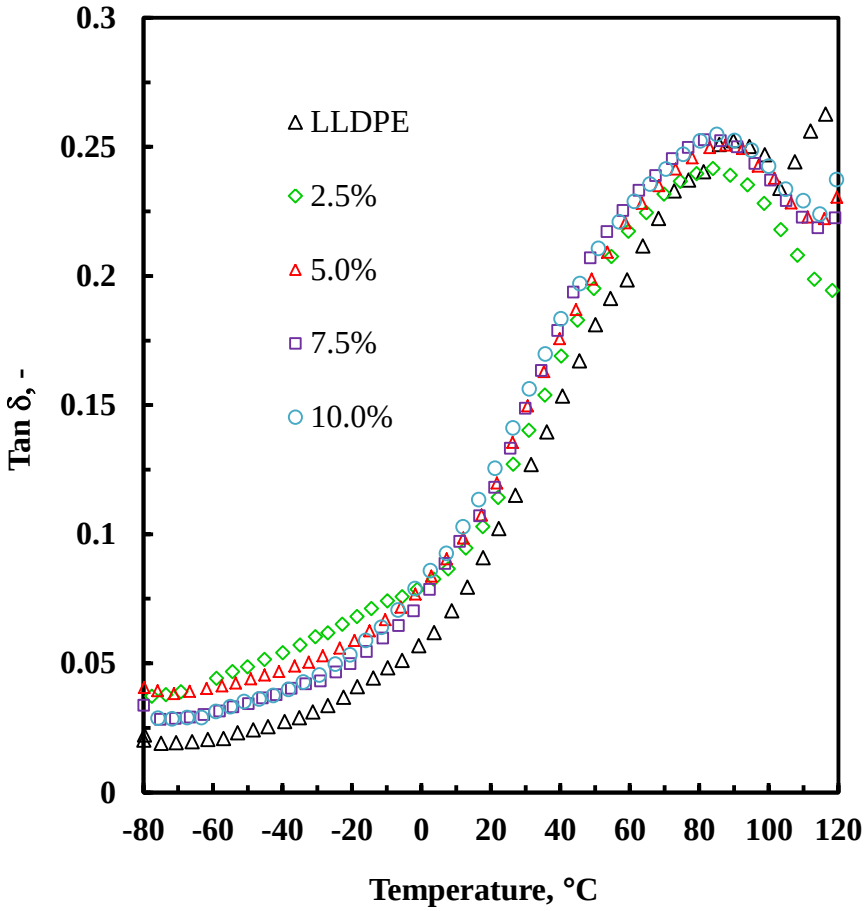

Figure 41. Temperature dependence of the loss factor (tan δ) of LLDPE and its organo-vermiculite composites

f) Flammability

Neat LLDPE is highly combustible and also has very high melt viscosity. During the cone calorimeter tests, in the organo-vermiculite composites we observed the formation of a char layer that may have served as a mass and energy transport barrier (Gilman *et al.*, 2000; Bourbigot *et al.*, 2006). This char had some cracks and voids that may have been formed due to the internal pressure from the released degradation products and due to its contraction and collapse on cooling (Fig. 42).

The cone calorimeter results of time to ignition and to flame out, pHRR and tHR, of LLDPE and its organo-vermiculite composites during the combustion tests are summarised in Table 19.

The pHRR (external heat flux of 35 kW m^{-2}) of LLDPE was decreased by 33% when using 7.5 wt.% of organo-vermiculite. Compared with the neat polymer, the composites showed a broader curve, with a plateau value (Fig. 43). The sample containing only 2.5 wt.% organo-vermiculite was an exception as the time to ignition and the pHRR both increased.

Figure 42. Image of 5 wt.% LLDPE composite char residue after cone calorimeter test.

On the other hand, the time to ignition (t_{ign}) and total heat release (tHR) were not improved, as also pointed out previously by Bourbigot *et al.* (2006) and Laoutid *et al.* (2009). Actually, the time to ignition appeared to decrease with increasing organo-vermiculite content. At least two factors might have contributed to these findings: (1) the lower decomposition temperature of the organo-vermiculite (specifically, the surfactant) which formed volatile vapours; and (2) the lower heat capacity of the filler, i.e. the organo-vermiculite (and mica phase) heated faster and ignited the LLDPE matrix earlier (Si *et al.*, 2007; Pack and Rafailovich, 2011).

Table 19. Flammability data summary of LLDPE and its organo-vermiculite composites.

Property, Units	Organo-vermiculite, wt.%			
	0	2.5	5	7.5
Time to ignition (t_{ign}), s	54 ± 14	74 ± 17	50 ± 40	35 ± 19
Time to flameout, s	676 ± 94	511 ± 36	460 ± 40	457 ± 11
Peak heat release rate (pHRR), kW m^{-2}	758 ± 20	842 ± 168	575 ± 72	509 ± 29
Total heat release (tHR), MJ m^{-2}	140 ± 22	184 ± 7	170 ± 13	194 ± 2

The CO_2 production and the overall smoke production curves (not shown) also followed similar trends. The reduction in CO and CO_2 production was ascribed to the decrease in mass loss due to the presence of the clay. A possible adsorption of the released gases was not ruled out completely. Expanded vermiculite is known to have some proclivity for adsorbing gases, especially CO_2 (Schoeman, 1989; Muiambo *et al.*, 2010).

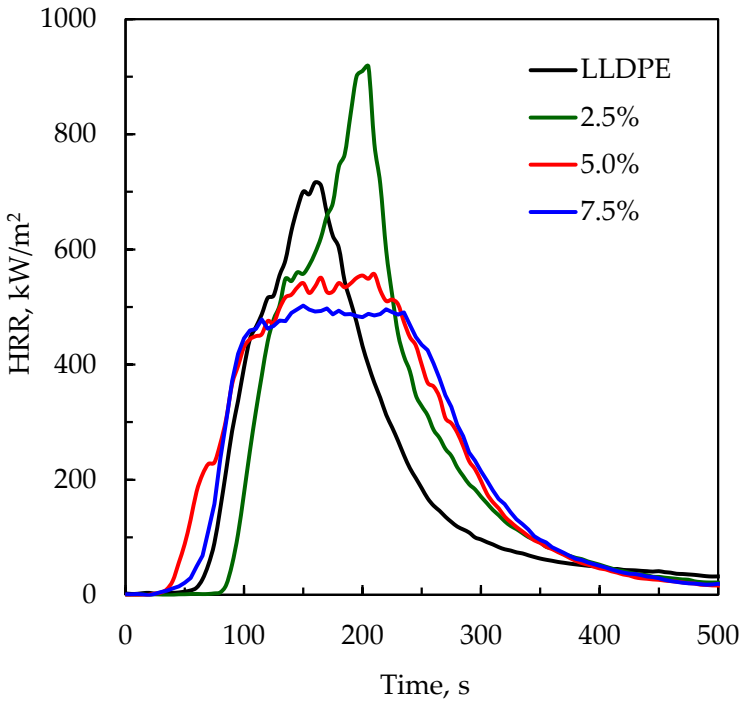

Figure 43. Cone calorimeter heat release rate curves for pressed LLDPE and its composites with organo-modified vermiculite.

7.1.4 Conclusions

According to the XRD results, all organo-vermiculite/LLDPE composites were vermiculite XRD-featureless, suggesting excellent dispersion throughout the matrix. However, visible clay particles were still present in all translucent samples, showing unaltered mica which retained its structure.

The initial mineralogical composition of the clay and the modification steps led to a mixture of well-exfoliated and well-dispersed organo-vermiculite layers and large stacks of unmodified mica sheets. Melt rheology at different temperatures suggested poor interaction between the polymer matrix and the clay layers.

The reinforcing effect in LLDPE was evident in all the compositions studied, even without a compatibiliser. The addition of only 2.5 wt.% organo-vermiculite to LLDPE improved both the tensile strength and the Young's modulus significantly.

All samples ignited easily, melted and burned profusely. The organo-vermiculite appeared to form a homogeneous exfoliated protective barrier layer at the sample surface. The composites with 5 wt.% and 7.5 wt.% organo-vermiculite showed reduced smoke-production rates, CO and CO_2 production rates, as well as a reduction of the pHRR from 758 ± 20 kW m^{-2} to 575 ± 72 kW m^{-2} and 509 ± 29 kW m^{-2}, respectively. However, all the composites showed an increase in the tHR.

7.2 UREA-VERMICULITE/PU COMPOSITES

7.2.1 Introduction

Polyurethanes (PU) represent an extensive class of polymers made by reaction of isocyanates with diols or polyols (Levchik and Weil, 2004). They have wide applications in several industrial sectors.

Flexible PU foams are highly flammable and are the main and most combustible components of upholstered furniture and mattresses. Nevertheless, rigid PU foams are among the best heat-insulating materials and one of the most used in the building industry (Levchik and Weil, 2004).

Halogen-based FR additives are traditionally used to improve the properties of PU composites (Tabuani *et al.*, 2012). However, due to health concerns and to increasing environmental scrutiny, PU formulators are searching for other FR materials that are environmentally friendly and cost-effective.

Flame-retarded thermoplastic polyurethane is used in wire and cable applications with aluminium hydroxide and magnesium hydroxide as fire-retardant additives. The use of mica and zinc borate is also reported in the literature. The latter is a synergist for aluminium or magnesium hydroxides (Levchik and Weil, 2004).

A key property of urea-vermiculite is its tendency to exfoliate when heated to high temperatures. During exfoliation it expands rapidly in a worm-like manner to form expanded material with a low density. The origin of this process lies in the vaporisation of the interlayer water and urea degradation products.

Expandable vermiculite can be compared to expandable graphite. A disadvantage of graphite-based flame retardants is the black colour and electrical conductivity they impart to the material. Hence the utility of urea-modified vermiculite was investigated as a flame retardant for PU composites.

7.2.2 *Experimental*

The urea-vermiculite was the Mg-urea-modified vermiculite prepared and characterised in detail in Chapter 4.

The ultra-low-viscosity liquid urethanes (Smooth-Cast© 300) were used as received from Smooth-On. Part A and Part B (100A:90B, wt.) were mixed thoroughly together with urea-vermiculite. The mixture was then poured into the mould in a single spot and left for 3 min. The reaction (gelation) proceeded from the middle and moved sideways. The urea-vermiculite/PU composites showed some tendency to sediment with time, before curing was complete. The white sheets were fully cured by pressing them at room temperature and 5 MPa for 10 min. A release agent (Universal Mold Release) was applied to the metallic plates to facilitate demoulding.

TGA experiments were performed by the dynamic method on a Mettler Toledo A851 TGA/SDTA instrument. A sample of about 15 mg was placed in an open 150 µl alumina pan. The temperature was scanned from 25 to 800 °C at a rate of 10 °C min^{-1}, with air flowing at a rate of 50 ml min^{-1}.

The combustion behaviour was assessed according to the ISO 5660-1 standard procedure in a Dual Cone Calorimeter (Fire Testing Technology (UK) Ltd). Measurements were carried out in triplicate. The sheet dimensions were 100 mm × 100 mm × 3 mm. The sheets were placed on aluminium foil and exposed, separated horizontally, to an external heat flux of 35 kW m^{-2}. A hold-down frame was used to minimise the swelling and consequent interference from intumescence. The exhaust gas flow rate was set at 24 ℓ s^{-1}. The HRR, pHRR and MLR were calculated from the oxygen consumption and obtained directly from the Fire Testing Technology "ConeCalc" software.

7.2.3 Results and discussion

a) TGA

The thermal decomposition behaviour of neat PU and of the urea-vermiculite composites (in air) are shown in Fig. 44 and summarised in Table 20.

All compositions exhibited two thermal decomposition steps. The neat PU volatilised completely, before 700 °C, but the composites still retained a residue even at 800 °C. The quantity of the residue at 800 °C corresponded closely to the nominal urea-vermiculite content.

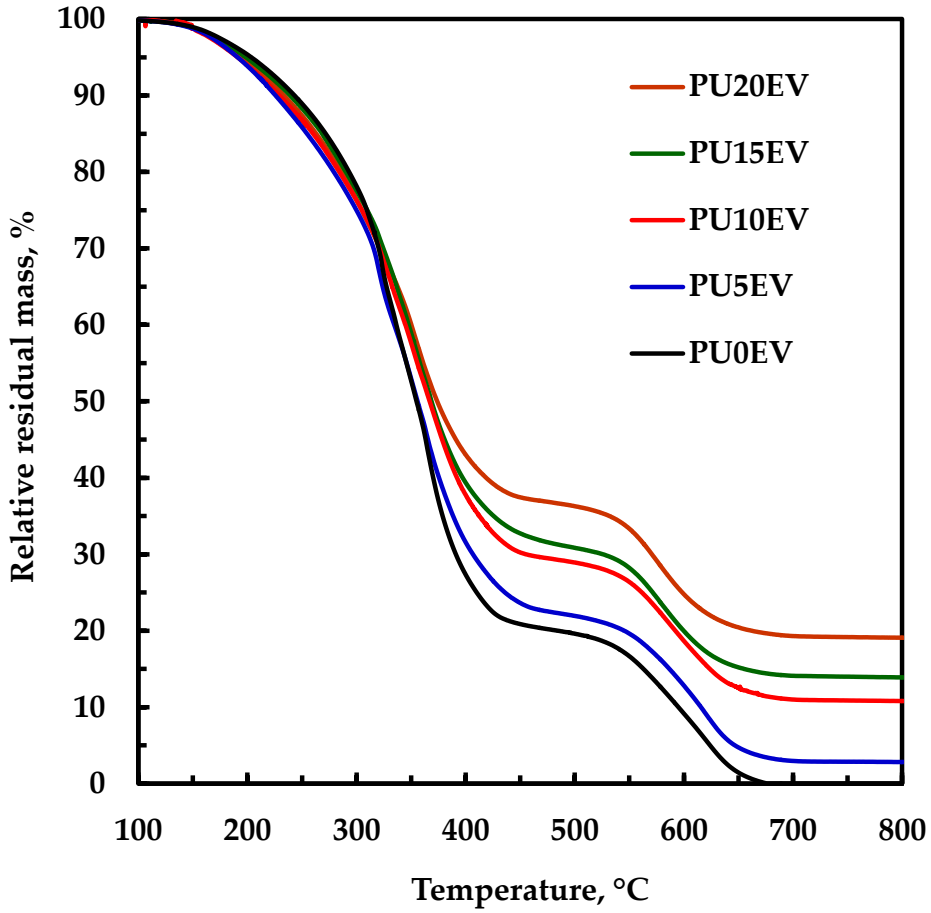

Figure 44. Thermal degradation plots of PU and its composites with urea-vermiculite, in air

Table 20. TGA summary of the PU composites

Sample (wt.%)	Residual mass (wt.%)			
	200 °C	400 °C	600 °C	800 °C
PUEV0 (neat)	95	27	9	0
PUEV5 (5%)	94	32	13	4
PUEV10 (10%)	94	38	19	11
PUEV15 (15%)	95	39	20	14
PUEV20 (20%)	94	43	25	19

b) Flammability

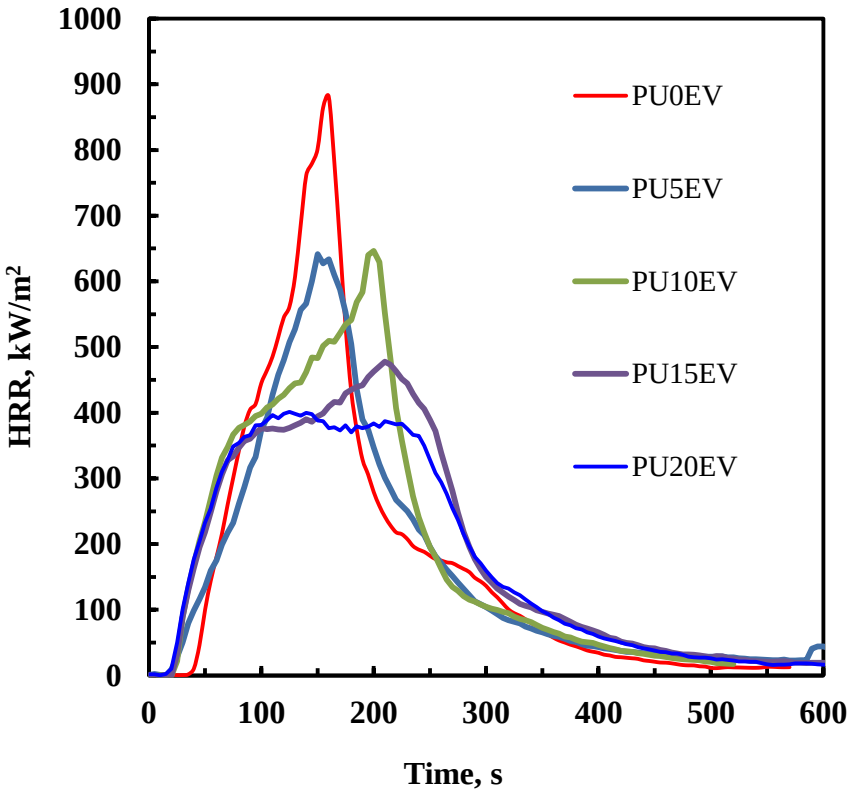

Figure 45. Cone calorimeter average peak HRR for PU and its composites with urea-vermiculite

Fig. 45 compares the heat release rate for PU composites with that of their PU reference polymer. The data in Table 21 summarise the cone calorimeter results.

The heat release curves for the neat PU exhibited the shape characteristic of thermally thin samples (Schartel and Hull, 2007). Thermally thin samples are identified by a sharp peak in their HRR curves as the whole sample is pyrolysed at once.

Table 21. Flammability data summary of PU composites

Property, Units	Urea-vermiculite, wt.%					
	0	**5**	**10**	**15**	**20**	**20T**
Time to ignition (t_{ign}), s	40 ± 2	25 ± 2	24 ± 1	26 ± 1	22 ± 4	28 ± 2
Time to flameout, s	521 ± 33	527 ± 98	563 ± 53	517 ± 9	538 ± 8	798 ± 102
Peak heat release rate (pHRR), kW m^{-2}	900 ± 5	779 ± 115	483 ± 20	647 ± 96	433 ± 29	377 ± 13
Total heat release (tHR), MJ m^{-2}	104 ± 1	107 ± 17	112 ± 4	107 ± 1	107 ± 3	98 ± 1
MAHRE (kW m^{-2})	374 ± 9	399 ± 32	371 ± 11	332 ± 7	312 ± 7	203 ± 4
pHRR/t_{ign}, kW $m^{-2}s^{-1}$	23 ± 1	31 ± 6	25 ± 3	20 ± 1	20 ± 2	14 ± 1

Compared with the neat PU, the pHRR of the composites was greatly reduced while the tHR was almost not affected. As expected, the t_{ign} was negatively affected, due to the clay-catalysed polymer decomposition (Berta *et al.*, 2006; Tabuani *et al.*, 2012; Kiliaris and Papaspyrides, 2010). However, when the filler was concentrated at the top of one of the sides (sample denoted 20T), subjected directly to the cone heat flux, the composite showed better fire performance (Appendix XI-c)). The tHR was still high due to fact that the composite had two burning stages: the first one retarded by the filler and second one corresponding to the underlying material.

The prominence of the second stage offers a hint about the poor bonding between the expanded vermiculite flakes and the molten PU.

Figure 46. Image of 10 wt.% PU composite char residue after cone calorimeter test.

Fig. 46 shows the appearance of the 10 wt.% composite's residue char after the cone calorimeter test. This image also indicates clearly that the urea-vermiculite flakes could not bond properly to the PU matrix. This lack of bonding between PU char and the exfoliated flakes allowed the consumption of the exposed polymer as well as the underlying material. Some flakes were even swept away from the pyrolysis zone while exfoliating.

The urea-vermiculite composites featured lower CO, CO_2 and smoke production rates owing to the reduction in the rate of mass loss. The observed trends mirror those observed for the HRR (Fig. 45) almost perfectly.

7.2.4 Conclusions

PU and its urea-vermiculite composites exhibited two thermal degradation steps, with the residual mass, at 800 °C, corresponding to the urea-vermiculite content.

The cone calorimeter results revealed that the fire performance of urea-vermiculite in PU composites is greatly affected by the distribution of the FR additive along the vertical direction of incidence of the heat flux. The addition of 20 wt.% urea-vermiculite lowered the pHRR from 900 ± 5 kW m^{-2} to 377 ± 13 kW m^{-2} and the tHR from 104 ± 1 MJ m^{-2} to 98 ± 1 MJ m^{-2}.

The urea-vermiculite formed an exfoliated but non-cohesive protective barrier layer on top of the PU composites. It provided protection to some extent. However, after all the urea-vermiculite had expanded, the loose flakes offered efficient protection only at high loadings. This poor bonding between the PU char and the exfoliated flakes also allowed the consumption of the underlying PU. As a consequence, the tHR did not improve, even for high filler loadings.

7.3 UREA-VERMICULITE/PVC COMPOSITES

7.3.1 Introduction

Polyvinyl chloride (PVC) is a very versatile polymer used in diverse applications, including flooring, rigid pipes, flexible hoses, conveyor belting, and wire and cable insulation. Neat PVC features a relatively high chlorine content of 56.7 wt.%. That makes it more resistant to ignition and burning than most organic polymers (Coaker, 2003). However, the conventional plasticisers used in the manufacture of flexible PVC detract from this outstanding fire resistance.

PVC is the second-largest contributor after wood to fires in non-domestic premises and its use in electrical cable insulation is one of the main sources of PVC in fires. Thus FR and smoke-suppressant (SS) additives must be incorporated in order to meet product test specifications such as the oxygen index, HRR, smoke evolution, or the extent of burning (Coaker, 2003). Levchik and Weil (2005) and Weil *et al.* (2006) reviewed the chemical additives that have been considered to achieve acceptable fire properties in the principal PVC application areas. In particular, phosphate esters are useful as FR plasticisers in flexible PVC (Levchik and Weil, 2005).

Neat PVC is thermally unstable and prone to autocatalytic dehydrochlorination (Starnes Jr and Ge, 2004). The addition of thermal stabilisers is required to allow processing at elevated temperatures (Folarin and Sadiku, 2011). However, pyrolysis of PVC yields an isotropic carbon char residue (Otani, 1965) and this contributes to the mechanisms of flame-retardant action (Folarin and Sadiku, 2011).

Plasticised PVC is flexible and offers versatile applications from semi-rigid to very soft materials; it is also cost-effective (Matheson *et al.*, 1992; Jimenez *et al.*, 2001).

The utility of urea-vermiculite as a flame retardant for PVC, plasticised with 60 phr (parts per hundred parts of resin) of a phosphate ester, was investigated.

7.3.2 *Experimental*

TPC Paste Resin Co, Ltd supplied the PVC emulsion grade PG680. It was a free-flowing powder with a K-value of 69. Reofos 50, a synthetic isopropylated triaryl phosphate ester plasticiser, was supplied by Chemtura.

The urea-vermiculite was the Mg-urea-modified vermiculite prepared and characterised in detail in Chapter 4.

The different urea-vermiculite/PVC compounds were prepared using the plastisol route. PVC powder (100 g), Reofos 50 (60 g) and an adequate amount of urea-vermiculite were mixed together in a high-shear mixer for 10 min. The paste mixture was immediately poured into a mould (100 mm x 100 mm x 4 mm) and heated for 10 min in a convection oven set at 120 °C. Thereafter the sheets were cured at 150 °C and 5 MPa in a hot press for 5 min. The samples were made by varying the urea-vermiculite content, from 0 wt.% (neat) to 20 wt.%. The mass ratio of PVC and the plasticiser was kept constant for all samples to maintain the same phosphorous content.

TGA was performed by the dynamic method on a Mettler Toledo A851 TGA/SDTA instrument. For TGA, a sample of about 15 mg was placed in an open 150 µℓ alumina pan. The temperature was scanned from 25 to 800 °C at a rate of 10 °C min^{-1} with air flowing at a rate of 50 ml min^{-1}.

7.3.3 *Results and discussion*

a) TGA

PVC thermograms, in air, show three degradation steps (Fig. 47). The first two steps are related to PVC's dehydrochlorination (with the formation of double bonds) and to the degradation of the plasticiser (Dunn and Ennis, 1970; Jimenez *et al.*, 2001). The last thermal event corresponds to the degradation of the oxidised PVC (Annakutty and Kishore, 1993; Jimenez *et al.*, 2001).

For the PVC compound and for the urea-vermiculite composites the maximum degradation rate was observed during the first step at T_{max} = 289 ± 2 °C.

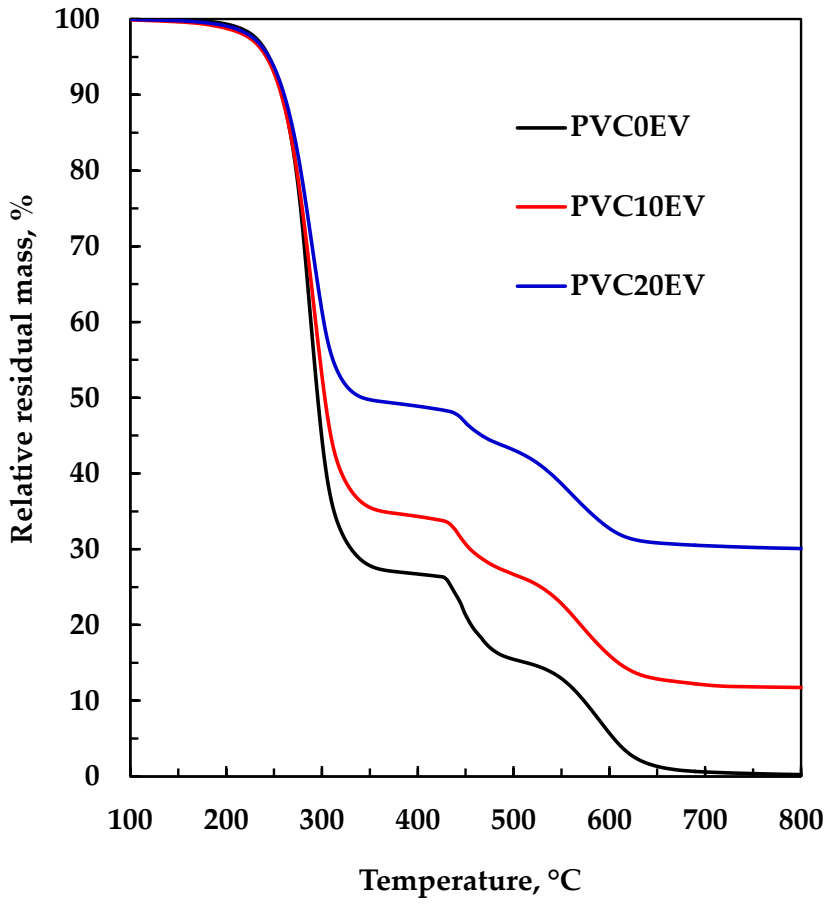

Figure 47. TGA curves of neat PVC and composites containing 10 wt% and 20 wt.% of urea-vermiculite

The typical urea-vermiculite thermal degradation steps were overlapped by those from the PVC and could not be clearly observed. The amount of the residual mass, in the composites, corresponded to more than the urea-vermiculite added and raised with the increment of the quantity of the filler (Table 22). This result suggests that urea-vermiculite induces char formation in PVC during thermal degradation, in air.

Table 22. TGA summary of the PVC composites

Sample (wt.%)	Tmax, °C	Residual mass, wt.%		
		400 °C	600 °C	800 °C
PVCEV0 (neat)	287	27	6	0
PVCEV10 (10%)	291	34	16	12
PVCEV20 (20%)	289	49	33	30

b) Flammability of urea-vermiculite/PVC composites

The urea-vermiculite/PVC cone calorimeter results are summarised in Table 23. Additional results are also shown in Appendix IX. Representative heat release rate (HRR) curves obtained from the cone calorimeter tests are presented in Fig. 48.

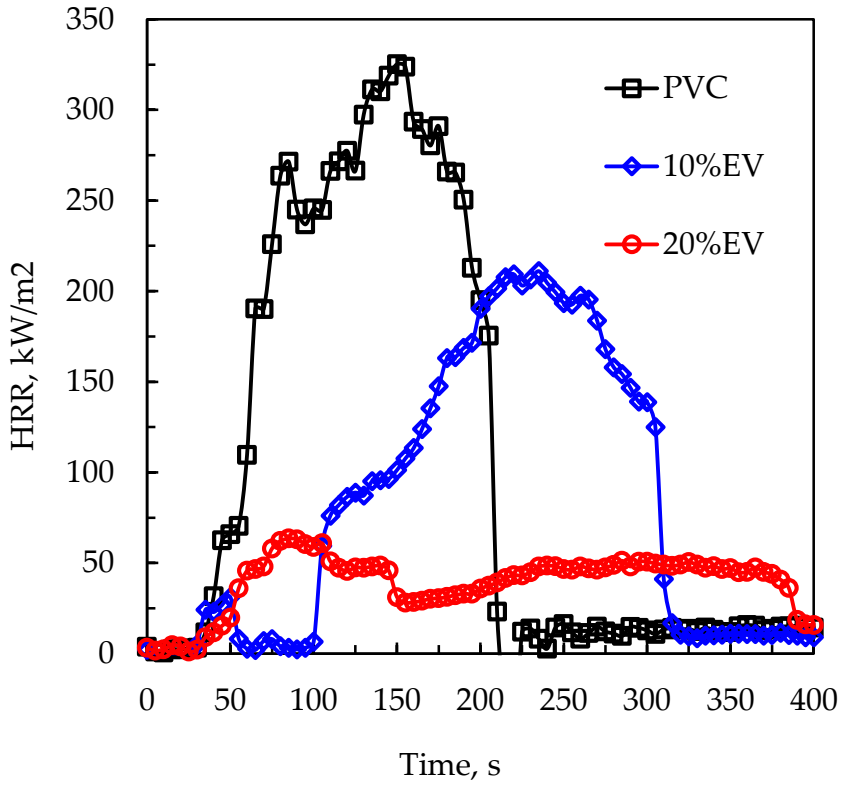

Figure 48. Cone calorimeter average pHRR for PVC compound and its composites with 10 and 20 wt.% urea vermiculite

All the neat PVC compound samples ignited and flamed briefly. This gave rise to the sharp peak in the HRR at short times. All the neat PVC samples produced a large amount of smoke. From Fig. 49 (a) and (b), showing the PVC samples on the cone calorimeter sample holder after flameout, it can be seen that the PVC composites continued releasing smoke even after flameout. A considerably expanded residue was observed due to the action of the urea-vermiculite filler. This latter fact is consistent with the TGA findings.

The heat release curves for the neat plasticised PVC compound exhibited the shape characteristic of thermally thin samples (Schartel and Hull, 2007).

Table 23. Flammability data summary of PVC composites

Property, Units	**Urea vermiculite, wt.%**		
	0	**10**	**20**
Time to ignition (t_{ign}), S	35 ± 3	33 ± 6	59 ± 6
Time to flameout, S	146 ± 59	174 ± 143	122 ± 27
Peak heat release rate (pHRR), kW m^{-2}	325 ± 11	229 ± 16	60 ± 23
Total heat release (tHR), MJ m^{-2}	55 ± 11	42 ± 14	7 ± 2
pHRR/t_{ign}, kW $m^{-2}s^{-1}$	9.3 ± 0.8	7.1 ± 0.9	1.5 ± 0.9

HRR curves characteristic of thermally thick, char-producing samples show a sudden rise to a plateau value. However, the HRR curves for the samples containing urea-vermiculite were a bit more complex. Most of them ignited briefly, almost flamed out and then reignited, i.e. the flame was not sustainable. In some cases, at the initial stage of the test, they were manually reignited at least once because they were flaming out instantaneously. Apparently the first ignition consumed the available flammable volatiles (induced by the spark) and the samples flamed out. The subsequent abrupt reignition was due to the increase in the amount of flammable volatiles because of the continued pyrolysis and smoking while not burning. On the other hand, the halogen entering the vapour phase also contributed to a "flame poisoning effect", i.e. the

reaction and termination of oxygen-based chain branching, free radical reactions occurring in the flame (Matheson et al., 1992; Weil et al., 2009).

The profuse smoke evolution suggests that the composite samples were pyrolysed while at the same time a glowing combustion occurred at the surface. The urea-vermiculite composites featured lower CO, CO_2 and SPRs. Their trends were identical to those observed for the HRR (Fig. 48).

The lower "fire performance index" (PI = pHRR/t_{ign}) of the composite containing 20 wt.% of urea-vermiculite is a clear indication of better cone calorimetry performance. Such improvement with respect to the pHRR and tHR is attributed to a combination of factors, which will now be discussed.

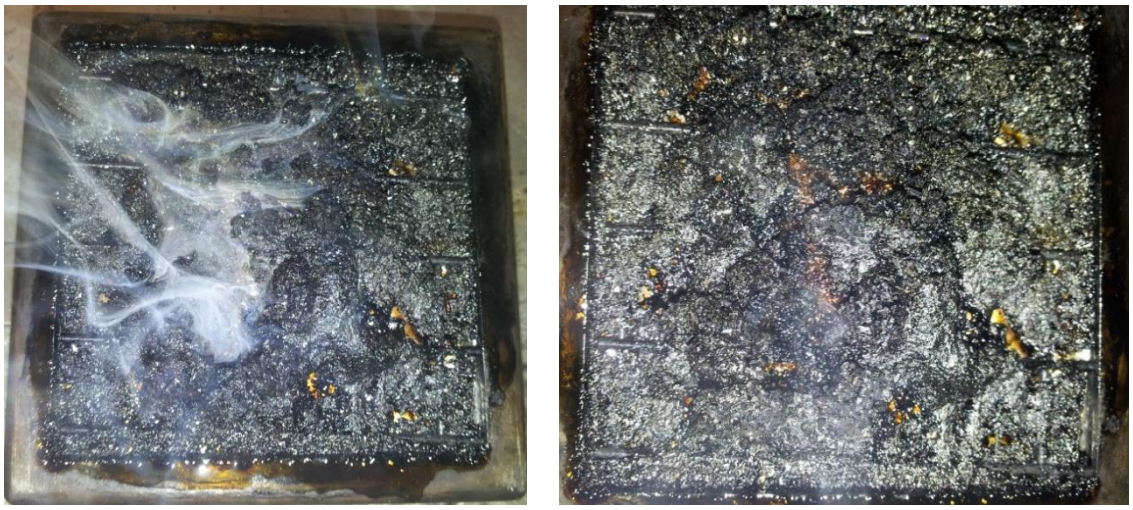

Figure 49. Images of char residue of 10 wt.% urea-vermiculite/PVC after cone calorimeter tests: (a-left) just after flame flameout and still smoking, and (b-right) after complete extinction of flame and smoke

Firstly, the expansion of the urea-vermiculite formed a low-density layer of 'worm-like' structures which provided a protective barrier at the polymer surface. This limited heat transfer to the substrate and thus slowed down the rate of thermal degradation. On the other hand, the release of the HCl by the decomposing PVC apparently also prevented flaming combustion during the latter part of the cone calorimeter tests. This can be attributed to a dilution effect on the air–fuel mixture in the gas phase. However, the halogen entering the gas phase also contributed to a

"flame poisoning effect", i.e. the slowing down of the free radical chain reactions occurring in the flame (Weil *et al.*, 2006). In combination, these two effects explain why the cone calorimeter test proceeded without a visible flame following an initial short-lived ignition. It degenerated into a bulk pyrolysis experiment in combination with a surface glowing-combustion event.

7.3.4 Conclusions

The cone calorimeter test proceeded without a visible flame following an initial short-lived ignition which degenerated into a bulk pyrolysis experiment in combination with a surface glowing-combustion event. These results revealed that addition of 20 wt.% urea-vermiculite lowered the pHRR from 325 ± 11 kW m^{-2} to 60 ± 23 kW m^{-2} and the total heat release from 55 ± 11 MJ m^{-2} to only 7 ± 2 MJ m^{-2}. All samples containing 20 wt.% urea-vermiculite ignited and burned only very briefly before flameout.

The urea-vermiculite forms an exfoliated protective barrier layer. In addition, the simultaneous release of halogen species by the polymer matrix and the exfoliating vermiculite prevents the formation of a flammable air–fuel mixture.

The cone calorimetry results also showed that urea-vermiculite allowed thermal stabilisation of the condensed phase at high temperatures, but had little influence on the vapour phase behaviour.

REFERENCES

Alexandre, M., Dubois, P., 2000. Polymer-layered silicate nanocomposites: preparation, properties and uses of a new class of materials. Materials Science and Engineering: R: Reports 28, 1-63.

Annakutty, K.S., Kishore, K., 1993. Novel polymeric flame retardant plasticizers for poly(vinyl chloride). European Polymer Journal 29, 1387-1390.

Berta, M., Lindsay, C., Pans, G., Camino, G., 2006. Effect of chemical structure on combustion and thermal behaviour of polyurethane elastomer layered silicate nanocomposites. Polymer Degradation and Stability 91, 1179-1191.

Bourbigot, S., Duquesne, S., Jama, C., 2006. Polymer Nanocomposites: How to Reach Low Flammability? Macromolecular Symposia 233, 180-190.

Chrissopoulou, K., Altintzi, I., Anastasiadis, S.H., Giannelis, E.P., Pitsikalis, M., Hadjichristidis, N., Theophilou, N., 2005. Controlling the miscibility of polyethylene/layered silicate nanocomposites by altering the polymer/surface interactions. Polymer 46, 12440-12451.

Coaker, A.W., 2003. Fire and flame retardants for PVC. Journal of Vinyl and Additive Technology 9, 108-115.

Dufton, P.W., 1995. Fire - Additives and Materials. Smithers Rapra Technology.

Dunn, P., Ennis, B.C., 1970. Thermal analysis of compounded poly(vinyl chloride). Journal of Applied Polymer Science 14, 355-364.

Durmus, A., Kasgoz, A., Macosko, C.W., 2007. Linear low density polyethylene (LLDPE)/clay nanocomposites. Part I: Structural characterization and quantifying clay dispersion by melt rheology. Polymer 48, 4492-4502.

Durmuş, A., Woo, M., Kaşgöz, A., Macosko, C.W., Tsapatsis, M., 2007. Intercalated linear low density polyethylene (LLDPE)/clay nanocomposites prepared with oxidized polyethylene as a new type compatibilizer: Structural, mechanical and barrier properties. European Polymer Journal 43, 3737-3749.

Folarin, O.M., Sadiku, E.R., 2011. Thermal stabilizers for poly(vinyl chloride): A review. International Journal of Physical Sciences 6, 4323-4330.

Gilman, J.W., Jackson, C.L., Morgan, A.B., Harris, R., Manias, E., Giannelis, E.P., Wuthenow, M., Hilton, D., Phillips, S.H., 2000. Flammability Properties of Polymer−Layered-Silicate Nanocomposites. Polypropylene and Polystyrene Nanocomposites†. Chemistry of Materials 12, 1866-1873.

Gomes, E.D., Visconte, L.Y., Pacheco, E.a.V., 2009. Thermal characterization of polypropylene/vermiculite composites. Journal of Thermal Analysis and Calorimetry 97, 571-575.

Hotta, S., Paul, D.R., 2004. Nanocomposites formed from linear low density polyethylene and organoclays. Polymer 45, 7639-7654.

Intratec, 2013. Technology economics: LLDPE via solution process. Intratec Solutions LCC, p. 10.

Jimenez, A., Lopez, J., Iannoni, A., Kenny, J.M., 2001. Formulation and mechanical characterization of PVC plastisols based on low-toxicity additives. Journal of Applied Polymer Science 81, 1881-1890.

Kiliaris, P., Papaspyrides, C.D., 2010. Polymer/layered silicate (clay) nanocomposites: An overview of flame retardancy. Progress in Polymer Science 35, 902–958.

Laoutid, F., Bonnaud, L., Alexandre, M., Lopez-Cuesta, J.M., Dubois, P., 2009. New prospects in flame retardant polymer materials: From fundamentals to nanocomposites. Materials Science and Engineering R: Reports 63, 100-125.

Lee, J.-H., Jung, D., Hong, C.-E., Rhee, K.Y., Advani, S.G., 2005. Properties of polyethylene-layered silicate nanocomposites prepared by melt intercalation with a PP-g-MA compatibilizer. Composites Science and Technology 65, 1996-2002.

Levchik, S.V., Weil, E.D., 2004. Thermal decomposition, combustion and fire-retardancy of polyurethanes—a review of the recent literature. Polymer International 53, 1585-1610.

Levchik, S.V., Weil, E.D., 2005. Overview of the recent literature on flame retardancy and smoke suppression in PVC. Polymers for Advanced Technologies 16, 707-716.

Li, B., Jia, H., Guan, L., Bing, B., Dai, J., 2009. A novel intumescent flame-retardant system for flame-retarded LLDPE/EVA composites. Journal of Applied Polymer Science 114, 3626-3635.

Liu, B., Ding, Q., Zhang, J., Hu, B., Shen, J., 2005. Preparation and properties of new EPDM/vermiculite nanocomposites. Polymer Composites 26, 706-712.

Matheson, A.F., Charge, R., Corneliussen, T., 1992. Properties of PVC compounds with improved fire performance for electrical cables. Fire Safety Journal 19, 55-72.

Mathot, V.B.F., 1984. Temperature dependence of some thermodynamic functions for amorphous and semi-crystalline polymers. Polymer 25, 579-599.

Muiambo, H.F., Focke, W.W., Atanasova, M., Der Westhuizen, I.V., Tiedt, L.R., 2010. Thermal properties of sodium-exchanged palabora vermiculite. Applied Clay Science 50, 51-57.

Otani, S., 1965. On the carbon fiber from the molten pyrolysis products. Carbon 3, 31-38.

Pack, S., Rafailovich, M.H., 2011. Self-extinguishing polymer–clay nanocomposites, in: Mittal, V. (Ed.), Thermally stable and flame retardant polymer nanocomposites. Cambridge, New York, pp. 237-275.

Paul, D.R., Robeson, L.M., 2008. Polymer nanotechnology: Nanocomposites. Polymer 49, 3187-3204.

Qiu, Z.-C., Zhang, J.-J., Zhou, Y., Song, B.-Y., Chang, J.-J., Yang, K.-K., Wang, Y.-Z., 2011. Biodegradable poly(p-dioxanone) reinforced and toughened by organo-modified vermiculite. Polymers for Advanced Technologies 22, 993-1000.

Rosa, M.L., Tankink, A., Hoch, M., 2008. Highly flexible halogen free and flame retardant thermoplastic cable compounds modified with EVM polymers, 57th International Wire & Cable Symposium, Rhode Island, pp. 125-133.

Schartel, B., Hull, T.R., 2007. Development of fire-retarded materials—Interpretation of cone calorimeter data. Fire and Materials 31, 327-354.

Schoeman, J.J., 1989. Mica and vermiculite in South Africa. Journal of The South African Institute of Mining and Metallurgy 89, 1-12.

Si, M., Zaitsev, V., Goldman, M., Frenkel, A., Peiffer, D.G., Weil, E., Sokolov, J.C., Rafailovich, M.H., 2007. Self-extinguishing polymer/organoclay nanocomposites. Polymer Degradation and Stability 92, 86-93.

Starnes Jr, W.H., Ge, X., 2004. Mechanism of autocatalysis in the thermal dehydrochlorination of poly(vinyl chloride). Macromolecules 37, 352-359.

Tabuani, D., Bellucci, F., Terenzi, A., Camino, G., 2012. Flame retarded Thermoplastic Polyurethane (TPU) for cable jacketing application. Polymer Degradation and Stability 97, 2594-2601.

Tjong, S.C., Meng, Y.Z., 2003. Impact-modified polypropylene/vermiculite nanocomposites. Journal of Polymer Science Part B: Polymer Physics 41, 2332-2341.

Tjong, S.C., Meng, Y.Z., Hay, A.S., 2002. Novel Preparation and Properties of Polypropylene–Vermiculite Nanocomposites. Chemistry of Materials 14, 44-51.

Utracki, L.A., 2004. Clay-Containing Polymeric Nanocomposites, Volumes 1-2. Smithers Rapra Technology.

Valášková, M., Simha Martynková, G., Matějka, V., Barabaszová, K., Plevová, E., Měřínská, D., 2009. Organovermiculite nanofillers in polypropylene. Applied Clay Science 43, 108-112.

Valášková, M., Tokarský, J., Barabaszová, K.Č., Matějka, V., Hundáková, M., Pazdziora, E., Kimmer, D., 2013. New aspects on vermiculite filler in polyethylene. Applied Clay Science 72, 110-116.

Wang, Z., Huang, P., Fan, W.C., Wang, Q., 1988. Measurements on the fire behaviour of PVC sheets using the cone calorimeter, Proceedings of the Asia-Oceania Symposium on Fire Science & Technology. International Association for Fire Safety Science, pp. 221-227.

Weil, E.D., Levchik, S., Moy, P., 2006. Flame and smoke retardants in vinyl chloride polymers - Commercial usage and current developments. Journal of Fire Sciences 24, 211-236.

Zhao, C., Qin, H., Gong, F., Feng, M., Zhang, S., Yang, M., 2005. Mechanical, thermal and flammability properties of polyethylene/clay nanocomposites. Polymer Degradation and Stability 87, 183-189.

Alexandre, M., Dubois, P., 2000. Polymer-layered silicate nanocomposites: preparation, properties and uses of a new class of materials. Materials Science and Engineering: R: Reports 28, 1-63.

Annakutty, K.S., Kishore, K., 1993. Novel polymeric flame retardant plasticizers for poly(vinyl chloride). European Polymer Journal 29, 1387-1390.

Berta, M., Lindsay, C., Pans, G., Camino, G., 2006. Effect of chemical structure on combustion and thermal behaviour of polyurethane elastomer layered silicate nanocomposites. Polymer Degradation and Stability 91, 1179-1191.

Bourbigot, S., Duquesne, S., Jama, C., 2006. Polymer Nanocomposites: How to Reach Low Flammability? Macromolecular Symposia 233, 180-190.

Chrissopoulou, K., Altintzi, I., Anastasiadis, S.H., Giannelis, E.P., Pitsikalis, M., Hadjichristidis, N., Theophilou, N., 2005. Controlling the miscibility of polyethylene/layered silicate nanocomposites by altering the polymer/surface interactions. Polymer 46, 12440-12451.

Coaker, A.W., 2003. Fire and flame retardants for PVC. Journal of Vinyl and Additive Technology 9, 108-115.

Dufton, P.W., 1995. Fire - Additives and Materials. Smithers Rapra Technology.

Dunn, P., Ennis, B.C., 1970. Thermal analysis of compounded poly(vinyl chloride). Journal of Applied Polymer Science 14, 355-364.

Durmus, A., Kasgoz, A., Macosko, C.W., 2007. Linear low density polyethylene (LLDPE)/clay nanocomposites. Part I: Structural characterization and quantifying clay dispersion by melt rheology. Polymer 48, 4492-4502.

Durmuş, A., Woo, M., Kaşgöz, A., Macosko, C.W., Tsapatsis, M., 2007. Intercalated linear low density polyethylene (LLDPE)/clay nanocomposites prepared with oxidized polyethylene as a new type compatibilizer: Structural, mechanical and barrier properties. European Polymer Journal 43, 3737-3749.

Folarin, O.M., Sadiku, E.R., 2011. Thermal stabilizers for poly(vinyl chloride): A review. International Journal of Physical Sciences 6, 4323-4330.

Gilman, J.W., Jackson, C.L., Morgan, A.B., Harris, R., Manias, E., Giannelis, E.P., Wuthenow, M., Hilton, D., Phillips, S.H., 2000. Flammability Properties of Polymer−Layered-Silicate Nanocomposites. Polypropylene and Polystyrene Nanocomposites†. Chemistry of Materials 12, 1866-1873.

Gomes, E.D., Visconte, L.Y., Pacheco, E.a.V., 2009. Thermal characterization of polypropylene/vermiculite composites. Journal of Thermal Analysis and Calorimetry 97, 571-575.

Hotta, S., Paul, D.R., 2004. Nanocomposites formed from linear low density polyethylene and organoclays. Polymer 45, 7639-7654.

Intratec, 2013. Technology economics: LLDPE via solution process. Intratec Solutions LCC, p. 10.

Jimenez, A., Lopez, J., Iannoni, A., Kenny, J.M., 2001. Formulation and mechanical characterization of PVC plastisols based on low-toxicity additives. Journal of Applied Polymer Science 81, 1881-1890.

Kiliaris, P., Papaspyrides, C.D., 2010. Polymer/layered silicate (clay) nanocomposites: An overview of flame retardancy. Progress in Polymer Science 35, 902–958.

Laoutid, F., Bonnaud, L., Alexandre, M., Lopez-Cuesta, J.M., Dubois, P., 2009. New prospects in flame retardant polymer materials: From fundamentals to nanocomposites. Materials Science and Engineering R: Reports 63, 100-125.

Lee, J.-H., Jung, D., Hong, C.-E., Rhee, K.Y., Advani, S.G., 2005. Properties of polyethylene-layered silicate nanocomposites prepared by melt intercalation with a PP-g-MA compatibilizer. Composites Science and Technology 65, 1996-2002.

Levchik, S.V., Weil, E.D., 2004. Thermal decomposition, combustion and fire-retardancy of polyurethanes—a review of the recent literature. Polymer International 53, 1585-1610.

Levchik, S.V., Weil, E.D., 2005. Overview of the recent literature on flame retardancy and smoke suppression in PVC. Polymers for Advanced Technologies 16, 707-716.

Li, B., Jia, H., Guan, L., Bing, B., Dai, J., 2009. A novel intumescent flame-retardant system for flame-retarded LLDPE/EVA composites. Journal of Applied Polymer Science 114, 3626-3635.

Liu, B., Ding, Q., Zhang, J., Hu, B., Shen, J., 2005. Preparation and properties of new EPDM/vermiculite nanocomposites. Polymer Composites 26, 706-712.

Matheson, A.F., Charge, R., Corneliussen, T., 1992. Properties of PVC compounds with improved fire performance for electrical cables. Fire Safety Journal 19, 55-72.

Mathot, V.B.F., 1984. Temperature dependence of some thermodynamic functions for amorphous and semi-crystalline polymers. Polymer 25, 579-599.

Muiambo, H.F., Focke, W.W., Atanasova, M., Der Westhuizen, I.V., Tiedt, L.R., 2010. Thermal properties of sodium-exchanged palabora vermiculite. Applied Clay Science 50, 51-57.

Otani, S., 1965. On the carbon fiber from the molten pyrolysis products. Carbon 3, 31-38.

Pack, S., Rafailovich, M.H., 2011. Self-extinguishing polymer–clay nanocomposites, in: Mittal, V. (Ed.), Thermally stable and flame retardant polymer nanocomposites. Cambridge, New York, pp. 237-275.

Paul, D.R., Robeson, L.M., 2008. Polymer nanotechnology: Nanocomposites. Polymer 49, 3187-3204.

Qiu, Z.-C., Zhang, J.-J., Zhou, Y., Song, B.-Y., Chang, J.-J., Yang, K.-K., Wang, Y.-Z., 2011. Biodegradable poly(p-dioxanone) reinforced and toughened by organo-modified vermiculite. Polymers for Advanced Technologies 22, 993-1000.

Rosa, M.L., Tankink, A., Hoch, M., 2008. Highly flexible halogen free and flame retardant thermoplastic cable compounds modified with EVM polymers, 57th International Wire & Cable Symposium, Rhode Island, pp. 125-133.

Schartel, B., Hull, T.R., 2007. Development of fire-retarded materials—Interpretation of cone calorimeter data. Fire and Materials 31, 327-354.

Schoeman, J.J., 1989. Mica and vermiculite in South Africa. Journal of The South African Institute of Mining and Metallurgy 89, 1-12.

Si, M., Zaitsev, V., Goldman, M., Frenkel, A., Peiffer, D.G., Weil, E., Sokolov, J.C., Rafailovich, M.H., 2007. Self-extinguishing polymer/organoclay nanocomposites. Polymer Degradation and Stability 92, 86-93.

Starnes Jr, W.H., Ge, X., 2004. Mechanism of autocatalysis in the thermal dehydrochlorination of poly(vinyl chloride). Macromolecules 37, 352-359.

Tabuani, D., Bellucci, F., Terenzi, A., Camino, G., 2012. Flame retarded Thermoplastic Polyurethane (TPU) for cable jacketing application. Polymer Degradation and Stability 97, 2594-2601.

Tjong, S.C., Meng, Y.Z., 2003. Impact-modified polypropylene/vermiculite nanocomposites. Journal of Polymer Science Part B: Polymer Physics 41, 2332-2341.

Tjong, S.C., Meng, Y.Z., Hay, A.S., 2002. Novel Preparation and Properties of Polypropylene−Vermiculite Nanocomposites. Chemistry of Materials 14, 44-51.

Utracki, L.A., 2004. Clay-Containing Polymeric Nanocomposites, Volumes 1-2. Smithers Rapra Technology.

Valášková, M., Simha Martynková, G., Matějka, V., Barabaszová, K., Plevová, E., Měřínská, D., 2009. Organovermiculite nanofillers in polypropylene. Applied Clay Science 43, 108-112.

Valášková, M., Tokarský, J., Barabaszová, K.Č., Matějka, V., Hundáková, M., Pazdziora, E., Kimmer, D., 2013. New aspects on vermiculite filler in polyethylene. Applied Clay Science 72, 110-116.

Wang, Z., Huang, P., Fan, W.C., Wang, Q., 1988. Measurements on the fire behaviour of PVC sheets using the cone calorimeter, Proceedings of the Asia-Oceania Symposium on Fire Science & Technology. International Association for Fire Safety Science, pp. 221-227.

Weil, E.D., Levchik, S., Moy, P., 2006. Flame and smoke retardants in vinyl chloride polymers - Commercial usage and current developments. Journal of Fire Sciences 24, 211-236.

Zhao, C., Qin, H., Gong, F., Feng, M., Zhang, S., Yang, M., 2005. Mechanical, thermal and flammability properties of polyethylene/clay nanocomposites. Polymer Degradation and Stability 87, 183-189.

CHAPTER 8
GENERAL CONCLUSIONS AND RECOMMENDATIONS

The present work has described different procedures and methods for the modification of Palabora vermiculite and its application in flame-retarded LLDPE, PU and PVC polymer composites.

Ion exchange of Palabora vermiculite with inorganic salts does not affect its macroscopic appearance nor destroy its crystalline structure. However, it changes slightly its d-spacing. K^+ ions from the biotite layers are not easily exchangeable, even when intercalated by long-chain organic surfactants or metal-urea complexes.

Inorganic cations and organic surfactants change vermiculite's expansion onset temperature, but do not change its maximum expansion ratio significantly. The expansion ratio is independent of the flake thickness and the nature of the modification. Neat vermiculite flakes are almost perfectly flat, while in the expanded state the individual sheets assume a buckled configuration. Application of a compressive force sufficient to compact an expanded vermiculite flake to the original dimensions, followed by equilibration with liquid water, reconstitutes vermiculite's structure. At low compressive forces the vermicular structure shows spring-like behaviour (with hysteresis). The interlayer mosaic-like bonding holds the sheets together and stabilises the system of mechanical interconnects, which prevents complete exfoliation/delamination.

The expansion onset temperature of vermiculite (over 450 °C) has been successfully tuned to within the activation temperature range of intumescent systems (209 ± 35 °C) through co-intercalation of metal-urea complexes. These exhibit both urea and water molecules, as blowing agents, surrounding the interlayer cations.

Na-vermiculite intercalates long-chain organic surfactants to almost the same extent as neat Mg-vermiculite and this process is restricted to 150% of the CEC. The XRD d-spacing values increased in proportion to the surfactant chain length. The d-spacing also increased with increasing surfactant:vermiculite ratio up to ca. 150% CEC, at which point it assumed an average value of 4.4 nm for the double-chain C10 surfactant.

Organo-vermiculite/LLDPE composites were translucent and their XRD diffractograms showed no features of vermiculite, suggesting excellent dispersion throughout the matrix. SEM and melt rheology suggested poor interaction between the polymer matrix and the clay layers. The addition of organo-vermiculite to LLDPE significantly improved the tensile strength and the Young's modulus. The organo-vermiculite was effective as a flame retardant for polyethylene in cone calorimeter tests. It exfoliated when exposed to heat and appeared to form a homogeneous protective barrier layer at the surface. Its presence reduced the pHRR and the rates of CO and CO_2 generation, as well as the smoke production rate (SPR).

The fire performance of urea-vermiculite in PU composites depended greatly on its distribution along the vertical direction of the heat flux incidence. The addition of 20 wt.% urea-vermiculite significantly lowered the pHRR. The urea-vermiculite formed an exfoliated but non-cohesive protective barrier layer on top of PU composites. The poor bonding between the PU char and the exfoliated flakes failed to prevent consumption of the underlying PU. As a consequence, fire performance parameters such as the tHR were not improved.

The urea-vermiculite/PVC cone calorimeter test proceeded without a visible flame following an initial short-lived ignition. In essence, the cone calorimeter test degenerated into a bulk pyrolysis experiment, although a glowing-combustion event occurred at the surface. Urea-vermiculite formed a heat–induced, swollen exfoliated protective barrier layer and the simultaneous release of halogen species by the PVC prevented the formation of a flammable air–fuel mixture. The addition of urea-vermiculite significantly lowered both the pHRR and the tHR.

In general, urea-vermiculite allowed thermal stabilisation of the condensed phase at high temperatures, but had little influence on the vapour phase behaviour. The amount of degradation products released by the urea-vermiculite (non-flammable vapours) was not sufficient to dilute the mixture of flammable vapours.

To the best of our knowledge, this is the first time that vermiculite's exfoliation onset temperature has been significantly lowered using ion-exchange methods. Further studies are encouraged to increase urea's co-intercalation in vermiculite and to improve understanding about the relationship between expansion ratio and the mass loss just before and during exfoliation.

Additional studies are also suggested in order to understand urea-vermiculite's behaviour in the presence of compatibilisers (which can provide good bonding between the clay layers and the polymer matrix), as well as in synergistic systems with other FR additives. There is definite potential in exploring synergistic systems, especially good char-formers that could improve the performance of the urea-vermiculite as a flame-retardant additive.

APPENDICES

Appendix I. Publications

Muiambo, H.F., Focke, W.W., Atanasova, M., Benhamida, A. 2015. Characterization of urea-modified Palabora vermiculite, *App. Clay Sci*. 105-106, 14-20.

Muiambo, H.F., Focke, W.W., Asante, J.K.O., 2015. Preparation and properties of LLDPE-organovermiculite composites**.** *Polymer* (*Submitted*)

Focke, W.W., **Muiambo, H.F**., Mhike, W., Kruger, H.J., Ofosu, O., 2014. Flexible PVC flame retarded with expandable graphite. *Polym. Degrad. Stabil*. 100, 63-69.

Muiambo, H.F., Focke, W.W., 2012. Ion-exchanged vermiculites with lower expansion onset temperatures. *Mol. Cryst. Liq*. Cryst. 555, 65-75.

Focke, W.W., **Muiambo, H.F.**, Kruger, H.J., van der Westhuizen, I., Frederich Labuschagne, J.W.J., 2012. Characterizing intumescent powders with SEM and TMA. Book of Abstracts: 11th International Conference on the Frontiers of Polymers and Advanced Materials (ICFPAM), Pretoria, South Africa.

Appendix II. Conference presentations

Muiambo, H.F., Focke, W.W. Preparation and properties of LLDPE-organovermiculite composites. Presented at the XV International Clay Conference, 7–11 July 2013, Rio de Janeiro, Brazil.

Muiambo, H.F., Benhamida, A., Focke, W.W. Nanomorphology versus nanodispersion in melt-extruded vermiculite/LLDPE composites. Presented at SIDA – VIII Regional Meeting, 1–3 August 2013, Bagamoyo, Tanzania.

Muiambo, H.F., Benhamida, A., Focke, W.W. Assessment of organo-vermiculite dispersion in melt-extruded LLDPE composites. Presented at Les Journées d'Etudes des Matériaux Polymères (JEMP'2013), 2–3 October 2013, Béjaia, Algérie.

Appendix III. SEM images of neat vermiculite

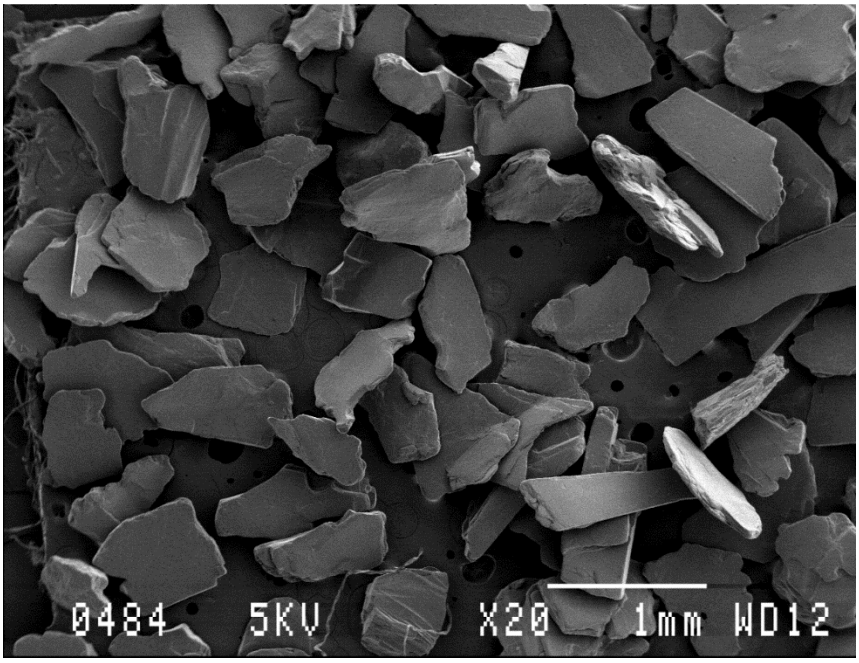

Appendix III-a) Very low magnification SEM image of neat vermiculite

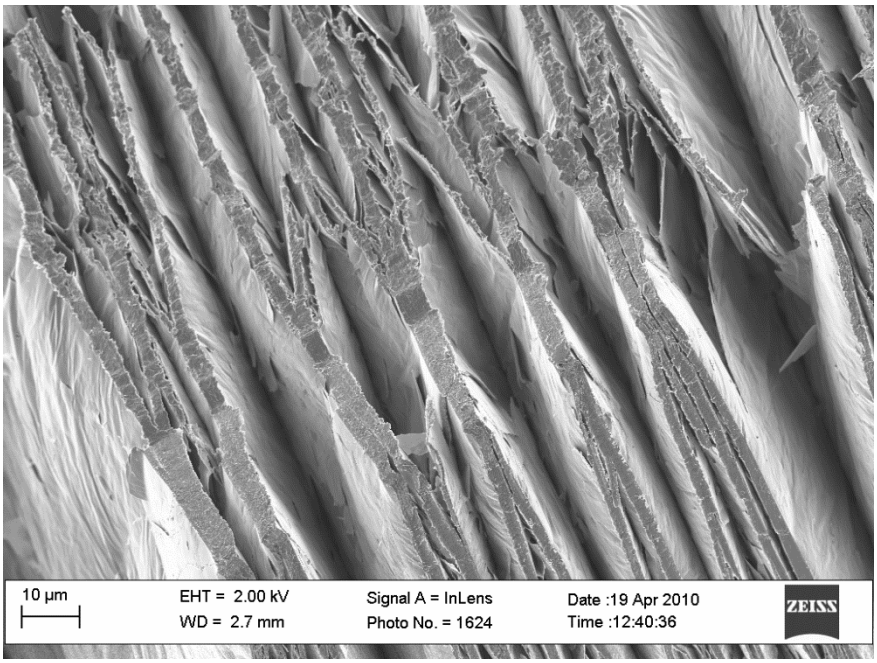

Appendix III-b) SEM image of heat-expanded Na-exchanged vermiculite

Appendix IV. ESEM micrographs of the expansion of Na-vermiculite

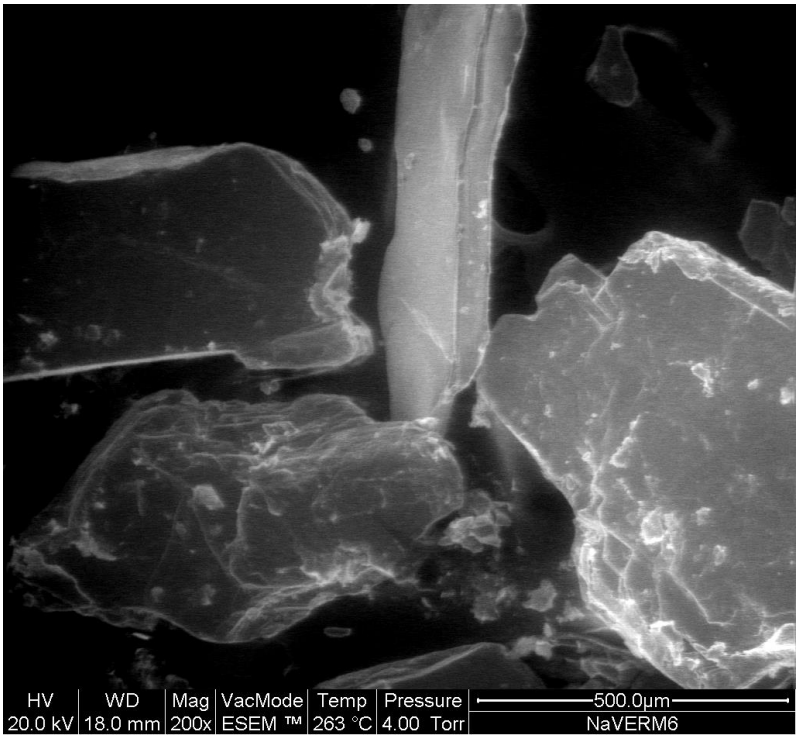

Appendix IV-a) Just before exfoliation, which commenced at 263 °C

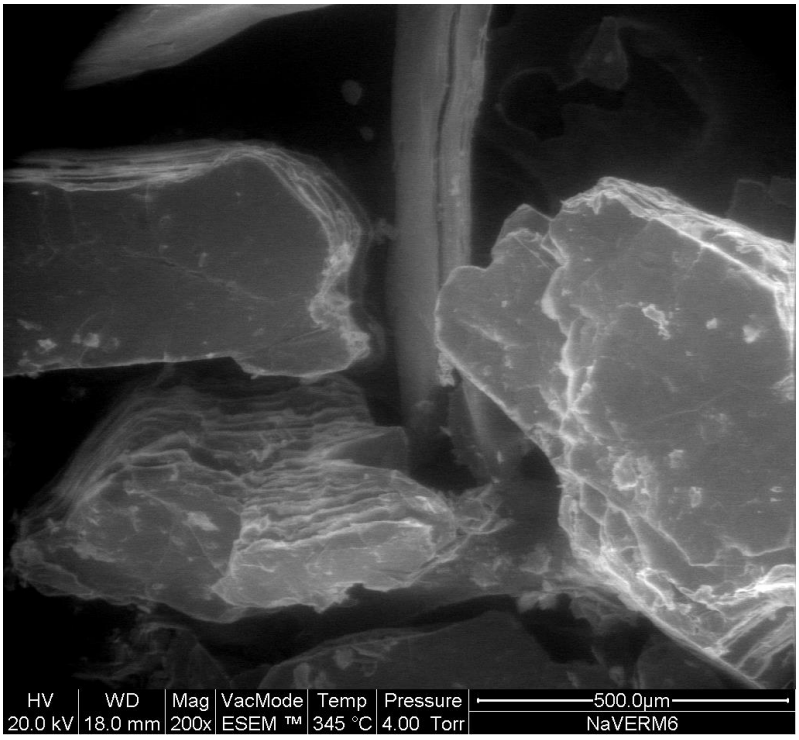

Appendix IV-b) During exfoliation at 345 °C

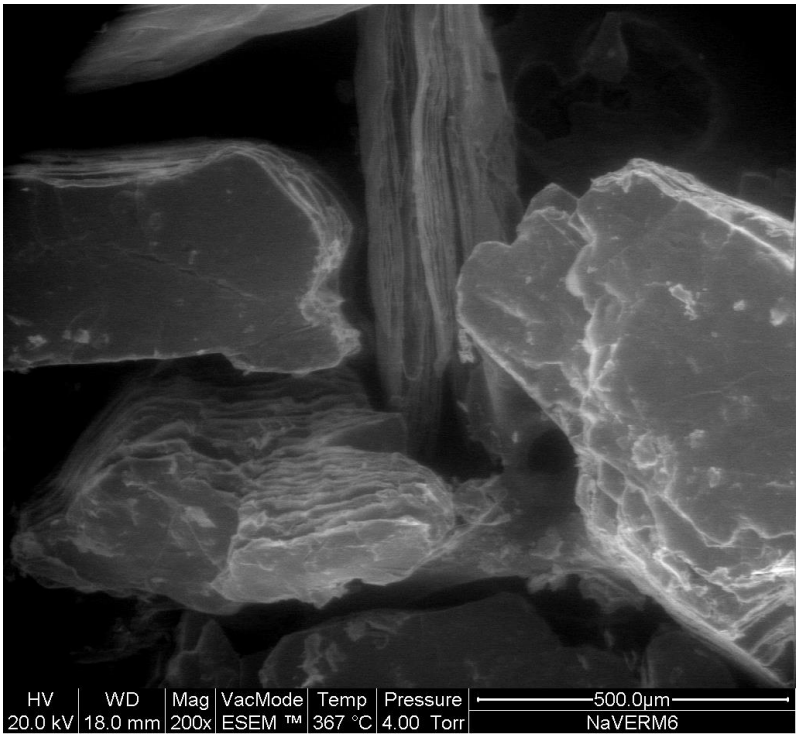

Appendix IV-c) During exfoliation at 367 °C

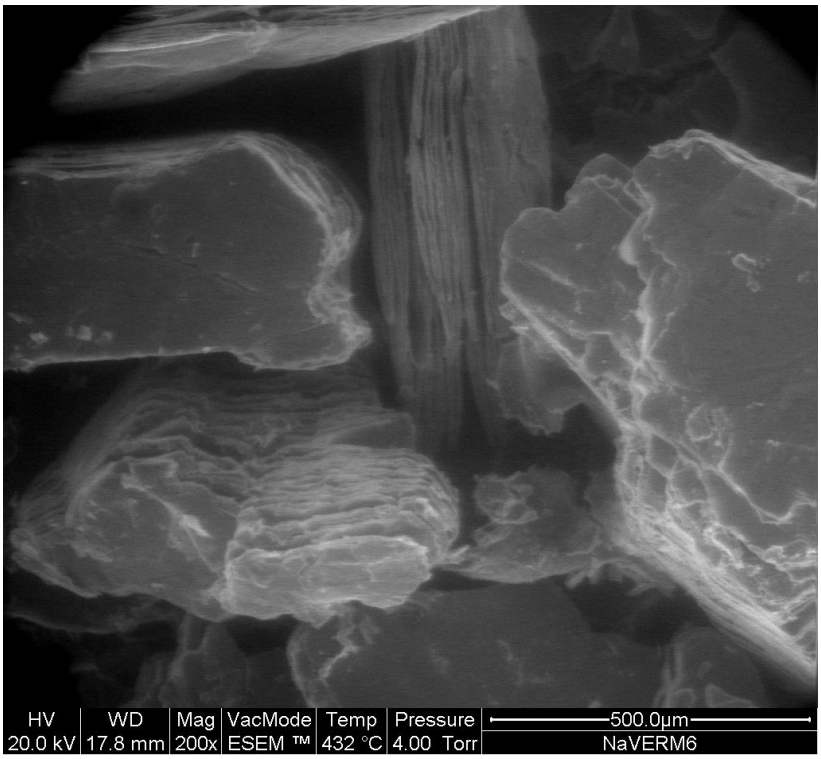

Appendix IV-d) After exfoliation at 432 °C

Appendix V. Vermiculite production in South Africa from 1994 to 2009 (Potter, 1996–2009; Cordier, 2010)

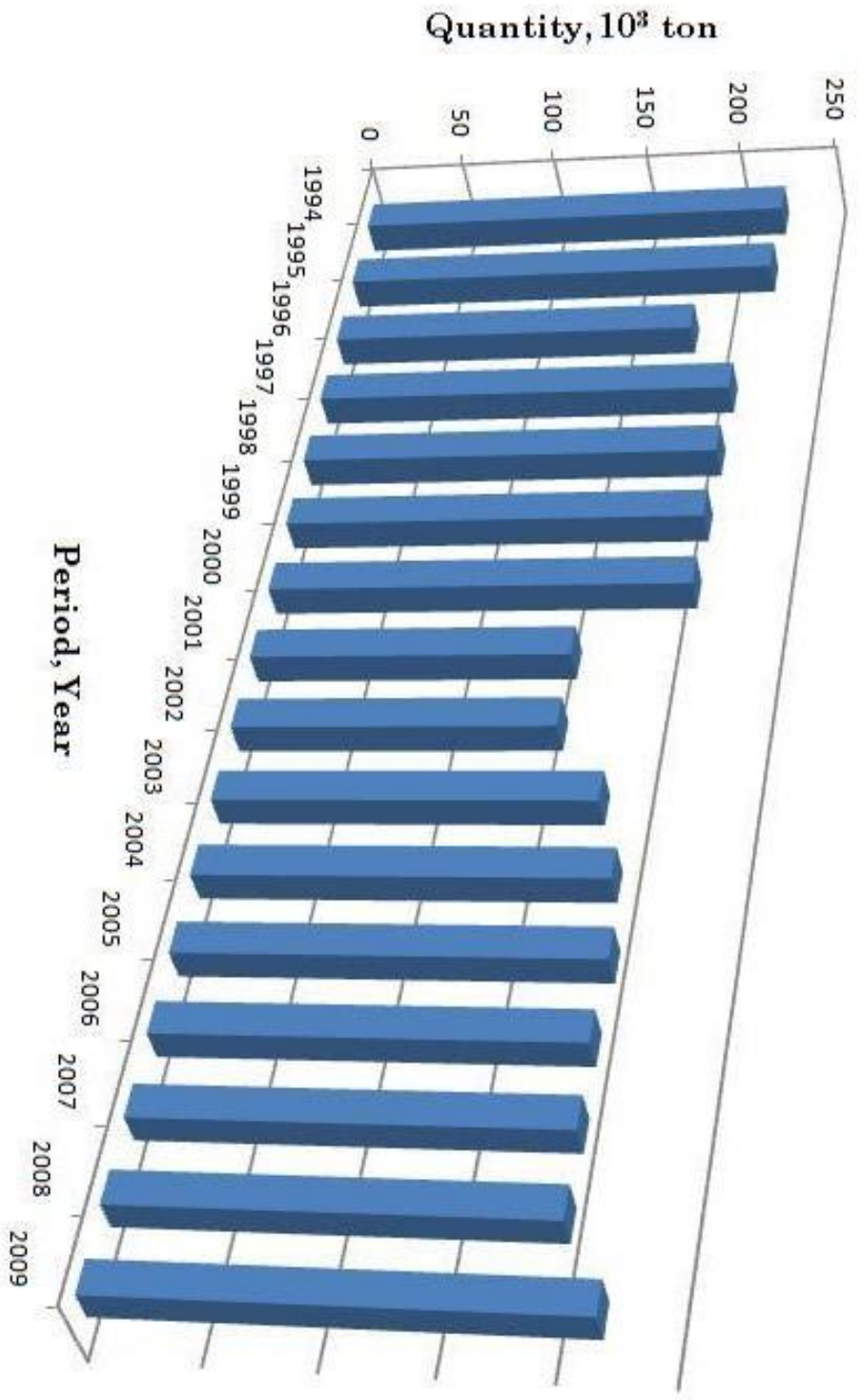

Appendix VI. Mandoval Vermiculite technical data sheet

MANDOVAL VERMICULITE

TECHNICAL DATA

TO: _____

FAX NO: _____

Raw Vermiculite
Vermiculite is a micaceous mineral. Mandoval's vermiculite consists of golden/brown flakes carefully classified into 5 grade each having a specified range of particle size.

Exfoliation of Vermiculite
Exfoliation occures at right angles to the cleavage planes, causing the flakes to expand into concertina-shaped granules.

Commercial exfoliation of vermiculite is achieved by passing the crude vermiculite in a controlled manner through a furnace chamber at elevated temperatures. Vermiculite reabsorbs some moisture after exfoliation.

Sintering Temperature
About 1,260°C.

Melting Point
About 1,315°C.

Specific Heat
0.2.

Specific Gravity
2.6.

pH Value
8-8,6 owing to the presence of associated carbonaceous rock, the reaction is normally alkaline as these break down into alkali oxides/hydroxides.

Thermal Conductivity
Vermiculite has low thermal capacity and high thermal insulation properties. Thermal conductivity at normal atmospheric temperatures:
k = 0.062 - 0.065 W/m°C

Incombustibility
Vermiculite is incombustible.

Water Holding Capacity
Exfoliated vermiculite will readily hold water within the interlaminar voids. The water retained as a percentage of the air dry weight is 240%.

Cation Exchange Properties
The exchangeable cation normally present in vermiculite is magnesium. The cation exchange capacity is 90-100 milli-equivalents per 100 grams.

Vermiculite is clean to handle, non-abrasive, reflective, rot-proof, odourless, mouldable, non-irritant.

Typical Chemical Analysis
The chemical analysis of raw and exfoliated vermiculite is identical. The major elements are:

SiO_2	39.37%*
TiO_2	1.25%
Al_2O_3	12.08%
Fe_2O_3	5.45%
FeO	1.17%
MnO	0.30%
MgO	23.37%
CaO	1.46%
Na_2O	0.80%
K_2O	2.46%
H_2O + 105°C	5.17%
H_2O - 105°C	6.02%
CO_2	0.60%
P_2O_5	0.15%
Li_2O	0.03%
*Free silica content	<1.0%

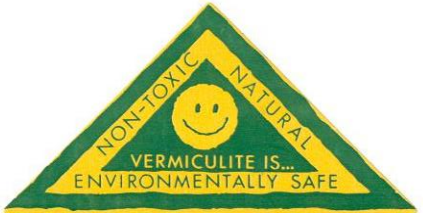

Insolubility
Vermiculite is insoluble in water and organic solvents

Sizes and Densities of the standard grades as packed per 100 litre bag.

Grade	Approx Size of Granule	Bag Mass	*kg/m³ *g/litre
Large	8mm & smaller	7kg	Max. 80
Medium	4mm & smaller	8kg	Max. 90
Fine	2mm & smaller	9kg	Max. 112
Superfine	1mm & smaller	10kg	Max. 125
Micron	0.5mm & smaller	10kg	Max. 125

Prices on request
Prices quoted are exclusive of VAT

(Prices are subject to change without notice)

MANDOVAL VERMICULITE CC
Reg.. No. CK2000/045769/23

2 Johnson Street, Alrode
P.O. Box 124114, Alrode
Tel: (011) 864-5205
Fax: (011 908-3049

E-Mail: mandoval@mandoval.co.za

Appendix VII. Effect of the TMA applied force (at 50 °C) on the compression ratio of (at 800 °C) expanded vermiculite flakes

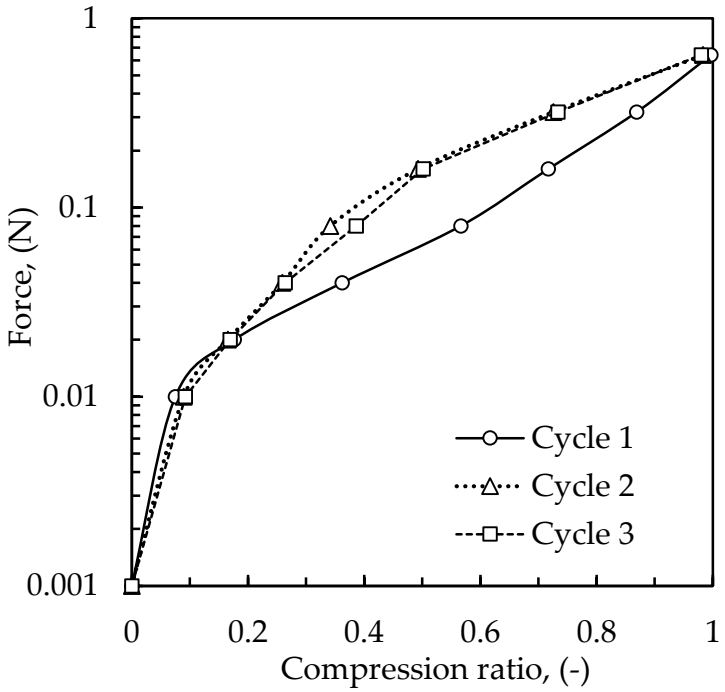

After the first expansion, the required force to compress the flakes is relatively low. From the second expansion, the required force to compress vermiculite flakes to a certain magnitude is similar.

Appendix VIII. SEM images of organo-vermiculite/LLDPE composites

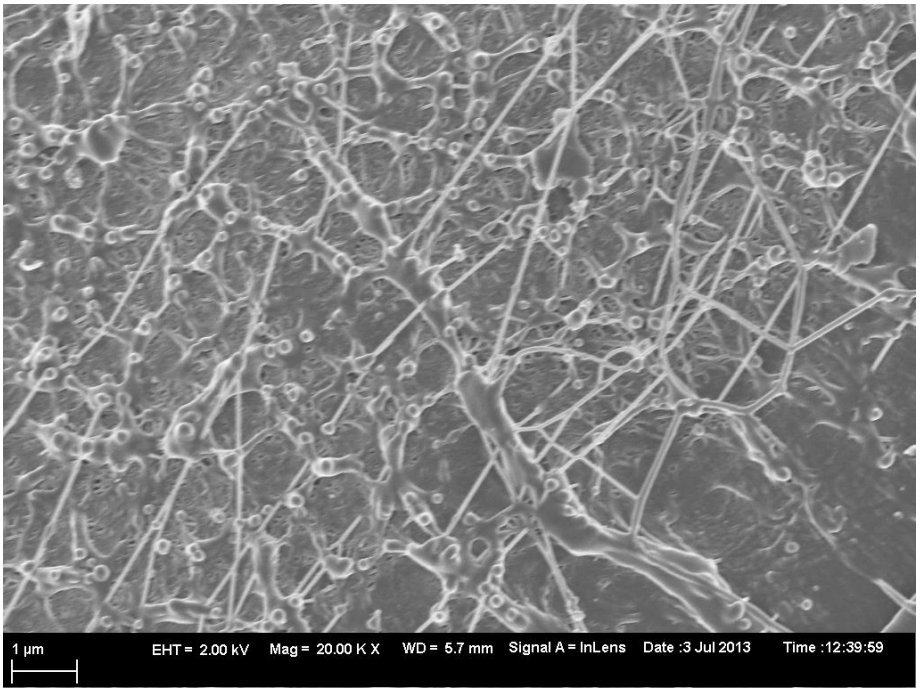

Appendix VIII-a) High magnification SEM image of neat LLDPE

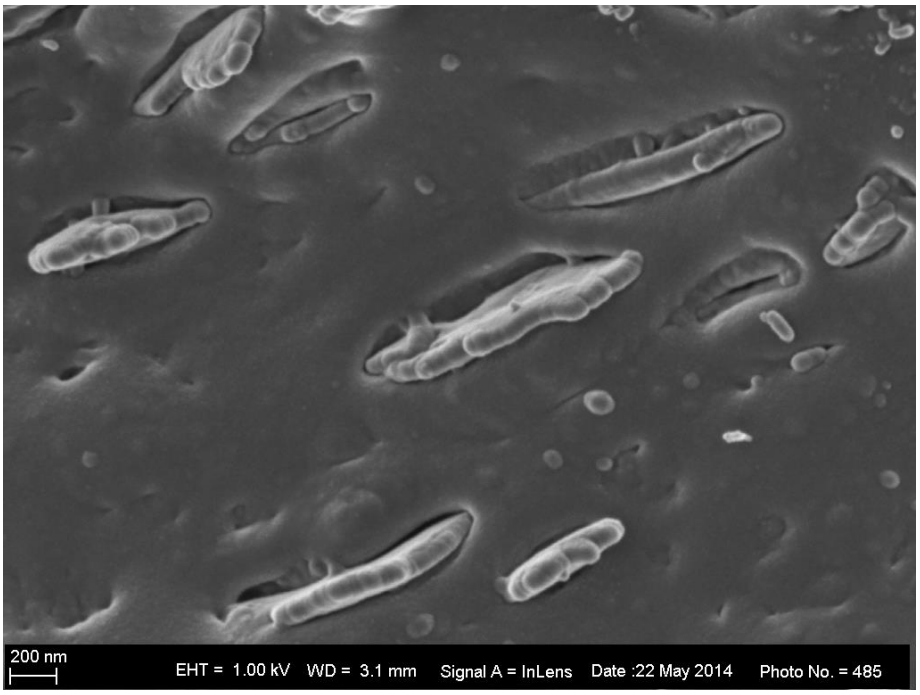

Appendix VIII-b) SEM images of fracture structure of organo-vermiculite-LLDPE composites

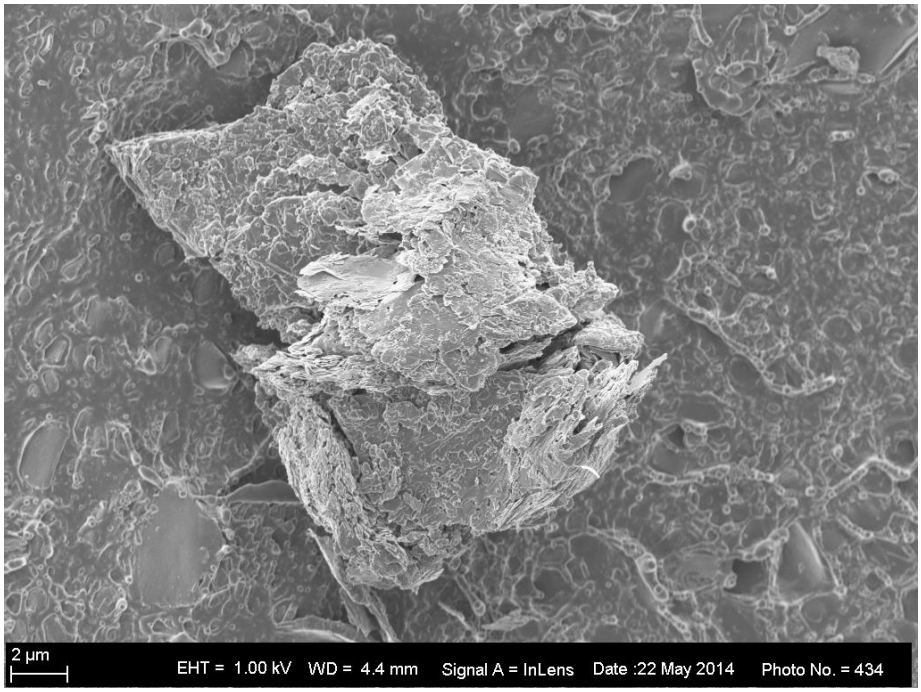

Appendix VIII-c) 5 wt.% organo-vermiculite. The clay particles are not interacting properly with the polymer matrix.

Appendix VIII-d) Large stacks of clay platelets present in all modified samples showing unaltered biotite layers, which retained their structure

Appendix IX. Cone calorimeter results of organo-vermiculite/LLDPE composites

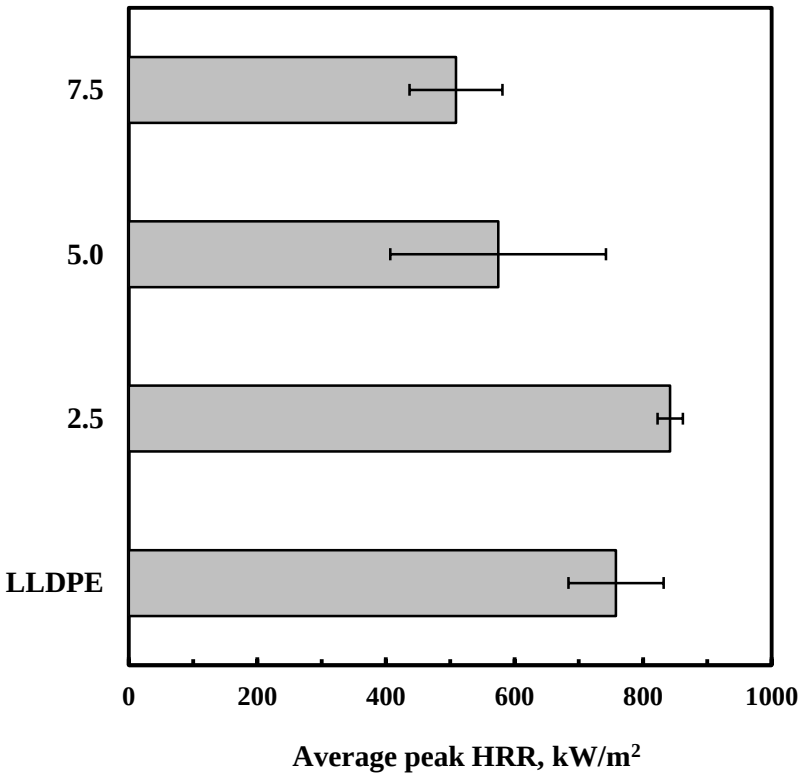

Appendix IX-a) Cone calorimeter pHRR for LLDPE and its composites with urea-vermiculite.

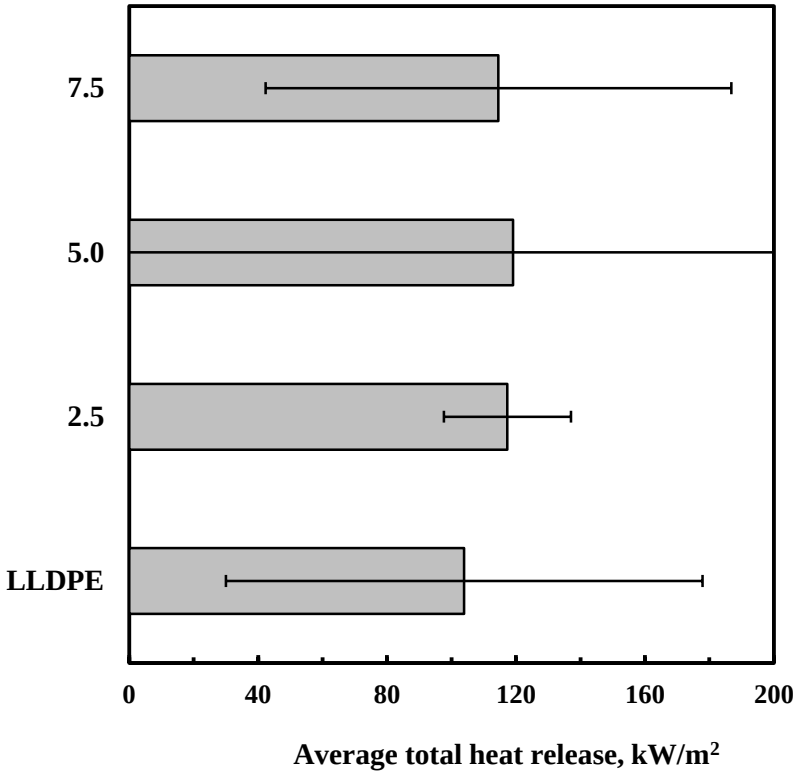

Appendix IX-b) Cone calorimeter tHR for LLDPE and its composites with urea-vermiculite.

Appendix X. Cone calorimeter data: composites of urea-vermiculite and plasticised PVC

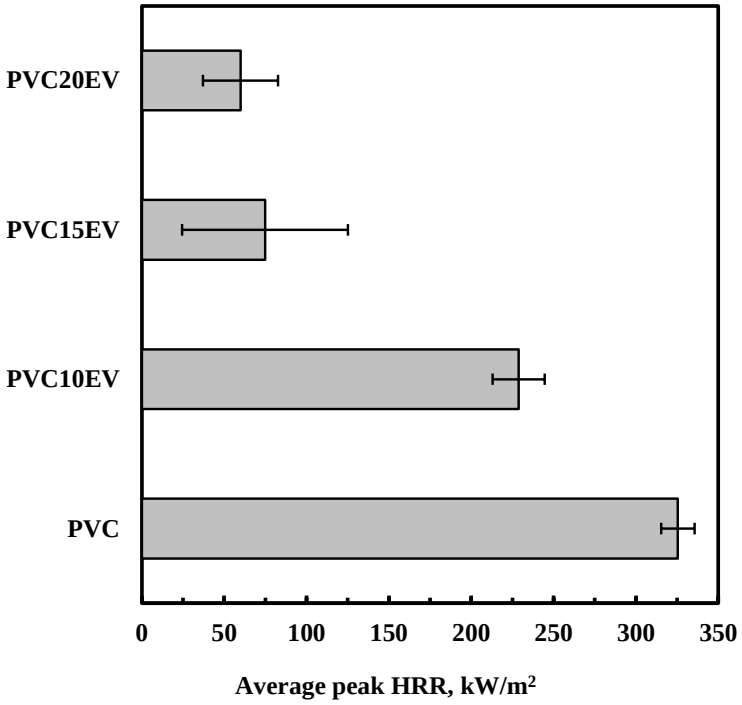

Appendix X-a) Cone calorimeter pHRR for the plasticised PVC compound and its composites with urea-vermiculite.

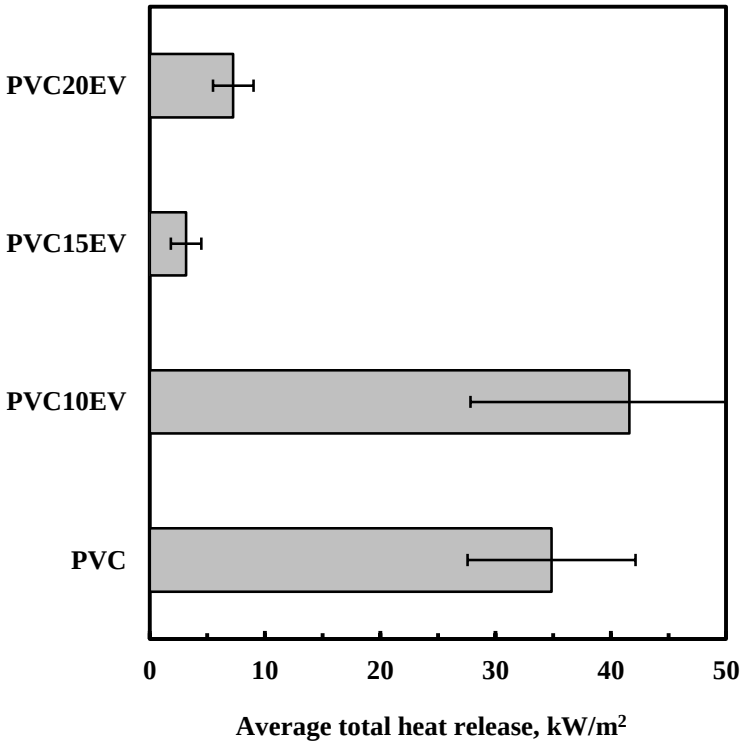

Appendix X-b) Cone calorimeter tHR for the plasticised PVC compound and its composites with urea-vermiculite.

Appendix XI. Cone calorimeter results of urea-vermiculite/PU composites

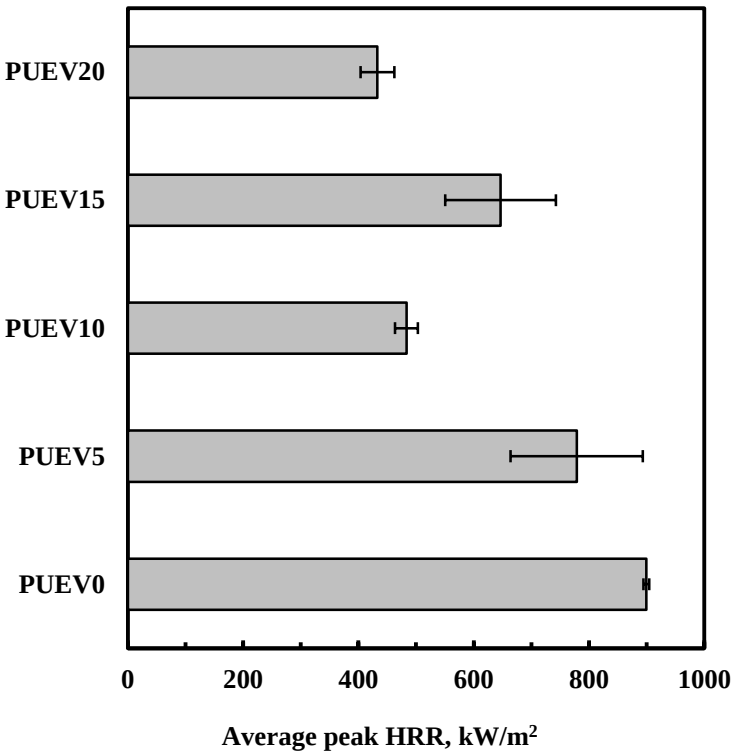

Appendix XI-a) Cone calorimeter pHRR for the PU compound and its composites with urea-vermiculite.

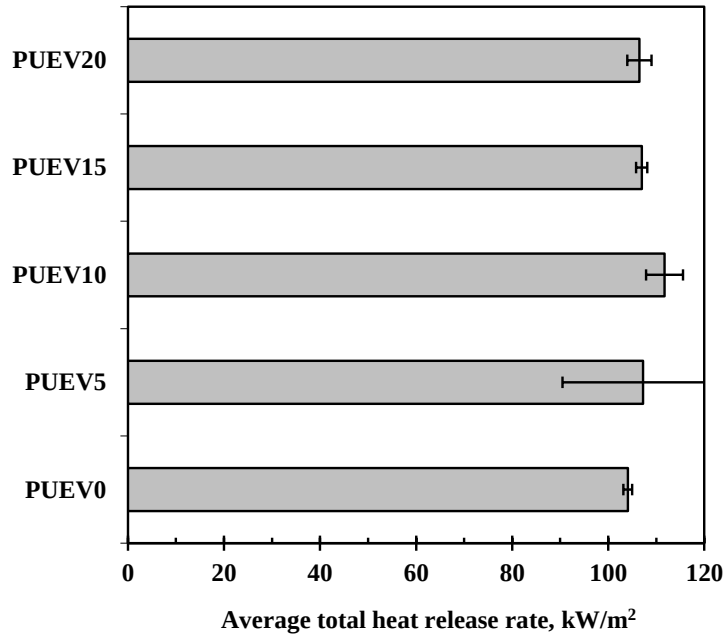

Appendix XI-b) Cone calorimeter tHR for the PU compound and its composites with urea-vermiculite.

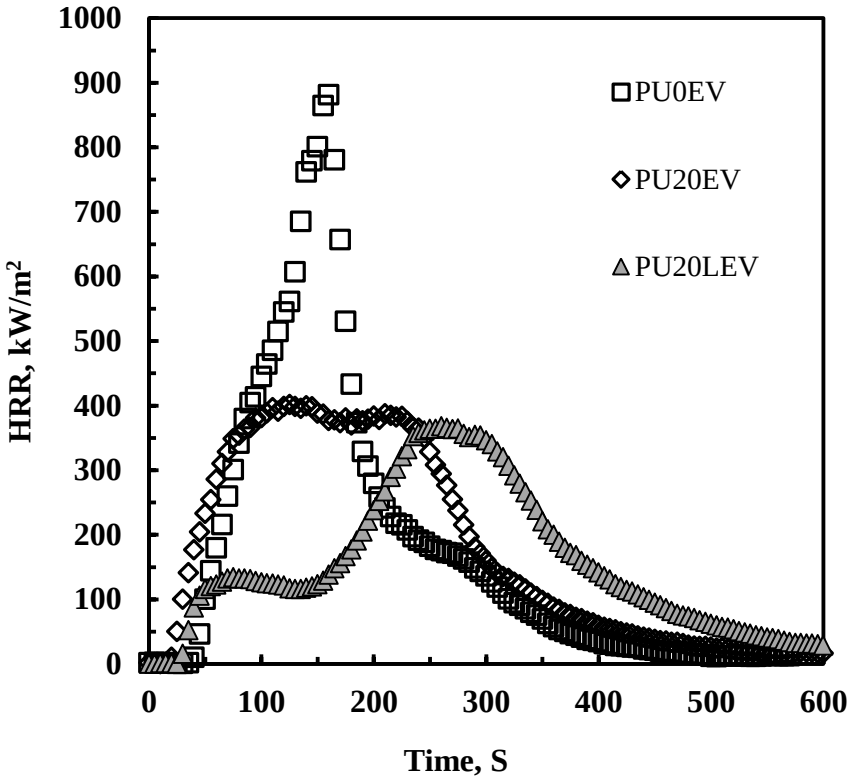

Appendix XI-c) Comparison of cone calorimeter heat release rate curves for PU compound and its composites with 20 wt.% urea-vermiculite.